
DATA-DRIVEN PARTICLE DYNAMICS: STRUCTURE-PRESERVING COARSE-GRAINING FOR EMERGENT BEHAVIOR IN NON-EQUILIBRIUM SYSTEMS

Quercus Hernández¹, Max Win¹, Thomas O’Connor², Paulo E. Arratia¹, and Nathaniel Trask¹

¹School of Engineering and Applied Science, University of Pennsylvania, 220 South 33rd Street, Philadelphia, PA 19104, USA.

²Department of Materials Science and Engineering, Carnegie Mellon University, Pittsburgh, PA, USA.

December 23, 2025

ABSTRACT

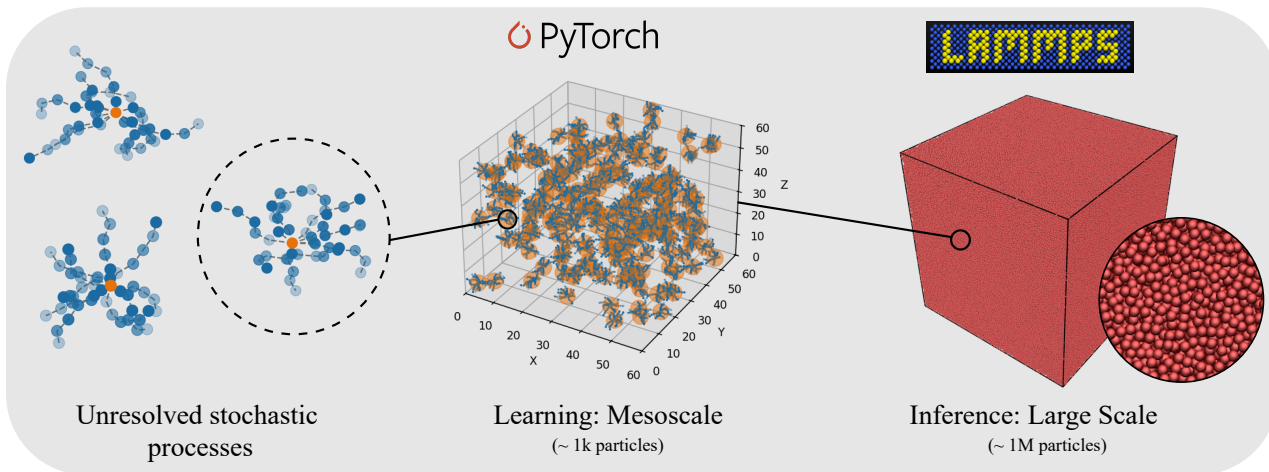
Multiscale systems are ubiquitous in science and technology, but are notoriously challenging to simulate as short spatiotemporal scales must be appropriately linked to emergent bulk physics. When expensive high-dimensional dynamical systems are coarse-grained into low-dimensional models, the entropic loss of information leads to emergent physics which are dissipative, history-dependent, and stochastic. To machine learn coarse-grained dynamics from time-series observations of particle trajectories, we propose a framework using the metriplectic bracket formalism that preserves these properties by construction; most notably, the framework guarantees discrete notions of the first and second laws of thermodynamics, conservation of momentum, and a discrete fluctuation-dissipation balance crucial for capturing non-equilibrium statistics. We introduce the mathematical framework abstractly before specializing to a particle discretization. As labels are generally unavailable for entropic state variables, we introduce a novel self-supervised learning strategy to identify emergent structural variables. We validate the method on benchmark systems and demonstrate its utility on two challenging examples: (1) coarse-graining star polymers at challenging levels of coarse-graining while preserving non-equilibrium statistics, and (2) learning models from high-speed video of colloidal suspensions that capture coupling between local rearrangement events and emergent stochastic dynamics. We provide open-source implementations in both PyTorch and LAMMPS, enabling large-scale inference and extensibility to diverse particle-based systems.

1 Introduction

Multiscale phenomena governing complex systems, from quantum materials to geophysical flows, exhibit emergent behaviors in which small-scale, potentially stochastic physics influences widely separated spatiotemporal scales. For example, quantum effects govern ferromagnetic ordering in magnetic materials [1], while topological entanglement leads to anomalous diffusion in polymer melts [2]. In geophysics, the bulk evolution of soil landscapes can be tied to microstructural events such as jamming transitions in dense suspensions [3, 4]. Bridging these disparate scales is an outstanding challenge for multiscale simulation, as computationally tractable strategies must avoid resolving prohibitively short spatiotemporal scales while preserving their influence on resolved ones. This process is typically referred to as “coarse-graining” and spans multiple applications. For example, in molecular physics, the resolution of electron motion by den-

sity functional theory (DFT) or vibrational motion by molecular dynamics (MD) would mandate $10^{12} - 10^{15}$ timestep simulations to resolve $O(1)$ s timescales, and many works aim to identify coarse-grained representations, either empirically by ansatz [5], through formal procedures [6, 7], or with machine learning (ML) to supervise pair potentials from DFT data [8]. In turbulence, full resolution of the energy cascade requires prohibitive resolution of the Kolmogorov scale; in practice, coarse-graining to either the Taylor microscale (in large eddy simulation/LES) or integral length scale (in unsteady Reynolds averaged simulation/URANS) provides tractable simulation; turbulence literature similarly reflects a trend from empirical ansatz [9], to formal coarse-graining procedures [10, 11, 12], to machine-learned LES/RANS models [13, 14, 15]. Our aim is to build a generally applicable framework that can machine learn a stochastic dynamical system governing large scale, easily measurable, dynamics while preserving the essential statistical character of unresolved physics.

A Coarse-grained acceleration of multibody physics



B Structure-preserving model direct from experiments

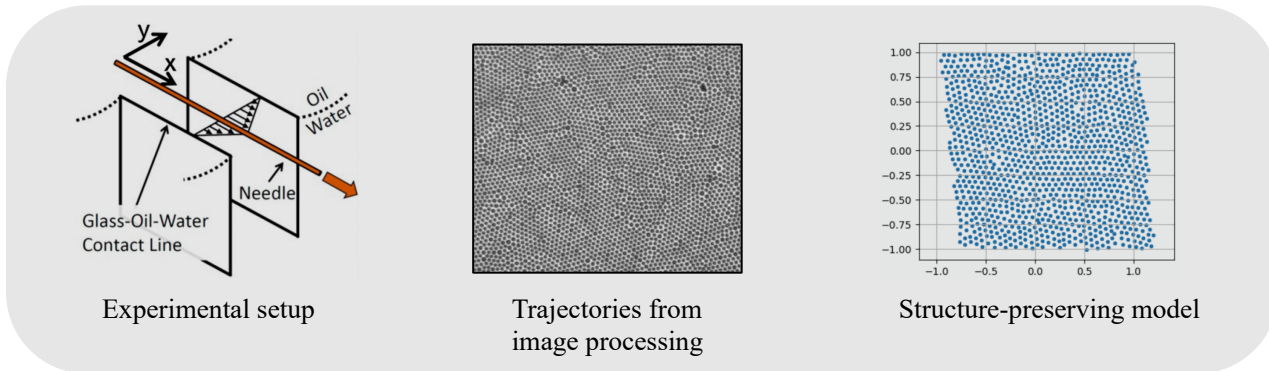


Figure 1: Exemplar applications using data-driven particle dynamics to bridge scales in simulated (top) and experimental (bottom) datasets. (A) Detailed simulation of polymers fully resolve stochastic fluctuations (left), in-silico experiments of a small domain supervise model discovery (middle), yielding a data-driven model for non-equilibrium bulk response solved in a massive parallel simulator (right). (B) A 2D suspension in an oscillatory shear flow provides a rich multiphysics/multiscale exemplar incorporating lubrication, electrostatics, contact, and stochasticity (left). Trajectories of particle data are extracted using computer vision techniques, providing complete top-down (but noisy) data to supervise model collection (center), ultimately yielding a model which predicts linkages between structure and emergent dynamics (right).

We address the challenge by building a unified “top-down” coarse-graining framework which can machine learn dynamics from partial observations of coarse-grained variables without labels for unobservable states, using bracket structure to build thermodynamically consistent representations of unobservable fluctuations. The current machine learning paradigm is largely “bottom-up”, where data and simulations must be collected at the most fundamental level to understand emergent dynamics [16]. This ab initio strategy naturally yields a potentially unwieldy hierarchy of models, linking descriptions of physics that bridge submolecular, molecular, mesoscopic, continuum, and systems/network scales. This is particularly relevant for experimental systems in which velocimetry or digital image correlation may yield observable fields but unobserved fields are either intractable or impossible to

measure (e.g. material structure or entropy, respectively); extracting predictive models direct from experiment is the primary goal of this work. Following the trend of self-supervised learning which has recently emerged in the machine learning community, we demonstrate how geometric structure in the unresolved physics at lower levels can be exploited to infer their effect on higher levels of the hierarchy without the need for labeled data. This enables one to e.g. learn a continuum scale model without DFT/MD labels, subverting the prevailing wisdom that top-down approaches cannot capture unresolved statistical features [16].

For a machine learned model to credibly describe coarse-grained representations of systems, emergent thermodynamic and stochastic structure must be preserved at a discrete level, independent of data availability, optimization error, or model

form error. Several frameworks offer candidate mathematical formalisms to identify this requisite structure. The Mori-Zwanzig (MZ) formalism [17, 18, 19, 20] interprets coarse-graining as a projection of full-order dynamics onto coarse-grained variables. Through projections, coarse-graining induces three terms: a mean-field coarsened dynamics; a non-Markovian/history-dependent dissipative memory kernel; and a stochastic term accounting for work done by unresolved physics. Although the full-order system may be reversible, MZ establishes the need to consistently treat non-Markovian stochasticity and dissipation; the work done on the system by fluctuations must exactly balance dissipation to ensure energy is conserved, providing so-called *detailed fluctuation-dissipation balance* [21, 22]. In non-equilibrium systems, this provides a formalism to model the transfer of energy from unresolved non-equilibrium fluctuations and resolved state variables via dissipative mechanisms. Through fluctuation-dissipation balance, we aim to infer the statistical character of fluctuations through labels of observable dissipative processes.

While powerful, the MZ formalism often requires restrictive Markovian assumptions to obtain tractable models [23]. The metriplectic/GENERIC formalism [24, 25, 26, 27, 28] provides an algebraic alternative where processes are described via reversible and irreversible brackets whose matrix representations admit natural parameterizations in tensor-based ML frameworks like PyTorch. A stochastic metriplectic model takes the form:

$$d\mathbf{x} = \left[\mathbf{L} \frac{\partial E}{\partial \mathbf{x}} + \mathbf{M} \frac{\partial S}{\partial \mathbf{x}} + k_B \frac{\partial}{\partial \mathbf{x}} \cdot \mathbf{M} \right] dt + d\tilde{\mathbf{x}} \quad (1)$$

for: state \mathbf{x} , energy and entropy functionals $E(\mathbf{x})$ and $S(\mathbf{x})$, Poisson matrix $\mathbf{L}(\mathbf{x}) = -\mathbf{L}^T$, friction matrix $\mathbf{M}(\mathbf{x}) = \mathbf{M}^T$, Boltzmann constant k_B and fluctuation $d\tilde{\mathbf{x}}$. Under the degeneracy constraint $\mathbf{L}\nabla S = \mathbf{M}\nabla E = \mathbf{0}$, one achieves constant energy and non-decreasing entropy in the $k_B = 0$ case. If fluctuations are posed which satisfy

$$\mathbb{E} \left[d\tilde{\mathbf{x}} d\tilde{\mathbf{x}}^T \right] = 2k_B \mathbf{M} dt,$$

detailed fluctuation-dissipation balance is achieved so that energy is preserved despite stochastic forcing. In the conventional literature, an analytically derived model is identified as metriplectic and inherits theoretical benefits. The current work instead poses a parameterized metriplectic bracket so that, *by construction*, any fit model preserves detailed balance and preserves statistical thermodynamical structure. This provides a linkage between observable dissipative processes and unobserved statistical structure.

In this manuscript, we prescribe a general construction of parametric $E, S, \mathbf{L}, \mathbf{M}$ as perturbations of non-canonical Hamiltonian systems which serves as a broadly applicable template, before specializing to a particle Hamiltonian appropriate for learning material/Lagrangian descriptions suitable for experimental particle tracking, data-driven MD, and large deformation solid mechanics. The particle bracket is adapted from classical particle methods [29, 30] and provides interpretable predictions of volume, internal energy, pressure, and temperature via an equation of state (EOS) which discretely preserves

Gibbs' relations. Our approach provides a new capability to recover a model from time-series observations of particle trajectories which extrapolates beyond equilibrium training data with the capacity to recover a conventional EOS. From a computational perspective, we provide an open-source LAMMPS implementation that exhibits weak scaling, with the potential to evaluate these models at the exascale.

This development enables the design of new experimental campaigns in which predictive models are rigorously extracted from particle-tracking data. Such a capability is particularly promising for systems which defy conventional first-principles modeling. Here, we exemplify this approach using an experimental dense colloidal suspension composed of nearly 5×10^4 particles undergoing shear deformation (see Fig. 1B). For such systems, predictive models have proven elusive [31, 32, 33, 34], with limited progress using supervised learning to identify configurational features that correlate with emergent suspension dynamics [35, 35, 36]. This challenging but tractable modeling task could be done for a few particles, but cannot scale up to millions of particles with conventional simulation. We demonstrate with our top-down approach a dynamical model that predicts deviations from linear shear profiles associated with rare dislocation events driven by force dipoles, establishing a nontrivial linkage between structure and emergent dynamics.

2 Prior literature

2.1 Candidate coarse-graining theories

A number of theoretical frameworks provide a principled foundation for coarse-graining. Mori and Zwanzig's initial works [18, 17] were generalized to optimal prediction extensions [23] and the metriplectic/GENERIC [24, 27] theories; Ottinger showed [37] that GENERIC can be derived as a special case of MZ. The renormalization group (RNG) theory [38], as well as information theoretic frameworks like relative entropy, iterative Boltzmann, and MaxEnt [39, 40, 41, 16], and more recent stochastic [42] provide alternative formalisms to coarse-grain. In the mechanics community, homogenization theory and the more finite element-centric variational multi-scale (VMS) method offer related projection-based variational techniques but lack an explicit tie to non-equilibrium thermodynamical/statistical behavior [43, 44].

In fluids, these frameworks have provided a theory-informed basis to develop turbulence and constitutive models, including representative earlier works in RNG [45, 46] and more recent MZ [11, 47, 12, 48] and VMS [49, 50, 51] works. In molecular dynamics, coarse-graining is arguably more mature, with excellent review articles [16, 52] elucidating the bottom-up/top-down divide, summarizing recent trends, and providing MD-specific ties to information theory. While some coarse-grained MD methods conjecture effective potentials in an ad hoc manner [5], several works have used MZ or variational/information-theoretic frameworks to provide rigorous justification of their functional form [53, 54, 6].

The present work requires a theory able to provide a machine-learnable ansatz for dynamics which can: prescribe the reversible, irreversible, and stochastic dynamics that emerge in coarse-grained descriptions; guarantee detailed fluctuation-dissipation balance; provide discrete notions of the first and second laws of thermodynamics; support a tractable computation amenable to end-to-end automatic differentiation; and identify internal variables describing unobservable physics. Interestingly, [16, 55] advocate “ultra-coarse-grained” state dynamics, where the state is enriched with an additional field which encodes unresolved structure; the self-supervised entropic variable identified in the present framework plays an analogous role.

2.2 Supervised learning: force matching, missing physics and closure modeling

In data-driven modeling, the inference of parameterized dynamics $\dot{X} = F(X, t; \theta)$ from either timeseries $\{X_i(\cdot)\}$ or labeled state-force pairs $\{X(t_i), F(t_i)\}$ is sometimes referred to as *force matching*. When a force is partially known but missing terms due to a coarse-graining procedure, different communities refer to this as *closure modeling*, *missing physics*, or *residual correction*. A typical configuration is to discretize in time and infer parameters θ by minimizing the residual associated with a given timestep (e.g. $\min_{\theta} \|X^{n+1} - X^n - F(X^n, t^n; \theta)\|^2$), to integrate the parameterized ODE and train over rolled-out trajectories, or to employ equality constrained optimization. For all configurations, it is assumed that labels for a fully observable state X are available.

In the MD community, while conventional approximants [56, 7] or atomic cluster expansions [57] have provided reliable bases for regressing F , neural architectures have surged in popularity due to their ability to extract information from high-dimensional inputs. While early works used neural networks [8] or Gaussian processes [58] to regress univariate force-distance relationships, contemporary graph architectures can process many-body geometric configurations of either particles or continuum meshes [59, 60, 61, 62, 63, 64, 65, 66, 67, 68]. Autoencoders can identify latent representations from bottleneck structure, providing candidate representations for reduced dynamics [69, 70, 71, 72]. In most instances, training data takes the form of ab initio DFT calculations that give a complete prescription of F from molecular configuration in the bottom-up configuration.

Recent work has shown that low force-matching residuals are insufficient benchmarks for coarse-grained models, while structural descriptors (e.g., radial distribution functions) and dynamical quantities (e.g., velocity autocorrelation functions, diffusion coefficients) are necessary benchmarks to qualify thermodynamic and stability performance [73]. Without physically consistent coupling between dynamics and fluctuations, many ML methods rely on *backmapping* [16], employing generative architectures trained on ab initio data to reproduce stochastic behavior in both continuum [74, 75, 76] and molecular [77, 78, 79] systems. Here, we demonstrate that metriplectic brackets prescribe thermodynamically valid fluctuations without ab initio training data, whereas popu-

lar physics-agnostic GNNs fail to capture correct statistical benchmarks. Jin et al [16] highlight a particular challenge in bottom-up coarse graining: the choice of coarse-grained variables and the identification of a model-form compatible with target ensemble statistics require careful constructions, often prompting overly simplistic Langevin descriptions of missing friction. Our approach provides a rich class of automatically compatible stochastic/dissipative processes.

2.3 Structure-preserving algorithms

While the incorporation of physical principles has broadly been recognized to improve scientific machine learning, recent works have distinguished between *physics-informed* techniques [80, 81] which impose physics by introducing penalties, compared to *structure-preserving* which integrate physics either by construction or via equality constraints [82]. Among other pathologies, the former loosely endows properties only to within optimization error, and therefore cannot provide detailed fluctuation dissipation balance [83, 84]. The latter has particularly been considered in computer vision and molecular dynamics, where substantial effort focuses on equivariant/invariant architectures which provide uniform predictions as input images/graphs are rotated or translated [85, 86, 87, 88, 89, 73, 90]. This is distinct from the notion of geometry in variational/geometric mechanics, where symmetries of governing brackets, rather than geometric transformations, guarantee notions of conservation or dissipation. For this work, we consider the latter when we define a data-driven coarse-graining approach to be structure preserving. In Fu’s assessment of ML-MD benchmarks [73], the former is shown to meet more stringent benchmarks but with millions of parameters; we achieve the same performance but with tens of thousands of parameters (a 10 – 1000× improvement in parameter efficiency, and therefore inference time).

Enforcing these symmetries are commonplace for reversible systems, where Hamiltonian networks [91, 92, 93], Lagrangian networks [94], and similar constructions yield architectures which conserve energy by design. Irreversible systems are only recently considered in the scientific ML literature; while early works considered physics-informed soft constraints [95, 96], strong imposition of dissipative structure has been considered only more recently with variational or port-Hamiltonian descriptions [97, 98, 99, 100, 101, 102]. Some consider metriplectic brackets [103, 104, 105], but with a construction that scales superlinearly in the degrees of freedom so that structure-preserving dynamics have been shown only for thousands of degrees of freedom. The present work prescribes metriplectic brackets in linear $O(N)$ complexity, allowing us to demonstrate weak parallel scaling at inference time in LAMMPS [106]. Open source code is provided (<https://github.com/PIMILab>) for both learning models in PyTorch and performing inference at massive scales in LAMMPS. The current work thus amounts to the first demonstration of learned metriplectic dynamics with $O(N)$ scaling enabling massively parallel inference.

3 Results

We consider a diverse set of physics to highlight important consequences of structure preservation in our approach:

- **Ideal gas.** Recovery of a continuum fluid system with a conventional equation of state allows us to demonstrate out-of-distribution performance for non-equilibrium flow predicted from equilibrium training data and viceversa.
- **Star polymer.** A conventional coarse-grained MD demonstrates performance superior to a well-calibrated empirical coarse-grained model and recovery of structural/dynamic statistics where conventional GNNs fail.
- **Viscoelastic solid.** The generality of the framework is highlighted by predicting a solid system, proving generalization to other energy functionals (i.e. strain energy) to treat continuum systems.
- **Jammed colloidal system.** Illustration of full capability of framework to bridge structure-dynamics to predict rare events in a complex multiphysics system from experimental data; lubrication/contact/electrostatic interactions governing defect dynamics are unresolved, yet learned stochastic dynamics capture their impact on statistics of defect dynamics.

In light of [73], which stresses the importance of structural/dynamical statistics benchmarks, we include comparisons to popular GNN architectures when predicting the Radial Distribution Function (RDF), Velocity Autocorrelation Function (VACF), and Mean Squared Displacement (MSD).

- **Graph Network-based Simulator (GNS).** We take Graph Network-based Simulator [107] as a representative state of the art “black-box” GNN model commonly used for scientific machine learning tasks.
- **Stochastic Graph Network-based Simulator (GNS-SDE).** We add an additional message passing network which imposes multiplicative Gaussian noise and uses a maximum likelihood loss [108] to ensure improved performance is not due to maximum likelihood training.
- **Conventional coarse-grained model (DPD).** We use the same maximum likelihood training to calibrate the parameters of a standard DPD model [5], providing a representative baseline for accuracy accessible to a conventional ad hoc coarse graining method. While accurate for an ideal gas, for the more complicated systems the calibrated DPD provides an overly “soft” potential, with lower amplitude peaks in RDF compared to our learned models.

Details for all benchmarks and comparison methods may be found in Appendix G.

3.1 Ideal gas

We first consider an ideal gas in a 3D periodic box over three different forcings to demonstrate out-of-distribution generalization, sketched in Fig. 2. Training is performed for vortex

forcing (TAYLOR-GREEN, [109]), while inference is tested under configurations unseen during training for an unforced system (SELF-DIFFUSION) and shear forcing via Lees-Edwards boundary conditions (SHEAR FLOW, [110]).

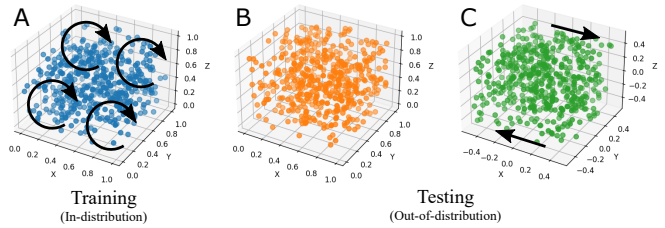


Figure 2: IDEAL GAS datasets. Flow configurations for (A) TAYLOR-GREEN training dataset, and (B) SELF DIFFUSION and (C) SHEAR FLOW testing datasets. We confirm generalization of non-equilibrium statistics in (B) and (C) despite distinct flow conditions held out during training.

Fig. 8 demonstrates good agreement between the proposed methodology and spatial statistics for long extrapolation rollouts. On the other hand, both GNS and GNS-SDE fail to capture the statistics of the flow, and are outperformed by classical DPD technique. We also present in Table 5 the relative error results of the same model tested under two different periodic boundary conditions without any additional training. We can observe that our method maintains its performance under extrapolation to unseen flows while the traditional GNN methods diverge in longer rollouts.

We further include two additional tests to provide visual intuition of our algorithm’s performance in inference; these cases have not been held out during training. Fig. 9 shows how the proposed method achieves the correct average velocity shear profile with respect to the reference solution for the SHEAR FLOW dataset. Fig. 9 shows the inferred SELF-DIFFUSION mixing of a domain scaled up to $L = 2$.

To demonstrate the capability to predict non-equilibrium dynamics when trained under equilibrium conditions, we also trained the model under quiescent equilibrium conditions and evaluated its rollout performance under externally driven flows. As shown in Fig. 11 the equilibrium-trained model reproduces the key dynamical statistics, confirming that the metriplectic structure generalizes beyond its training regime. However, its performance slightly deteriorates when trained on both equilibrium and non-equilibrium data due to the model not having encountered the broader velocity distributions present in non-equilibrium states.

3.2 Challenging coarse graining experiment: Star polymer

A star polymer melt in a 3D periodic box provides a conventional coarse-grained MD exemplar, for which bottom-up ML is natural, but the feasibility to capture statistics in a “top-down” configuration is unclear. Each polymer is composed of a core atom and 10 arms bonded by a finite extensible nonlinear elastic (FENE) potential, whereas the interaction between

polymers is modeled by a Lennard-Jones potential. Two different internal configurations are considered: 1 and 5 beads per arm, which results in less and higher coarse-graining levels (Fig. 3). The fully resolved datasets are generated using LAMMPS [106] and then coarse-grained by computing the center of mass position and velocity of each polymer.

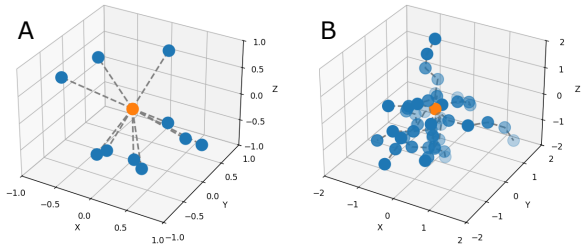


Figure 3: Representative star polymers coarse grained into a single data-driven particle in STAR POLYMER datasets. (A) STAR POLYMER 11 with 1 core, 10 arms and 1 bead per arm. (B) STAR POLYMER 51 with 1 core, 10 arms and 5 beads per arm.

The results are shown in Fig. 4 and Table 5. We observe that, similar to the previous dataset, the correct statistics are obtained while GNN baselines fail to predict statistical structure. Both GNS and GNS-SDE predict a nearly flat RDF, meaning that the prediction lacks spatial structure and correlations. Both the VACF and MSD deviate from the ground truth by orders of magnitude, which suggests that they overestimate the velocity and dissipation. Similarly, the deviation in the MSD shows an overestimation of the diffusion regime, totally misrepresenting the stochastic dynamics of the system. This highlights the major qualitative impact physical structure preservation has on even simple systems, and that “black-box” techniques are poor candidates for coarse-graining, as the well-calibrated DPD model outperforms these methods with drastically fewer parameters. In contrast, our method outperforms the well-calibrated model by a factor of $2 \times -10 \times$ in relative error.

3.3 Weak scaling study

Table 4 shows the per timestep performance of the tested models in a serial implementation. The models have been optimized with the TorchScript compiler and run on a single GPU over a $T = 2000$ timestep run. As expected, the conventional DPD model exhibits the highest computational efficiency among the models evaluated, primarily due to its minimal architecture with only four trainable parameters. Our method is within a factor of two of GNS/GNS-SDE, as we employ multiple internal neural networks; illustrating that the current framework is of comparable computational complexity to conventional ML pair potentials. Importantly, all coarse-grained models achieve significantly faster runtimes than the fully resolved dynamics, demonstrating the computational benefits of coarse-graining.

Given a trained model, we provide code to perform inference in LAMMPS [106] as a custom pair style. LAMMPS is an

exascale code, and thus provides a means of taking models trained on small systems and performing inference on arbitrarily large numbers of particles. In Fig. 5 we demonstrate weak scaling up to 8 million coarse-grained particles over 64 processors.

4 Extension to general physics problems

The previous examples assumed a specific choice of internal energy, appropriate for a fluid-like system which stores energy only via dilatation. We now demonstrate how broader classes of physics may be considered by extending the definition of potential energy functional to handle additional inputs by adding a tensorial strain energy dependence appropriate for solid systems. This allows the model to account for reversible effects stored elastically as shear stresses, which are not present in fluids. The derivation of dissipative and noise terms is independent of this addition and remains unchanged; this case serves as an example for how to add additional reversible physics in the framework.

4.1 Viscoelastic solid

We consider next a viscoelastic material under shear to demonstrate the capture of strain energy (Fig. 12). This task is equivalent to discovering the underlying constitutive law of the system, encoded in the learned strain energy potential and the dissipative forces. The predictions of the model, also reported in Table 5, are in good agreement with the reference finite element solution, up to a large 50% strain. The model is also able to complete a full cycle starting from rest and returning to its original configuration after a relaxation period. On the other hand, thermodynamically inconsistent baseline models fail to capture the constitutive behaviour characteristic of solid-like dynamics, resulting in unphysical spatial correlations (Fig. 12, denoted as “Ours no U^{dev} ”). Moreover, we have performed an ablation study, illustrating that neglecting the new strain energy term precludes prediction of spatial statistics. This is due to the lack of restoring elastic forces which drive the conservative behaviour of deviatoric stress terms.

4.2 Experimental dataset: jammed colloidal system

Finally, we consider an experimental dataset consisting of a dense colloidal particle suspension undergoing cyclic shear deformation [111, 112, 32]. Here, particles are confined to a two-dimensional (2D) monolayer, which allows for visualization of the evolving microstructure; the suspension is a bidisperse (50% by number) mixture of 4:1 and 5:6 μm -diameter sulfate latex particles (Invitrogen) adsorbed at the interface between water and oil (decane). This material is subjected to a linear shear deformation in a custom-made interfacial stress rheometer (ISR) [113, 112, 111], which provides bulk rheological data. In short, a thin magnetized needle is embedded in the monolayer inside an open channel formed by two walls (Fig. 1B); a static Helmholtz field keeps the needle centered in the channel, while additional electromagnets move the needle back and forth, uniformly shearing the suspension

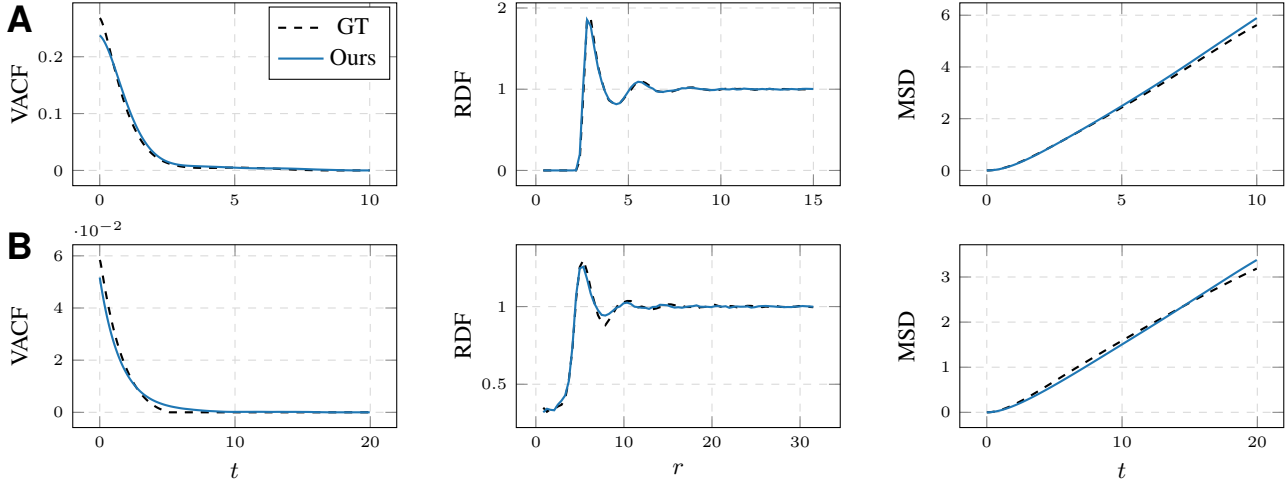


Figure 4: Correlation metrics for the (A) STAR POLYMER 11 and (B) STAR POLYMER 51 datasets, establishing recovery of structure and dissipative response. Other deep learning baselines (GNS, GNS-SDE) fail to recover structural or dynamical statistics and produce unstable results (outside the plotting range). In contrast, a classical model such as DPD captures some dynamical information but inaccurately.

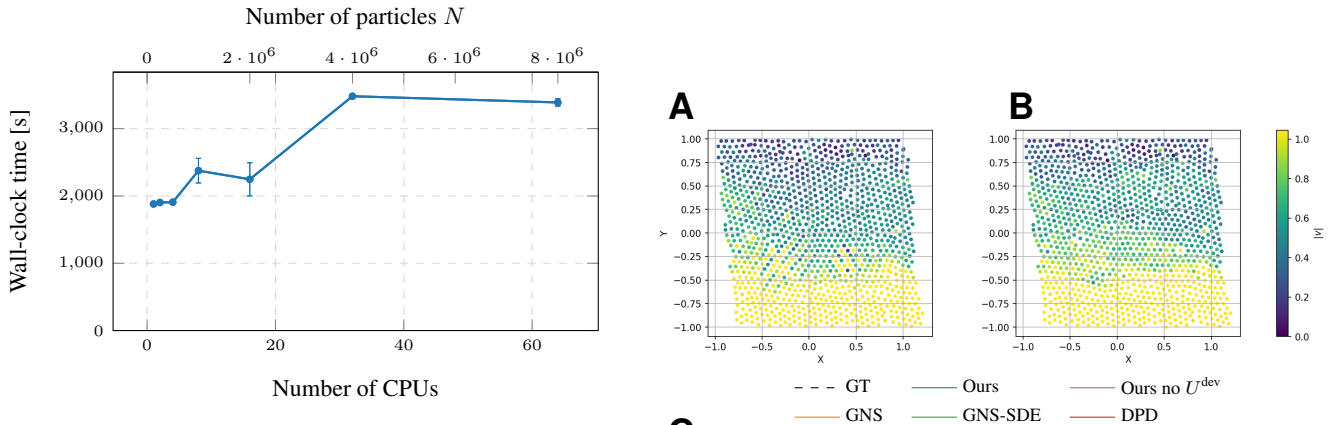


Figure 5: Computation time required for a fixed number of CPUs per processor without GPU acceleration. A flat curve denotes weak scaling, demonstrating that systems of arbitrary size may be considered by scaling CPUs proportional to numbers of particles.

monolayer in the channel. This setup allows for the visualization/characterization of particle position/trajectories using high-resolution optical microscopy. Images are processed using an in-house particle tracking algorithm and velocities are obtained with finite differences. For more details on the experimental setup, please see [112, 111, 32]. This experimental dataset integrates fluid- and solid-like behavior of jammed polycrystalline suspensions, as well as electrostatics, lubrication and contact physics, highlighting the broad applicability of the framework in multiphysics settings.

Figure 6 shows snapshots of the experimental (A) and model-predicted (B) sheared colloidal suspension color-coded by their local speed $|V|$. The model successfully reproduces

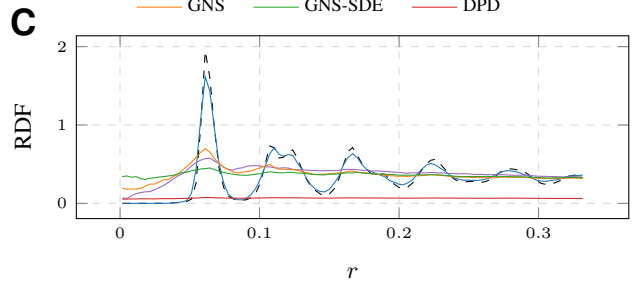


Figure 6: Predicting dynamics and structure of experimental colloidal systems undergoing shear deformation. Dynamics: instantaneous snapshot of jammed colloidal system with particles color-coded by velocity magnitude $|V|$ for (A) experimental dataset and (B) model prediction showing good agreement. (C) Structure: Model can predict the experimental sample radial distribution function (RDF). Neither conventional GNNs or DPD are able to predict structure.

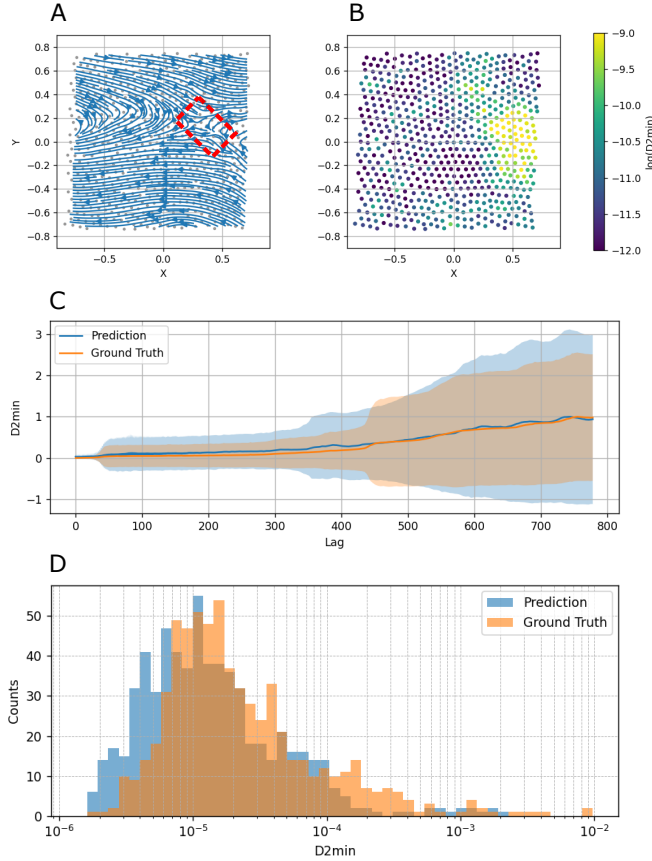


Figure 7: Dynamical properties of the model predictions on the experimental dataset for a domain crop. (A) Streamlines computed from displacements for a lag of 200 snapshots of the first cycle. The red square identifies a hyperbolic motion of a dislocation event fully predicted by the neural network. Predicting the force dipole driving the displacement hopping has been a major challenge. (B) Non-affine squared displacement field (D_{\min}^2), where the hotspots represent non-affine deformation clusters, highlighting that the learned model is able to identify local dislocation events. (C) Normalized mean and standard deviation of D_{\min}^2 for different lag times on a peak-to-peak cycle. While the magnitude of the force dipole driving the displacement is underestimated, after normalization we observe qualitative agreement with experiment. (D) Histogram of non-affine displacements for lag 150.

key flow features, including regions of relatively high particle speed near the moving needle (bottom of image) and low particle speed near the stationary wall (top). Figure 6C shows strong agreement between the experimental and model-predicted radial distribution function (RDF). The RDF indicates that the suspension is disordered at long range but exhibits short-range order, consistent with crystalline domains only a few hundred particles in size. These domains are separated by extensive grain boundaries composed of disordered configurations. Notably, our model outperforms several

commonly used methods in predicting the experimental RDF (Fig. 6).

Next, we explore the sample dynamical properties using the proposed framework. Fig. 7A shows streamlines associated with particle motions during shear. We find the expected hyperbolic motion of dislocations associated with the force quadrupole, consistent with the geometry of a single plastic event found in incompressible elastic media [114] and in the experimental dataset [111]. The learned model also predicts local non-affine deformations at the particle scale, as shown in Fig. 7B. Here, we quantify non-affine (particle) rearrangements using the quantity D_{\min}^2 [115, 111]. This quantity, computed between 2 instants, measures how much each particle and its nearest “shells” of neighbors move unlike a continuous elastic solid; it is the mean squared residual displacement after subtracting the best affine transformation [115, 111]. Measures of D_{\min}^2 are used to identify discrete, local plastic rearrangements, which are a key feature of the shear transformation zone (STZ) picture of plasticity. Figure 7C shows predictions of the mean and standard deviation trends of D_{\min}^2 (non-affine deformation) as a function of time for one full deformation cycle, while Fig. 7D shows the distribution of non-affine rearrangements at a particular phase (lag 150) in the deformation cycle. Both analyses reveal the good agreement between the experimental dataset and the model. In addition, we compare the statistics of the same dislocation metric histograms of both the reference and the predicted simulations (Fig. 13) and observe that, up to a constant factor of 20%, the model can reproduce the statistics of local non-affine rearrangements. Overall, the model is mechanistically resolving the force dipole driving displacement events but underestimating the magnitude of the interaction. Nevertheless, the model successfully captures the underlying mechanisms governing dislocation dynamics, which is a notoriously difficult task [32, 34, 36]. Importantly, though these rare events initiate through mechanisms below the coarse-graining length-scale, we obtain correct emergent statistics documented through the D_{\min}^2 field.

5 Discussion

We have presented a top-down deep learning methodology to construct physical models of conservative, dissipative, and stochastic effects which are consistent with the laws of thermodynamics and detailed fluctuation-dissipation balance. The model is supervised by time-series data for position and velocity only, with a self-supervised technique identifying emergent entropic variables that govern dissipative physics. The technique successfully captures the coarse-grained response of molecular systems using only top-down information, providing a new alternative to traditional bottom-up models which require complete characterization (e.g. via ab initio MD for particles, or other characterization of driving forces). We have further demonstrated that diverse physics may be handled by modifying the internal energy functional, allowing us to capture viscoelasticity and electrokinetic suspensions in a common framework.

The presented methodology is mostly agnostic to the architectural choice of the machine-learnable quantities. The algorithm could be improved with more sophisticated architectures such as cross-attention [116] or conditioning over parametric variables such as differing molecule types. One might also use, e.g. graph autoencoders to directly map from microstructure configuration to the emergent entropy variable rather than using self-supervised learning [117, 118]. We have chosen to demonstrate the framework with simple dense network architectures to highlight the significance of structure-preservation without relying on large datasets or transformers which may not be tractable to curate in data-sparse experimental settings.

Let \mathbf{x} be a set of a dynamical system state variables. In metriplectic dynamics, the deterministic evolution of \mathbf{x} is given by

$$d\mathbf{x} = \left[\mathbf{L} \frac{\partial E}{\partial \mathbf{x}} + \mathbf{M} \frac{\partial S}{\partial \mathbf{x}} + k_B \frac{\partial}{\partial \mathbf{x}} \cdot \mathbf{M} \right] dt + d\tilde{\mathbf{x}}. \quad (2)$$

where $E(\mathbf{x})$ and $S(\mathbf{x})$ are functionals prescribing generalized energy and entropy of the system, $\mathbf{L}(\mathbf{x}) = -\mathbf{L}^T$ is a skew-symmetric Poisson matrix and $\mathbf{M}(\mathbf{x}) = \mathbf{M}^T$ is a symmetric positive semi-definite friction matrix. These two terms prescribe the reversible and irreversible dynamics of the system, respectively. By imposing the degeneracy conditions,

$$\mathbf{L} \nabla S = \mathbf{M} \nabla E = \mathbf{0},$$

the dynamics satisfy the following discrete versions of the first and second laws of thermodynamics independent of the choice of state variables; these degeneracy conditions are challenging to impose in machine learning contexts. The stochastic effects $d\tilde{\mathbf{x}}$ are directly related to the dissipative effects via the fluctuation-dissipation theorem [21, 22]:

$$d\tilde{\mathbf{x}} d\tilde{\mathbf{x}}^T = 2k_B \mathbf{M} dt, \quad (3)$$

where k_B is the Boltzmann constant, meaning that $d\tilde{\mathbf{x}}$ is an infinitesimal of order $1/2$. Intuitively, the extra mechanical work induced by random fluctuation should be balanced with the dissipation forces to maintain thermodynamical equilibrium. We prove in Appendix B conservation properties and fluctuation-dissipation principles for dynamics of this class.

Proposition 5.1. (2) satisfies energy conservation $dE = 0$ if $\mathbf{M} \nabla E = \mathbf{0}$ and $d\tilde{\mathbf{x}} \cdot \nabla E = 0$.

Proof. See proof in Proposition B.2. \square

We next demonstrate a general construction for metriplectic dynamics as a dissipative/stochastic perturbation of an arbitrary non-canonical Hamiltonian system. While we later specialize this to particles, the technique can be applied to any discrete system (e.g. finite element simulations or circuit models). Assume that the state \mathbf{x} can be partitioned into reversible and irreversible variables $\mathbf{x} = (\mathbf{x}_{\text{rev}}, \mathbf{x}_{\text{irr}})$ such that in the absence of irreversibility

$$d\mathbf{x}_{\text{rev}} = \mathbf{L}_{\text{rev}} \frac{\partial E}{\partial \mathbf{x}_{\text{rev}}} dt,$$

or in other words, $\mathbf{L}_{\text{rev}} = -\mathbf{L}_{\text{rev}}^T$ prescribes non-canonical Hamiltonian dynamics for \mathbf{x}_{rev} . Under the further assumption

that the reversible state can be written in terms of generalized position-momentum coordinates such that $\mathbf{x}_{\text{rev}} = (\mathbf{q}, \mathbf{p})$ and $\mathbf{x} = (\mathbf{q}, \mathbf{p}, \mathbf{x}_{\text{irr}})$, we define the Poisson matrix as a block system

$$\mathbf{L} = \begin{bmatrix} \mathbf{L}_{\text{rev}} & \mathbf{0} \\ \mathbf{0} & \mathbf{0} \end{bmatrix}$$

If we assume that the entropic variable depends only on the irreversible state $S(\mathbf{x}_{\text{irr}})$ then the degeneracy condition $\mathbf{L} \nabla S = \mathbf{0}$ holds trivially. To construct noise and dissipation compatible with the other degeneracy conditions $\mathbf{M} \nabla E = \mathbf{0}$ and $d\tilde{\mathbf{x}} \cdot \nabla E = 0$, we express the noise based on the Cholesky decomposition of $\mathbf{M} = \mathbf{Q}\mathbf{Q}^T$ as $d\tilde{\mathbf{x}} = \mathbf{Q}d\mathbf{W}$. We enforce the degeneracy condition via the ansatz,

$$Q_{ji} = C_{ijk} \frac{\partial E}{\partial x_k},$$

where C_{ijk} is a sparse 3-tensor with the skew-symmetry $C_{ijk} = -C_{ikj}$. See Proposition B.4 for the detailed derivation specifying a precise functional form.

With the degeneracy conditions satisfied, we have thus arrived at a construction for a metriplectic system. We construct metriplectic ML architectures via the following ‘‘metriplectic cookbook’’:

1. Select reversible \mathbf{x}_{rev} and irreversible variables \mathbf{x}_{irr} such that $\mathbf{x} = (\mathbf{x}_{\text{rev}}, \mathbf{x}_{\text{irr}})$.
2. Develop parameterized energies and entropies, assuming functional dependencies $E(\mathbf{x}_{\text{rev}}, \mathbf{x}_{\text{irr}})$ and $S(\mathbf{x}_{\text{irr}})$.
3. Develop a parametrization of $d\tilde{\mathbf{x}}$ (and consequently \mathbf{M}) consistent with the fluctuation-dissipation theorem.
4. Use the metriplectic Eq. (2) to determine the dynamical equations.
5. Use maximum likelihood to fit the model to data, using a marginal distribution over subsets of degrees of freedom to minibatch and maintain $O(1)$ /particle complexity training.
6. Introduce a self-supervised ‘‘teacher network’’ to identify unobservable \mathbf{x}_{irr} labels during training.

5.1 Data-driven particle dynamics

Consider now a collection of N particles with positions \mathbf{r}_i and velocities $\mathbf{v}_i = \frac{d\mathbf{r}_i}{dt}$ for $i \in V = \{1, \dots, N\}$. We introduce energy and entropy functionals

$$E = \sum_i \left[\frac{1}{2} m_i \mathbf{v}_i^2 + U_i \right], \quad S = \sum_i S_i,$$

where: $m_i = m$ is a particle mass, assumed to be constant; S_i is a per particle entropy; $U_i = U(\mathcal{V}_i, S_i)$ is a function prescribing per particle internal energy; and $\mathcal{V}_i(\mathbf{r}_1, \dots, \mathbf{r}_N)$ is a per particle volume which will be prescribed as a function of neighboring particle positions. We identify this with the general framework of the previous section by selecting generalized position and momentum $(\mathbf{q}_i, \mathbf{p}_i)$ as $\mathbf{x}_{\text{rev},i} = (\mathbf{r}_i, \mathbf{v}_i)$ and selecting entropy as the irreversible variable $\mathbf{x}_{\text{irr},i} = S_i$.

Recall the first law of thermodynamics $dU = TdS - PdV$, from which we may define per particle temperature and pressure as partials of U

$$T_i = \frac{\partial U_i}{\partial S_i}, \quad P_i = -\frac{\partial U_i}{\partial \mathcal{V}_i}.$$

For these choices, the gradients of energy and entropy are given by

$$\frac{\partial E}{\partial \mathbf{x}_i} = \begin{bmatrix} \frac{\partial U}{\partial \mathbf{r}_i} \\ m_i \mathbf{v}_i \\ T_i \end{bmatrix}, \quad \frac{\partial S}{\partial \mathbf{x}_i} = \begin{bmatrix} \mathbf{0} \\ \mathbf{0} \\ 1 \end{bmatrix}.$$

Substituting these expressions into Eq. (2) we obtain per particle dynamics

$$\begin{aligned} \underbrace{\begin{bmatrix} d\mathbf{r}_i \\ d\mathbf{v}_i \\ dS_i \end{bmatrix}}_{d\mathbf{x}_i} &= \sum_j \frac{1}{m} \underbrace{\begin{bmatrix} \mathbf{0} & \mathbf{I}\delta_{ij} & \mathbf{0} \\ -\mathbf{I}\delta_{ij} & \mathbf{0} & \mathbf{0} \\ \mathbf{0} & \mathbf{0} & \mathbf{0} \end{bmatrix}}_{\mathbf{L}_{ij}} \underbrace{\begin{bmatrix} \frac{\partial U}{\partial \mathbf{r}_j} \\ m\mathbf{v}_j \\ T_j \end{bmatrix}}_{\frac{\partial E}{\partial \mathbf{x}_j}} dt \\ &+ \sum_j M_{ij} \underbrace{\begin{bmatrix} \mathbf{0} \\ \mathbf{0} \\ 1 \end{bmatrix}}_{\frac{\partial S}{\partial \mathbf{x}_j}} dt + k_B \sum_j \frac{\partial}{\partial \mathbf{x}_j} \cdot M_{ij} dt + \underbrace{\begin{bmatrix} d\tilde{\mathbf{r}}_i \\ d\tilde{\mathbf{v}}_i \\ d\tilde{S}_i \end{bmatrix}}_{d\tilde{\mathbf{x}}_i}. \end{aligned} \quad (4)$$

5.2 Machine learnable parameterizations

To close this system of equations, we will introduce small neural networks shared across all particles to define:

- Particle volume $\mathcal{V}_i(\mathbf{r}_1, \dots, \mathbf{r}_N)$.
- Per particle internal energy $U_i(\mathcal{V}_i, S_i)$
- Thermal fluctuations $d\tilde{\mathbf{x}} = \mathbf{Q}d\mathbf{W}$.

After specifying these terms, \mathbf{M} may be calculated from \mathbf{Q} , providing a closed system of equations in Eq. (4). For simplicity all neural networks are taken as shallow multilayer perceptrons, unless otherwise noted. There is substantial room for improvement to adopt more sophisticated e.g. graph attention networks or transformers. We have been able to achieve state-of-the-art results with simple architectures and so choose to present this work with minimal complexity in the ML architecture; the simple MLPs adopted here have the added benefit of being amenable to finite difference calculation of gradients at inference time, allowing a fast implementation in LAMMPS.

We stress that in contrast to traditional particle methods, the operators are not constructed to discretize a known PDE; rather, we impose algebraic symmetries which impose structure preservation to build a ‘‘model skeleton’’, and then use observational data to ‘‘flesh out the skeleton’’.

5.2.1 Volume definition

To obtain a method which scales as $O(N)$ in the number of particles, we prescribe \mathcal{V} to include only contributions from particles within a neighborhood of radius h , denoted as $\mathcal{N}_i =$

$\{j \in V, |\mathbf{r}_{ij}| < h\}$ and parameterize the volume

$$\frac{1}{\mathcal{V}_i} = \sum_{j \in \mathcal{N}_i} W_{ij} = \sum_{j \in \mathcal{N}_i} \exp \left[\text{MLP}_{\mathcal{V}} \left(\frac{|\mathbf{r}_{ij}|}{h}; \theta_{\mathcal{V}} \right) \right] \left(1 - \frac{|\mathbf{r}_{ij}|^2}{h^2} \right)_+, \quad (5)$$

where for convenience we define the inverse volume $d_i = \mathcal{V}_i^{-1}$, $\mathbf{r}_{ij} = \mathbf{r}_i - \mathbf{r}_j$ denotes the relative positions between particle i and neighboring particles $j \in \mathcal{N}_i$, and $|\cdot|$ denotes the Euclidean norm.

This amounts to a message passing/aggregation network with no attention mechanism. We require only that W be positive to ensure a positive volume for each particle. In light of Noethers theorem, we require that W be invariant under shifts in coordinate to ensure momentum conservation, which we impose by using a radial kernel. More sophisticated graph attention mechanisms, deep message passing networks, and non-radial shift invariant architectures could be incorporated without compromising structure preservation.

We note that this architecture is inspired by classical particle methods such as SPH, where particle volume is defined via a kernel density estimate, see [29, 25], and other works which assign a ‘‘virtual’’ notion of volume to particles [119, 120].

5.2.2 Convexity and monotonicity of internal energy

In classical variational mechanics, the Gibbs relations mandate that internal energy must respect certain convexity and monotonicity constraints to preserve hyperbolicity in the resulting equations. Equivalently, from a simple physical perspective, pressure and temperature must be positive, requiring $\partial_{\mathcal{V}} U \leq 0$ and $\partial_S U \geq 0$. The second derivatives define the isothermal compressibility and the specific heat at constant volume, respectively, and must also be positive, i.e. U is convex in both arguments. In this work, we employ the recently proposed Constrained Monotonic Neural Network [121]:

$$U_i = \text{CMNN}_U(S_i, \mathcal{V}_i; \theta_U). \quad (6)$$

guaranteeing by construction that the first and second arguments be monotonically decreasing and increasing, respectively. This is achieved by enforcing the weight signs, and ensure the convexity by using softplus activation functions so that no constrained optimizers need to be used to obtain a thermodynamically consistent internal energy. For more details, see the Appendix D.

5.2.3 Stochastic fluctuations

When specializing the general ansatz (Eq. (2)) to a particle setting, additional care must be taken to ensure that forces satisfy conservation of linear and angular momentum. Motivated by [30], we assume a functional form for which random forcing in $d\tilde{\mathbf{v}}$ consists only of pairwise interactions, from which the degeneracy conditions enforce as a consequence:

$$\begin{aligned}
 md\tilde{\mathbf{v}}_i &= \sqrt{2k_B} \sum_{j \in \mathcal{N}_i} \left[A_{ij} d\bar{\mathbf{W}}_{ij} + B_{ij} \frac{\mathbf{I}}{D} \text{tr}(d\mathbf{W}_{ij}) \right] \mathbf{e}_{ij}, \\
 T_i d\tilde{S}_i &= -\frac{\sqrt{2k_B}}{2} \sum_{j \in \mathcal{N}_i} \left[A_{ij} d\bar{\mathbf{W}}_{ij} + B_{ij} \frac{\mathbf{I}}{D} \text{tr}(d\mathbf{W}_{ij}) \right] : \mathbf{e}_{ij} \mathbf{v}_{ij} \\
 &\quad + \sqrt{2k_B} \sum_{j \in \mathcal{N}_i} C_{ij} dV_{ij},
 \end{aligned} \tag{7}$$

where $A_{ij} = A_{ji}$, $B_{ij} = B_{ji}$ and $C_{ij} = C_{ji}$ are ij -symmetric functions of the position and entropy of the particles, D is the dimension of the problem and $\mathbf{e}_{ij} = \mathbf{r}_{ij}/|\mathbf{r}_{ij}|$ is the interdistance unitary vector. The Wiener differentials $d\mathbf{W}_{ij} = d\mathbf{W}_{ji}$ and $dV_{ij} = -dV_{ji}$ are symmetric and skew-symmetric, respectively, with regard to particle labels i, j . Their components are independent zero mean and unit variance Gaussian increments which are uncorrelated in components and particle index except if they belong to the same interaction (more details in Appendix A).

Unlike in [30], where A , B , and C were chosen to arrive at an accurate discretization of the fluctuating Navier-Stokes equations, we instead define shallow MLPs to identify state-dependent nonlinear scalings of the fluctuations

$$\begin{aligned}
 A_{ij} &= \text{MLP}_A \left(\frac{|\mathbf{r}_{ij}|}{h}, T_i; \theta_A \right) \cdot \text{MLP}_A \left(\frac{|\mathbf{r}_{ij}|}{h}, T_j; \theta_A \right), \\
 B_{ij} &= \text{MLP}_B \left(\frac{|\mathbf{r}_{ij}|}{h}, T_i; \theta_B \right) \cdot \text{MLP}_B \left(\frac{|\mathbf{r}_{ij}|}{h}, T_j; \theta_B \right), \\
 C_{ij} &= \text{MLP}_C \left(\frac{|\mathbf{r}_{ij}|}{h}, T_i; \theta_C \right) \cdot \text{MLP}_C \left(\frac{|\mathbf{r}_{ij}|}{h}, T_j; \theta_C \right),
 \end{aligned}$$

parametrized by $\theta_A, \theta_B, \theta_C$, which ensures the symmetry over particle pair indices and the functional dependency of viscosity with temperature. Additionally, we include the Boltzmann constant k_B and the particle mass m as trainable parameters to tune the relative importance of stochastic fluctuations relative to conservative dynamics. This is optional and can be replaced with their actual value, consistent with the units of the studied problem.

5.3 Dynamic equations

With the specified parameterization and using the metriplectic equation in Eq. (4), we can finally summarize the dynamic equations of the method:

$$\begin{aligned}
 d\mathbf{r}_i &= \mathbf{v}_i dt \\
 m d\mathbf{v}_i &= -\frac{\partial U}{\partial \mathbf{r}_i} dt + \mathbf{F}_{\text{diss}}^{\mathbf{v}} + \mathbf{F}_{\text{div}}^{\mathbf{v}} + m d\tilde{\mathbf{v}}_i \\
 T_i dS_i &= F_{\text{diss}}^S + F_{\text{div}}^S + T_i d\tilde{S}_i
 \end{aligned}$$

where F_{diss} are the dissipative terms and F_{div} the divergence terms of the dynamics, balanced out by the fluctuation-dissipation theorem. The developed formulation ensures the following conservation laws:

Proposition 5.2. *The metriplectic equation in Eq. (4) satisfies momentum conservation $d\mathbf{P} = 0$.*

Proof. See proof in Proposition B.1. \square

Proposition 5.3. *The metriplectic equation in Eq. (4) satisfies energy conservation $dE = 0$.*

Proof. See proof in Proposition B.2. \square

5.4 Self-supervision of entropy

While position and velocity are easily measurable either in experimental or by post-processed synthetic data (e.g. fully resolved MD data), calculating entropy would require an enumeration of microstates which is intractable for the vast majority of cases. To fully supervise the system, we therefore need to generate time-series labels of \mathbf{x}_{irr} . This has been a challenge for several works which have aimed to machine learn metriplectic dynamics [105, 95], limiting their applicability to small degree of freedom systems. In this work we adopt a self-supervised approach which allows scalability to massive numbers of degrees of freedom.

To generate labels for S_i , we introduce an auxiliary edge convolutional operator [122] which constructs a closure for the entropy in terms of position and velocity

$$S_i = \frac{1}{|\mathcal{N}_i|} \sum_{j \in \mathcal{N}_i} \text{MLP}_S \left(\frac{|\mathbf{r}_{ij}|}{h}, \mathbf{v}_{ij}; \theta_S \right).$$

In principle, this architecture could incorporate position-velocity information from a finite time history. For simplicity however, we present results using only information from the current timestep. In light of the fluctuation-dissipation theorem, we conjecture that knowledge of the energy dissipated (present in the position and velocity fields) is sufficient to identify the magnitude of the corresponding entropy increment.

We highlight that this architecture is *not* a closure in the dynamics—at the conclusion of training M is prescribed, the self-supervision network is discarded, and at inference time entropy is instead evolved by solution of Equation 2.

5.5 Training via log-likelihood

Let $\mathcal{D} = \{(\mathbf{x}_{\text{rev}}^t, \mathbf{x}_{\text{rev}}^{t+1})\}_{t=0}^{N_{\text{train}}}$ be a dataset consisting of position-velocity pairs. To train the system, we construct a joint probability distribution $p(\mathbf{x}_{\text{rev}}^{t+1}, \mathbf{x}_{\text{irr}}^{t+1} | \mathbf{x}_{\text{rev}}^t, \mathbf{x}_{\text{irr}}^t)$ corresponding to a numerical integration of Equation 2 and train the architectures with maximum likelihood. We denote all trainable parameters via

$$\Theta = \{\theta_V, \theta_U, \theta_A, \theta_B, \theta_C, \theta_S, k_B, m\}$$

and define the maximum log-likelihood objective

$$\Theta^* = \arg \min_{\Theta} \text{NLL}(x^1, \dots, x^T).$$

Through a marginalization procedure detailed in Appendix C, we can split the problem as per particle-wise loss corresponding to the multivariate Gaussian distribution:

$$\begin{aligned}
 \boldsymbol{\mu}^{t+1} &= \begin{bmatrix} \mathbf{v}_i^t + \frac{d\mathbf{v}_i^t}{dt} \Delta t \\ S_i^t + \frac{dS_i^t}{dt} \Delta t \end{bmatrix}, \\
 \boldsymbol{\Sigma}_{ii}^{t+1} &= \begin{bmatrix} \Delta \tilde{\mathbf{v}}_i \Delta \tilde{\mathbf{v}}_i^T & \Delta \tilde{\mathbf{v}}_i \Delta \tilde{S}_i^T \\ \Delta \tilde{S}_i \Delta \tilde{\mathbf{v}}_i^T & \Delta \tilde{S}_i \Delta \tilde{S}_i^T \end{bmatrix}.
 \end{aligned}$$

Thus the final loss function is defined as

$$\mathcal{L} = \frac{1}{N_{\text{train}}} \sum_{t=0}^{N_{\text{train}}} \frac{1}{N} \sum_{i=0}^N \left[\frac{1}{2} \ln |\Sigma_{ii}^{t+1}| + \frac{1}{2} (\mathbf{x}_i^{t+1} - \boldsymbol{\mu}_i^{t+1})^T (\Sigma_{ii}^{t+1})^{-1} (\mathbf{x}_i^{t+1} - \boldsymbol{\mu}_i^{t+1}) \right],$$

which can be minimized using standard batch gradient descent.

5.6 Test metrics

The benchmark algorithms are trained in fair conditions using the same training procedure and integrator as the presented method (see Appendix F for more details). All methods are tested over long rollouts of temporal length 25 times the training set to ensure steady-state statistics are achieved. Three metrics are considered: velocity autocorrelation function, radial distribution function and mean squared displacement, defined as the following ensemble averages:

$$\begin{aligned} \text{VACF}(t) &= \langle \mathbf{v}(\tau) \cdot \mathbf{v}(\tau + t) \rangle, \\ \text{RDF}(r) &= \frac{\langle \rho(r) \rangle}{\rho}, \\ \text{MSD}(t) &= \langle |\mathbf{r}(\tau) - \mathbf{r}(\tau + t)|^2 \rangle, \end{aligned}$$

where $\rho(r)$ is the local number density of particles at distance r and τ is a dummy variable representing the initial reference time over which ensemble averages are computed. Reproducing all three correlation metrics is necessary to correctly capture the dynamic behavior of the molecular dynamic system [123]:

- VACF: This metric evaluates how the velocity of a particle at one time is correlated with its velocity at a later time, and provides insight into the momentum relaxation of the system. The integral of the function is the self-diffusion coefficient of the system.
- RDF: This metric measures how the particle density varies as a function of distance from a reference particle. It is related to the structural organization and relative arrangements of particles, and is strongly determined by the conservative forces of the system.
- MSD: This metric quantifies the average squared distance that particles travel over time. It is used to characterize the diffusive behavior of particles and distinguish between different transport regimes. It is related to the VACF via the Green-Kubo relations [124, 125].

The VACF, RDF, and MSD curves are compared with the ground truth statistics through the point-wise L2 relative error:

$$\varepsilon_{\mathbf{y}} = \frac{|\mathbf{y}_{\text{GT}} - \mathbf{y}_{\text{pred}}|}{|\mathbf{y}_{\text{GT}}|}.$$

The code was implemented using Pytorch Geometric [126], and is publicly available online at <https://github.com/PIMILab>. All the experiments were performed using Adam optimizer [127] and run on a single NVIDIA H200 GPU. The dataset generation and hyperparameter details can be found in Appendix G.

5.7 Extension to new physics

To extend the method to viscoelastic, we first need to recall the law of thermodynamics for deformed bodies [128] as $dU = TdS + \boldsymbol{\sigma} : d\boldsymbol{\varepsilon}$. By applying a volumetric and deviatoric decomposition of the stress tensor $\sigma^{\alpha\beta} = -P\delta^{\alpha\beta} + \tau^{\alpha\beta}$, we obtain $dU = TdS - Pd\mathcal{V} + \boldsymbol{\tau} : d\bar{\boldsymbol{\varepsilon}}$ where \mathcal{V} is the volume and $\boldsymbol{\tau}$ and $\bar{\boldsymbol{\varepsilon}}$ are the traceless stress and strain tensors. This is the same as the previous equation of state in Eq. (6) with an additional shear elastic energy component. Now we may define per particle temperature, pressure and deviatoric stress as partials of U

$$T_i = \frac{\partial U_i}{\partial S_i}, \quad P_i = -\frac{\partial U_i}{\partial \mathcal{V}_i}, \quad \boldsymbol{\tau}_i = \frac{\partial U_i}{\partial \bar{\boldsymbol{\varepsilon}}_i}.$$

To model the traceless strain tensor, we propose a similar parametrization to Eq. (5) but enforce symmetries via

$$\begin{aligned} \boldsymbol{\varepsilon}_i &= \sum_{j \in \mathcal{N}_i} \mathbf{W}_{ij} = \sum_{j \in \mathcal{N}_i} \frac{1}{2} (\mathbf{l}_{ij} + \mathbf{l}_{ij}^T), \\ \mathbf{l}_{ij} &= \text{MLP}_{\boldsymbol{\varepsilon}} \left(\frac{\mathbf{u}_{ij}}{h}, \frac{\mathbf{r}_{ij}^0}{h}; \theta_{\boldsymbol{\varepsilon}} \right) - \text{MLP}_{\boldsymbol{\varepsilon}} \left(\mathbf{0}, \frac{\mathbf{r}_{ij}^0}{h}; \theta_{\boldsymbol{\varepsilon}} \right), \end{aligned}$$

where \mathbf{l}_{ij} is a lower triangular matrix whose entries are computed using a multilayer perceptron parametrized by $\theta_{\boldsymbol{\varepsilon}}$, $\mathbf{r}_{ij}^0 = \mathbf{r}_i^0 - \mathbf{r}_j^0$ is the undeformed configuration relative positions and $\mathbf{u}_{ij} = \mathbf{r}_{ij} - \mathbf{r}_{ij}^0$ is the displacement with respect to the reference configuration. This parametrization ensures zero strain under zero displacements and is also invariant under coordinate transformations. Finally, we subtract the trace to obtain a traceless strain tensor which will give rise to shear stresses,

$$\bar{\boldsymbol{\varepsilon}}_i = \boldsymbol{\varepsilon}_i - \frac{\mathbf{I}}{D} \text{tr}(\boldsymbol{\varepsilon}_i) = \sum_{j \in \mathcal{N}_i} \bar{\mathbf{W}}_{ij},$$

where D is the dimension of the problem. This formulation is inspired in large strain elasticity, but many other options could be considered based on classic SPH deformation gradient tensor or equivariant architectures. In regard to the internal energy model, we assume additive internal energies with similar monotonicity and convexity constraints as in the fluid model case (convex in the strain argument, as its second derivative represent the elasticity tensor):

$$\begin{aligned} U_i &= U_i^{\text{vol}} + U_i^{\text{dev}} = \text{CMNN}_{U^{\text{vol}}}(S_i, \mathcal{V}_i; \theta_{U^{\text{vol}}}) \\ &\quad + \text{CMNN}_{U^{\text{dev}}}(S_i, I(\bar{\boldsymbol{\varepsilon}}_i); \theta_{U^{\text{dev}}}), \end{aligned}$$

where $I(\bar{\boldsymbol{\varepsilon}}_i)$ are the $D - 1$ non-zero invariants of the traceless strain tensor. The additional terms in the conservative dynamics equation can be found in the Appendix A.1.

The results are evaluated with L2 relative error in position and RDF function to evaluate the structural fidelity of the predictions. As for the dynamics, we use the non-affine displacement (D_{min}^2) which evaluates how much the local neighbourhood of a particle deviates from an affine transformation between two time snapshots.

$$D_{\text{min}}^2(t_1, t_2) = \min_{\mathbf{J}} \langle |\mathbf{u}_i(t_1) - \mathbf{J}\mathbf{u}_j(t_2)|^2 \rangle,$$

where \mathbf{J} is the best least squares fit local deformation gradient.

Acknowledgements

We thank Pep Español and George Karniadakis for their insightful feedback and valuable discussions throughout the development of this work. We also acknowledge Joel T. Clemmer for his assistance with the LAMMPS code implementation and Aleksandra Vojvodic for the computational resources. The authors acknowledge support from the Department of Energy under the MMICCs program and the Department of Defense under the "Complexity, Nonlocality, and Uncertainty in Heterogeneous Solids" MURI program.

References

- [1] Jin Soo Lim, Diomedes Saldana-Greco, and Andrew M Rappe. Improper magnetic ferroelectricity of nearly pure electronic nature in helicoidal spiral camn 7 o 12. *Physical Review B*, 97(4):045115, 2018.
- [2] Thomas C O'Connor, Ting Ge, Michael Rubinstein, and Gary S Grest. Topological linking drives anomalous thickening of ring polymers in weak extensional flows. *Physical review letters*, 124(2):027801, 2020.
- [3] Douglas J Jerolmack and Karen E Daniels. Viewing earth's surface as a soft-matter landscape. *Nature Reviews Physics*, 1(12):716–730, 2019.
- [4] Robert Kostynick, Hadis Matinpour, Shravan Pradeep, Sarah Haber, Alban Sauret, Eckart Meiburg, Thomas Dunne, Paulo Arratia, and Douglas Jerolmack. Rheology of debris flow materials is controlled by the distance from jamming. *Proceedings of the National Academy of Sciences*, 119(44):e2209109119, 2022.
- [5] Robert D Groot and Patrick B Warren. Dissipative particle dynamics: Bridging the gap between atomistic and mesoscopic simulation. *The Journal of chemical physics*, 107(11):4423–4435, 1997.
- [6] Jhih-Wei Chu, Gary S Ayton, Vinod Krishna, Sergei Izvekov, Gregory A Voth, Avisek Das, and Hans C Andersen. The multiscale coarse-graining method. i. a rigorous bridge between atomistic and coarse-grained models. *The Journal of chemical physics*, 128(24), 2008.
- [7] Sergei Izvekov and Gregory A Voth. A multiscale coarse-graining method for biomolecular systems. *The Journal of Physical Chemistry B*, 109(7):2469–2473, 2005.
- [8] Jörg Behler and Michele Parrinello. Generalized neural-network representation of high-dimensional potential-energy surfaces. *Physical review letters*, 98(14):146401, 2007.
- [9] Joseph Smagorinsky. General circulation experiments with the primitive equations: I. the basic experiment. *Monthly weather review*, 91(3):99–164, 1963.
- [10] Massimo Germano, Ugo Piomelli, Parviz Moin, and William H Cabot. A dynamic subgrid-scale eddy viscosity model. *Physics of fluids a: Fluid dynamics*, 3(7):1760–1765, 1991.
- [11] Eric J. Parish and Karthik Duraisamy. A dynamic subgrid-scale model for large eddy simulations based on the mori–zwanzig formalism. *Journal of Computational Physics*, 349:154–175, 2017.
- [12] Zhen Li, Xin Bian, Bruce Caswell, and George Em Karniadakis. Construction of dissipative particle dynamics models for complex fluids via the mori–zwanzig formulation. *Soft matter*, 10(43):8659–8672, 2014.
- [13] Julia Ling, Andrew Kurzawski, and Jeremy Templeton. Reynolds averaged turbulence modelling using deep neural networks with embedded invariance. *Journal of Fluid Mechanics*, 807:155–166, 2016.
- [14] Karthik Duraisamy. Perspectives on machine learning-augmented reynolds-averaged and large eddy simulation models of turbulence. *Physical Review Fluids*, 6(5):050504, 2021.
- [15] Dmitrii Kochkov, Jamie A Smith, Ayya Alieva, Qing Wang, Michael P Brenner, and Stephan Hoyer. Machine learning-accelerated computational fluid dynamics. *Proceedings of the National Academy of Sciences*, 118(21):e2101784118, 2021.
- [16] Jaehyeok Jin, Alexander J Pak, Aleksander EP Durrneric, Timothy D Loose, and Gregory A Voth. Bottom-up coarse-graining: Principles and perspectives. *Journal of chemical theory and computation*, 18(10):5759–5791, 2022.
- [17] Robert Zwanzig. Ensemble method in the theory of irreversibility. *The Journal of Chemical Physics*, 33(5):1338–1341, 1960.
- [18] Hazime Mori. Transport, collective motion, and brownian motion. *Progress of theoretical physics*, 33(3):423–455, 1965.
- [19] Hermann Grabert. *Projection operator techniques in nonequilibrium statistical mechanics*, volume 95. Springer, 2006.
- [20] Robert Zwanzig. *Nonequilibrium statistical mechanics*. Oxford university press, 2001.
- [21] Herbert B Callen and Theodore A Welton. Irreversibility and generalized noise. *Physical Review*, 83(1):34, 1951.
- [22] Rep Kubo. The fluctuation-dissipation theorem. *Reports on progress in physics*, 29(1):255, 1966.
- [23] Alexandre J Chorin, Ole H Hald, and Raz Kupferman. Optimal prediction and the mori–zwanzig representation of irreversible processes. *Proceedings of the National Academy of Sciences*, 97(7):2968–2973, 2000.
- [24] Philip J Morrison. Bracket formulation for irreversible classical fields. *Physics Letters A*, 100(8):423–427, 1984.
- [25] Joseph P Morris, Patrick J Fox, and Yi Zhu. Modeling low reynolds number incompressible flows using sph. *Journal of computational physics*, 136(1):214–226, 1997.

- [26] Miroslav Grmela and Hans Christian Öttinger. Dynamics and thermodynamics of complex fluids. i. development of a general formalism. *Physical Review E*, 56(6):6620, 1997.
- [27] Hans Christian Öttinger and Miroslav Grmela. Dynamics and thermodynamics of complex fluids. ii. illustrations of a general formalism. *Physical Review E*, 56(6):6633, 1997.
- [28] Philip J Morrison and Michael H Updike. Inclusive curvaturelike framework for describing dissipation: Metriplectic 4-bracket dynamics. *Physical Review E*, 109(4):045202, 2024.
- [29] Joe J Monaghan. Smoothed particle hydrodynamics. In: *Annual review of astronomy and astrophysics. Vol. 30 (A93-25826 09-90)*, p. 543-574., 30:543–574, 1992.
- [30] Pep Espanol and Mariano Revenga. Smoothed dissipative particle dynamics. *Physical Review E*, 67(2):026705, 2003.
- [31] KL Galloway, EG Teich, XG Ma, Ch Kammer, IR Graham, NC Keim, C Reina, DJ Jerolmack, AG Yodh, and PE Arratia. Relationships between structure, memory and flow in sheared disordered materials. *Nature Physics*, 18(5):565–570, 2022.
- [32] K Lawrence Galloway, Xiaoguang Ma, Nathan C Keim, Douglas J Jerolmack, Arjun G Yodh, and Paulo E Arratia. Scaling of relaxation and excess entropy in plastically deformed amorphous solids. *Proceedings of the National Academy of Sciences*, 117(22):11887–11893, 2020.
- [33] Patrick Charbonneau, Jorge Kurchan, Giorgio Parisi, Pierfrancesco Urbani, and Francesco Zamponi. Glass and jamming transitions: From exact results to finite-dimensional descriptions. *Annual Review of Condensed Matter Physics*, 8(1):265–288, 2017.
- [34] M Lisa Manning and Andrea J Liu. Vibrational modes identify soft spots in a sheared disordered packing. *Physical Review Letters*, 107(10):108302, 2011.
- [35] Ekin D Cubuk, Samuel Stern Schoenholz, Jennifer M Rieser, Brad Dean Malone, Joerg Rottler, Douglas J Durian, Efthimios Kaxiras, and Andrea J Liu. Identifying structural flow defects in disordered solids using machine-learning methods. *Physical review letters*, 114(10):108001, 2015.
- [36] David Richard, Misaki Ozawa, Sylvain Patinet, Ethan Stanifer, B Shang, Sean A Ridout, Bin Xu, Ge Zhang, PK Morse, J-L Barrat, et al. Predicting plasticity in disordered solids from structural indicators. *Physical Review Materials*, 4(11):113609, 2020.
- [37] Hans Christian Öttinger. General projection operator formalism for the dynamics and thermodynamics of complex fluids. *Physical Review E*, 57(2):1416, 1998.
- [38] Victor Yakhot and Leslie M. Smith. The renormalization group, the epsilon expansion, and derivation of turbulence models. *Journal of Scientific Computing*, 7:35–61, 1992.
- [39] M Scott Shell. Coarse-graining with the relative entropy. *Advances in chemical physics*, 161:395–441, 2016.
- [40] Sikandar Yusufoddin Mashayak, Mara N Jochum, Konstantin Koschke, Narayana R Aluru, Victor Rühle, and Christoph Junghans. Relative entropy and optimization-driven coarse-graining methods in votca. *PLoS one*, 10(7):e0131754, 2015.
- [41] Aviel Chaimovich and M Scott Shell. Coarse-graining errors and numerical optimization using a relative entropy framework. *The Journal of chemical physics*, 134(9), 2011.
- [42] Massimiliano Esposito. Stochastic thermodynamics under coarse graining. *Physical Review E - Statistical, Nonlinear, and Soft Matter Physics*, 85(4):041125, 2012.
- [43] Thomas J. R. Hughes, Gilberto R. Feijóo, Luca Mazzei, and Jean-Baptiste Quinicy. The variational multiscale method—a paradigm for computational mechanics. *Computer Methods in Applied Mechanics and Engineering*, 166(1–2):3–24, 1998.
- [44] Thomas J. R. Hughes, Guglielmo Scovazzi, and Leopoldo P. Franca. Multiscale and stabilized methods. In *Encyclopedia of Computational Mechanics*. Wiley, 2004.
- [45] Victor Yakhot and Steven A. Orszag. Renormalization group analysis of turbulence. i. basic theory. *Physical Review Letters*, 57(14):1722–1725, 1986.
- [46] Leslie M. Smith and Stephen L. Woodruff. Renormalization-group analysis of turbulence. *Annual Review of Fluid Mechanics*, 30:275–310, 1998.
- [47] Eric J. Parish and Karthik Duraisamy. Non-markovian closure models for large eddy simulations using the mori–zwanzig formalism. *Physical Review Fluids*, 2:014604, 2017.
- [48] Panagiotis Stinis. Higher order mori–zwanzig models for the euler equations. *Multiscale Modeling & Simulation*, 6(3):741–760, 2007.
- [49] Volker John and Songul Kaya. A finite element variational multiscale method for the navier–stokes equations. *SIAM Journal on Scientific Computing*, 26(5):1485–1503, 2005.
- [50] Thomas JR Hughes and Assad A Oberai. The variational multiscale formulation of les with application to turbulent channel flows. In *Geometry, mechanics, and dynamics*, pages 223–239. Springer, 2002.
- [51] Aniruddhe Pradhan and Karthik Duraisamy. Variational multiscale closures for finite element discretizations using the mori–zwanzig approach. *Computer Methods in Applied Mechanics and Engineering*, 368:113152, 2020.
- [52] Tanja Schilling. Coarse-grained modelling out of equilibrium. *Physics Reports*, 972:1–45, 2022.

- [53] Zhen Li, Xin Bian, Xiantao Li, and George Em Karniadakis. Incorporation of memory effects in coarse-grained modeling via the mori-zwanzig formalism. *The Journal of chemical physics*, 143(24), 2015.
- [54] Sergei Izvekov. Mori-zwanzig projection operator formalism: Particle-based coarse-grained dynamics of open classical systems far from equilibrium. *Physical Review E*, 104(2):024121, 2021.
- [55] James F Dama, Anton V Sinitskiy, Martin McCullagh, Jonathan Weare, Benoît Roux, Aaron R Dinner, and Gregory A Voth. The theory of ultra-coarse-graining. 1. general principles. *Journal of chemical theory and computation*, 9(5):2466–2480, 2013.
- [56] Furio Ercolessi and James B Adams. Interatomic potentials from first-principles calculations: the force-matching method. *Europhysics Letters*, 26(8):583, 1994.
- [57] Ralf Drautz. Atomic cluster expansion for accurate and transferable interatomic potentials. *Physical Review B*, 99(1):014104, 2019.
- [58] Albert P Bartók, Mike C Payne, Risi Kondor, and Gábor Csányi. Gaussian approximation potentials: The accuracy of quantum mechanics, without the electrons. *Physical review letters*, 104(13):136403, 2010.
- [59] Justin Gilmer, Samuel S Schoenholz, Patrick F Riley, Oriol Vinyals, and George E Dahl. Neural message passing for quantum chemistry. In *International conference on machine learning*, pages 1263–1272. PMLR, 2017.
- [60] Anuroop Sriram, Abhishek Das, Brandon M Wood, Siddharth Goyal, and C Lawrence Zitnick. Towards training billion parameter graph neural networks for atomic simulations. *arXiv preprint arXiv:2203.09697*, 2022.
- [61] Linfeng Zhang, Jiequn Han, Han Wang, Roberto Car, and Weinan E. Deep potential molecular dynamics: a scalable model with the accuracy of quantum mechanics. *Physical review letters*, 120(14):143001, 2018.
- [62] Nathaniel Thomas, Tess Smidt, Steven Kearnes, Lusann Yang, Li Li, Kai Kohlhoff, and Patrick Riley. Tensor field networks: Rotation-and translation-equivariant neural networks for 3d point clouds. *arXiv preprint arXiv:1802.08219*, 2018.
- [63] Maurice Weiler, Mario Geiger, Max Welling, Wouter Boomsma, and Taco S Cohen. 3d steerable cnns: Learning rotationally equivariant features in volumetric data. *Advances in Neural information processing systems*, 31, 2018.
- [64] Risi Kondor, Zhen Lin, and Shubhendu Trivedi. Clebsch–gordan nets: a fully fourier space spherical convolutional neural network. *Advances in Neural Information Processing Systems*, 31, 2018.
- [65] Johannes Brandstetter, Rob Hesselink, Elise van der Pol, Erik J Bekkers, and Max Welling. Geometric and physical quantities improve e (3) equivariant message passing. *arXiv preprint arXiv:2110.02905*, 2021.
- [66] Kristof Schütt, Pieter-Jan Kindermans, Huziel Enoc Saucedo Felix, Stefan Chmiela, Alexandre Tkatchenko, and Klaus-Robert Müller. Schnet: A continuous-filter convolutional neural network for modeling quantum interactions. *Advances in neural information processing systems*, 30, 2017.
- [67] Johannes Gasteiger, Janek Groß, and Stephan Günnemann. Directional message passing for molecular graphs. *arXiv preprint arXiv:2003.03123*, 2020.
- [68] Yi Liu, Limei Wang, Meng Liu, Yuchao Lin, Xuan Zhang, Bora Oztekin, and Shuiwang Ji. Spherical message passing for 3d molecular graphs. In *International Conference on Learning Representations (ICLR)*, 2022.
- [69] Steven L Brunton, Marko Budišić, Eurika Kaiser, and J Nathan Kutz. Modern koopman theory for dynamical systems. *arXiv preprint arXiv:2102.12086*, 2021.
- [70] Wujie Wang and Rafael Gómez-Bombarelli. Coarse-graining auto-encoders for molecular dynamics. *npj Computational Materials*, 5(1):125, 2019.
- [71] Wujie Wang and Rafael Gómez-Bombarelli. Learning coarse-grained particle latent space with auto-encoders. *Adv. Neural Inf. Process. Syst.*, 1, 2019.
- [72] Agnieszka Ilnicka and Gisbert Schneider. Designing molecules with autoencoder networks. *Nature Computational Science*, 3(11):922–933, 2023.
- [73] Xiang Fu, Zhenghao Wu, Wujie Wang, Tian Xie, Sinan Ketan, Rafael Gomez-Bombarelli, and Tommi Jaakkola. Forces are not enough: Benchmark and critical evaluation for machine learning force fields with molecular simulations. *Transactions on Machine Learning Research*, 2023. Survey Certification.
- [74] Tianyi Li, Luca Biferale, Fabio Bonaccorso, Martino Andrea Scarpolini, and Michele Buzzicotti. Synthetic lagrangian turbulence by generative diffusion models. *Nature Machine Intelligence*, 6(4):393–403, 2024.
- [75] Pan Du, Meet Hemant Parikh, Xiantao Fan, Xin-Yang Liu, and Jian-Xun Wang. Conditional neural field latent diffusion model for generating spatiotemporal turbulence. *Nature Communications*, 15(1):10416, 2024.
- [76] M Sardar, A Skillen, MJ Zimón, S Draycott, and A Revell. Spectrally decomposed denoising diffusion probabilistic models for generative turbulence super-resolution. *Physics of Fluids*, 36(11), 2024.
- [77] Niklas Gebauer, Michael Gastegger, and Kristof Schütt. Symmetry-adapted generation of 3d point sets for the targeted discovery of molecules. *Advances in neural information processing systems*, 32, 2019.
- [78] Frank Noé, Simon Olsson, Jonas Köhler, and Hao Wu. Boltzmann generators: Sampling equilibrium states of many-body systems with deep learning. *Science*, 365(6457):eaaw1147, 2019.
- [79] Minkai Xu, Lantao Yu, Yang Song, Chence Shi, Stefano Ermon, and Jian Tang. Geodiff: A geometric diffusion

- model for molecular conformation generation. *arXiv preprint arXiv:2203.02923*, 2022.
- [80] Isaac E Lagaris, Aristidis Likas, and Dimitrios I Fotiadis. Artificial neural networks for solving ordinary and partial differential equations. *IEEE transactions on neural networks*, 9(5):987–1000, 1998.
- [81] George Em Karniadakis, Ioannis G Kevrekidis, Lu Lu, Paris Perdikaris, Sifan Wang, and Liu Yang. Physics-informed machine learning. *Nature Reviews Physics*, 3(6):422–440, 2021.
- [82] Benjamin Sanderse, Panos Stinis, Romit Maulik, and Shady E Ahmed. Scientific machine learning for closure models in multiscale problems: A review. *arXiv preprint arXiv:2403.02913*, 2024.
- [83] Sifan Wang, Yujun Teng, and Paris Perdikaris. Understanding and mitigating gradient flow pathologies in physics-informed neural networks. *SIAM Journal on Scientific Computing*, 43(5):A3055–A3081, 2021.
- [84] Sifan Wang, Shyam Sankaran, Hanwen Wang, and Paris Perdikaris. An expert’s guide to training physics-informed neural networks. *arXiv preprint arXiv:2308.08468*, 2023.
- [85] Yi-Lun Liao and Tess Smidt. Equiformer: Equivariant graph attention transformer for 3d atomistic graphs. *arXiv preprint arXiv:2206.11990*, 2022.
- [86] Yi-Lun Liao, Brandon Wood, Abhishek Das, and Tess Smidt. Equiformerv2: Improved equivariant transformer for scaling to higher-degree representations. *arXiv preprint arXiv:2306.12059*, 2023.
- [87] Leon Klein, Andreas Krämer, and Frank Noé. Equivariant flow matching. *Advances in Neural Information Processing Systems*, 36:59886–59910, 2023.
- [88] Saro Passaro and C Lawrence Zitnick. Reducing so (3) convolutions to so (2) for efficient equivariant gnns. In *International conference on machine learning*, pages 27420–27438. PMLR, 2023.
- [89] Yusong Wang, Tong Wang, Shaoning Li, Xinheng He, Mingyu Li, Zun Wang, Nanning Zheng, Bin Shao, and Tie-Yan Liu. Enhancing geometric representations for molecules with equivariant vector-scalar interactive message passing. *Nature Communications*, 15(1):313, 2024.
- [90] Clement Vignac, Nagham Osman, Laura Toni, and Pascal Frossard. Midi: Mixed graph and 3d denoising diffusion for molecule generation. In *Joint European Conference on Machine Learning and Knowledge Discovery in Databases*, pages 560–576. Springer, 2023.
- [91] Samuel Greydanus, Misko Dzamba, and Jason Yosinski. Hamiltonian neural networks. *Advances in neural information processing systems*, 32, 2019.
- [92] Marco David and Florian Méhats. Symplectic learning for hamiltonian neural networks. *Journal of Computational Physics*, 494:112495, 2023.
- [93] Zhengdao Chen, Jianyu Zhang, Martin Arjovsky, and Léon Bottou. Symplectic recurrent neural networks. *arXiv preprint arXiv:1909.13334*, 2019.
- [94] Miles Cranmer, Sam Greydanus, Stephan Hoyer, Peter Battaglia, David Spergel, and Shirley Ho. Lagrangian neural networks. *arXiv preprint arXiv:2003.04630*, 2020.
- [95] Quercus Hernández, Alberto Badías, David González, Francisco Chinesta, and Elías Cueto. Structure-preserving neural networks. *Journal of Computational Physics*, 426:109950, 2021.
- [96] Quercus Hernández, Alberto Badías, Francisco Chinesta, and Elías Cueto. Thermodynamics-informed graph neural networks. *IEEE Transactions on Artificial Intelligence*, 5(3):967–976, 2022.
- [97] Yaofeng Desmond Zhong, Biswadip Dey, and Amit Chakraborty. Dissipative symoden: Encoding hamiltonian dynamics with dissipation and control into deep learning. *arXiv preprint arXiv:2002.08860*, 2020.
- [98] Andrew Sosanya and Sam Greydanus. Dissipative hamiltonian neural networks: Learning dissipative and conservative dynamics separately. *arXiv preprint arXiv:2201.10085*, 2022.
- [99] Shanshan Xiao, Jiawei Zhang, and Yifa Tang. Generalized lagrangian neural networks. *arXiv preprint arXiv:2401.03728*, 2024.
- [100] Shenglin Huang, Zequn He, and Celia Reina. Variational onsager neural networks (vonns): A thermodynamics-based variational learning strategy for non-equilibrium pdes. *Journal of the Mechanics and Physics of Solids*, 163:104856, 2022.
- [101] Haijun Yu, Xinyuan Tian, Weinan E, and Qianxiao Li. Onsagernet: Learning stable and interpretable dynamics using a generalized onsager principle. *Physical Review Fluids*, 6(11):114402, 2021.
- [102] Shaan A Desai, Marios Mattheakis, David Sondak, Pavlos Protopapas, and Stephen J Roberts. Port-hamiltonian neural networks for learning explicit time-dependent dynamical systems. *Physical Review E*, 104(3):034312, 2021.
- [103] Kookjin Lee, Nathaniel Trask, and Panos Stinis. Machine learning structure preserving brackets for forecasting irreversible processes. *Advances in Neural Information Processing Systems*, 34:5696–5707, 2021.
- [104] Zhen Zhang, Yeonjong Shin, and George Em Karniadakis. Gfinns: Generic formalism informed neural networks for deterministic and stochastic dynamical systems. *Philosophical Transactions of the Royal Society A*, 380(2229):20210207, 2022.
- [105] Anthony Gruber, Kookjin Lee, and Nathaniel Trask. Reversible and irreversible bracket-based dynamics for deep graph neural networks. *Advances in Neural Information Processing Systems*, 36:38454–38484, 2023.

- [106] Steve Plimpton. Fast parallel algorithms for short-range molecular dynamics. *Journal of computational physics*, 117(1):1–19, 1995.
- [107] Alvaro Sanchez-Gonzalez, Jonathan Godwin, Tobias Pfaff, Rex Ying, Jure Leskovec, and Peter Battaglia. Learning to simulate complex physics with graph networks. In *International conference on machine learning*, pages 8459–8468. PMLR, 2020.
- [108] Naura Dridi, Lucas Drumetz, and Ronan Fablet. Learning stochastic dynamical systems with neural networks mimicking the euler-maruyama scheme. In *2021 29th European Signal Processing Conference (EUSIPCO)*, pages 1990–1994. IEEE, 2021.
- [109] Geoffrey Ingram Taylor and Albert Edward Green. Mechanism of the production of small eddies from large ones. *Proceedings of the Royal Society of London. Series A-Mathematical and Physical Sciences*, 158(895):499–521, 1937.
- [110] Arthur W Lees and Samuel F Edwards. The computer study of transport processes under extreme conditions. *Journal of Physics C: Solid State Physics*, 5(15):1921, 1972.
- [111] Nathan C Keim and Paulo E Arratia. Mechanical and microscopic properties of the reversible plastic regime in a 2d jammed material. *Physical review letters*, 112(2):028302, 2014.
- [112] Nathan C Keim and Paulo E Arratia. Yielding and microstructure in a 2d jammed material under shear deformation. *Soft Matter*, 9(27):6222–6225, 2013.
- [113] Carlton F Brooks, Gerald G Fuller, Curtis W Frank, and Channing R Robertson. An interfacial stress rheometer to study rheological transitions in monolayers at the air-water interface. *Langmuir*, 15(7):2450–2459, 1999.
- [114] Guillemette Picard, Armand Ajdari, François Lequeux, and Lydéric Bocquet. Elastic consequences of a single plastic event: A step towards the microscopic modeling of the flow of yield stress fluids. *The European Physical Journal E*, 15(4):371–381, 2004.
- [115] M.L. Falk and J.S. Langer. Dynamics of viscoplastic deformation in amorphous solids. *Phys. Rev. E*, 57(6):7192–7205, 1998.
- [116] A Waswani, N Shazeer, N Parmar, J Uszkoreit, L Jones, A Gomez, L Kaiser, and I Polosukhin. Attention is all you need. In *NIPS*, 2017.
- [117] Junhyun Lee, Inyeop Lee, and Jaewoo Kang. Self-attention graph pooling. In *International conference on machine learning*, pages 3734–3743. pmlr, 2019.
- [118] Zhen Zhang, Jiajun Bu, Martin Ester, Jianfeng Zhang, Chengwei Yao, Zhi Yu, and Can Wang. Hierarchical graph pooling with structure learning. *arXiv preprint arXiv:1911.05954*, 2019.
- [119] Edmond Kwan-yu Chiu, Qiqi Wang, Rui Hu, and Antony Jameson. A conservative mesh-free scheme and generalized framework for conservation laws. *SIAM Journal on Scientific Computing*, 34(6):A2896–A2916, 2012.
- [120] Nathaniel Trask, Pavel Bochev, and Mauro Perego. A conservative, consistent, and scalable meshfree mimetic method. *Journal of Computational Physics*, 409:109187, 2020.
- [121] Davor Runje and Sharath M Shankaranarayana. Constrained monotonic neural networks. In *International Conference on Machine Learning*, pages 29338–29353. PMLR, 2023.
- [122] Yue Wang, Yongbin Sun, Ziwei Liu, Sanjay E Sarma, Michael M Bronstein, and Justin M Solomon. Dynamic graph cnn for learning on point clouds. *ACM Transactions on Graphics (tog)*, 38(5):1–12, 2019.
- [123] David Chandler and Jerome K Percus. Introduction to modern statistical mechanics, 1988.
- [124] Melville S Green. Markoff random processes and the statistical mechanics of time-dependent phenomena. ii. irreversible processes in fluids. *The Journal of chemical physics*, 22(3):398–413, 1954.
- [125] Ryogo Kubo. Statistical-mechanical theory of irreversible processes. i. general theory and simple applications to magnetic and conduction problems. *Journal of the physical society of Japan*, 12(6):570–586, 1957.
- [126] Matthias Fey and Jan Eric Lenssen. Fast graph representation learning with pytorch geometric. *arXiv preprint arXiv:1903.02428*, 2019.
- [127] Diederik P Kingma. Adam: A method for stochastic optimization. *arXiv preprint arXiv:1412.6980*, 2014.
- [128] Lev Davidovich Landau, LP Pitaevskii, Arnold Markovich Kosevich, and Evgenii Mikhailovich Lifshitz. *Theory of elasticity: volume 7*, volume 7. Elsevier, 2012.
- [129] Prajit Ramachandran, Barret Zoph, and Quoc V Le. Searching for activation functions. *arXiv preprint arXiv:1710.05941*, 2017.

A Dynamical equations

This section provides derivations of the complete dynamical equations, from the starting point of the metriplectic problem to the particle discretization used in this work. By recalling the formulation of the main text, consider now a collection of N particles with positions \mathbf{r}_i and velocities $\mathbf{v}_i = \frac{d\mathbf{r}_i}{dt}$ for $i \in V = \{1, \dots, N\}$. We introduce energy and entropy functionals

$$E = \sum_i \left[\frac{1}{2} m_i \mathbf{v}_i^2 + U_i \right], \quad S = \sum_i S_i,$$

where: $m_i = m$ is a particle mass, assumed to be constant; S_i is a per particle entropy; $U_i = U(\mathcal{V}_i, S_i, \bar{\mathbf{e}}_i)$ is a function prescribing per particle internal energy; and $\mathcal{V}_i(\mathbf{r}_1, \dots, \mathbf{r}_N)$ is a per particle volume which will be prescribed as a function of neighboring particle positions. The dynamic equations of the system is described by the metriplectic equation:

$$\underbrace{\begin{bmatrix} d\mathbf{r}_i \\ d\mathbf{v}_i \\ dS_i \end{bmatrix}}_{d\mathbf{x}_i} = \sum_j \frac{1}{m} \underbrace{\begin{bmatrix} \mathbf{0} & \mathbf{I}\delta_{ij} & \mathbf{0} \\ -\mathbf{I}\delta_{ij} & \mathbf{0} & \mathbf{0} \\ \mathbf{0} & \mathbf{0} & \mathbf{0} \end{bmatrix}}_{\mathbf{L}_{ij}} \underbrace{\begin{bmatrix} \frac{\partial U}{\partial \mathbf{r}_j} \\ m\mathbf{v}_j \\ T_j \end{bmatrix}}_{\frac{\partial E}{\partial \mathbf{x}_j}} dt + \sum_j \mathbf{M}_{ij} \underbrace{\begin{bmatrix} \mathbf{0} \\ \mathbf{0} \\ 1 \end{bmatrix}}_{\frac{\partial S}{\partial \mathbf{x}_j}} dt + k_B \sum_j \frac{\partial}{\partial \mathbf{x}_j} \cdot \mathbf{M}_{ij} dt + \underbrace{\begin{bmatrix} d\tilde{\mathbf{r}}_i \\ d\tilde{\mathbf{v}}_i \\ d\tilde{S}_i \end{bmatrix}}_{d\tilde{\mathbf{x}}_i}, \quad (8)$$

subject to the fluctuation-dissipation theorem:

$$d\tilde{\mathbf{x}} d\tilde{\mathbf{x}}^T = 2k_B \mathbf{M} dt. \quad (9)$$

The stochastic differentials $d\tilde{\mathbf{x}}_i = (d\tilde{\mathbf{r}}_i, d\tilde{\mathbf{v}}_i, d\tilde{S}_i)$ are defined as:

$$\begin{aligned} d\tilde{\mathbf{r}}_i &= \mathbf{0} \\ m d\tilde{\mathbf{v}}_i &= \sqrt{2k_B} \sum_{j \in \mathcal{N}_i} \left[A_{ij} d\bar{\mathbf{W}}_{ij} + B_{ij} \frac{\mathbf{I}}{D} \text{tr}(d\mathbf{W}_{ij}) \right] \mathbf{e}_{ij}, \\ T_i d\tilde{S}_i &= -\frac{\sqrt{2k_B}}{2} \sum_{j \in \mathcal{N}_i} \left[A_{ij} d\bar{\mathbf{W}}_{ij} + B_{ij} \frac{\mathbf{I}}{D} \text{tr}(d\mathbf{W}_{ij}) \right] : \mathbf{e}_{ij} \mathbf{v}_{ij} + \sqrt{2k_B} \sum_{j \in \mathcal{N}_i} C_{ij} dV_{ij}, \end{aligned} \quad (10)$$

where $A_{ij} = A_{ji}$, $B_{ij} = B_{ji}$ and $C_{ij} = C_{ji}$ are symmetric functions of the position and entropy of the particles, D is the dimension of the problem and $\mathbf{e}_{ij} = \mathbf{r}_{ij}/|\mathbf{r}_{ij}|$ is the interdistance unitary vector. The Wiener differentials $d\mathbf{W}_{ij} = d\mathbf{W}_{ji}$ and $dV_{ij} = -dV_{ji}$ are symmetric and skew-symmetric with respect to particle labels i, j . Their components are independent zero mean and unit variance Gaussian increments which are uncorrelated in components and particle index except if they belong to the same interaction. This logic can be compactly expressed by using Kronecker deltas with the following differential rules:

$$\begin{aligned} d\mathbf{W}_{ii'}^{\alpha\alpha'} d\mathbf{W}_{jj'}^{\beta\beta'} &= (\delta_{ij}\delta_{i'j'} + \delta_{i'j}\delta_{ij'}) \delta^{\alpha\beta} \delta^{\alpha'\beta'} dt, \\ dV_{ii'} dV_{jj'} &= (\delta_{ij}\delta_{i'j'} - \delta_{i'j}\delta_{ij'}) dt, \\ d\mathbf{W}_{ii'}^{\alpha\alpha'} dV_{jj'} &= 0, \end{aligned} \quad (11)$$

where indices i, j and i', j' denote pairs of particles (latin subscripts) and α, β and α', β' denote the matrix component indices (greek superscripts). Last, we define the traceless symmetric matrix $d\bar{\mathbf{W}}_{ij}$ as

$$d\bar{\mathbf{W}}_{ij} = \frac{1}{2}(d\mathbf{W}_{ij} + d\mathbf{W}_{ij}^T) - \frac{\mathbf{I}}{D} \text{tr}(d\mathbf{W}_{ij}). \quad (12)$$

A.1 Computation of conservative terms

This section aims to derive the conservative terms of the dynamics. Isolating the reversible terms in Eq. (8), we obtain the usual Hamilton's equations in our chosen coordinates:

$$\begin{bmatrix} d\mathbf{r}_i \\ d\mathbf{v}_i \\ dS_i \end{bmatrix}_{\text{rev}} = \begin{bmatrix} \mathbf{v}_i \\ -\frac{1}{m} \frac{\partial U}{\partial \mathbf{r}_i} \\ 0 \end{bmatrix} dt.$$

We now focus on the non-trivial term, which is the momentum equation. By expanding the gradient and using the chain rule:

$$-\frac{\partial U}{\partial \mathbf{r}_i} = -\sum_k \frac{\partial U_k}{\partial \mathbf{r}_i} = -\sum_k \left[\frac{\partial U_k}{\partial \mathcal{V}_k} \frac{\partial \mathcal{V}_k}{\partial \mathbf{r}_i} + \frac{\partial U_k}{\partial \bar{\mathbf{e}}_k} \frac{\partial \bar{\mathbf{e}}_k}{\partial \mathbf{r}_i} \right]. \quad (13)$$

First, the volumetric term gives rise to a hydrostatic pressure force. By using the equation of state relationships and the volume definition, we get:

$$\begin{aligned} -\sum_k \frac{\partial U_k}{\partial \mathcal{V}_k} \frac{\partial \mathcal{V}_k}{\partial \mathbf{r}_i} &= -\sum_k (-P_k) \left(-\frac{1}{d_k^2} \right) \frac{\partial d_i}{\partial \mathbf{r}_i} = -\sum_k \frac{P_k}{d_k^2} \sum_j \frac{\partial W_{kj}}{\partial \mathbf{r}_i} = -\sum_{k,j} \frac{P_k}{d_k^2} \frac{\partial W_{kj}}{\partial \mathbf{r}_{kj}} \frac{\partial \mathbf{r}_{kj}}{\partial \mathbf{r}_i} \\ &= -\sum_{k,j} \frac{P_k}{d_k^2} \frac{\partial W_{kj}}{\partial \mathbf{r}_{kj}} (\delta_{ik} - \delta_{ij}) = -\sum_j \frac{P_i}{d_i^2} \frac{\partial W_{ij}}{\partial \mathbf{r}_{ij}} + \sum_k \frac{P_k}{d_k^2} \frac{\partial W_{ki}}{\partial \mathbf{r}_{ki}} = \sum_j \left[\frac{P_j}{d_j^2} \frac{\partial W_{ji}}{\partial \mathbf{r}_{ji}} - \frac{P_i}{d_i^2} \frac{\partial W_{ij}}{\partial \mathbf{r}_{ij}} \right] \end{aligned}$$

For the elasticity extension, the deviatoric term contributes to the dynamics with a shear elastic restoring force. By using the chain rule, we obtain:

$$\begin{aligned} -\sum_k \frac{\partial U_k}{\partial \bar{\boldsymbol{\varepsilon}}_k^{\alpha\beta}} \frac{\partial \bar{\boldsymbol{\varepsilon}}_k^{\alpha\beta}}{\partial \mathbf{r}_i^\gamma} &= -\sum_k \boldsymbol{\tau}_k^{\alpha\beta} \sum_j \frac{\partial \bar{\mathbf{W}}_{kj}^{\alpha\beta}}{\partial \mathbf{r}_i^\gamma} = -\sum_k \boldsymbol{\tau}_k^{\alpha\beta} \sum_j \frac{\partial \bar{\mathbf{W}}_{kj}^{\alpha\beta}}{\partial \mathbf{u}_{kj}^\delta} \frac{\partial \mathbf{u}_{kj}^\delta}{\partial \mathbf{r}_i^\gamma} = -\sum_{k,j} \boldsymbol{\tau}_k^{\alpha\beta} \frac{\partial \bar{\mathbf{W}}_{kj}^{\alpha\beta}}{\partial \mathbf{u}_{kj}^\delta} \delta_{\delta\gamma} (\delta_{ik} - \delta_{ij}) \\ &= -\sum_j \boldsymbol{\tau}_i^{\alpha\beta} \frac{\partial \bar{\mathbf{W}}_{ij}^{\alpha\beta}}{\partial \mathbf{u}_{ij}^\gamma} + \sum_k \boldsymbol{\tau}_k^{\alpha\beta} \frac{\partial \bar{\mathbf{W}}_{ki}^{\alpha\beta}}{\partial \mathbf{u}_{ki}^\gamma} = \sum_j \left[\boldsymbol{\tau}_j^{\alpha\beta} \frac{\partial \bar{\mathbf{W}}_{ji}^{\alpha\beta}}{\partial \mathbf{u}_{ji}^\gamma} - \boldsymbol{\tau}_i^{\alpha\beta} \frac{\partial \bar{\mathbf{W}}_{ij}^{\alpha\beta}}{\partial \mathbf{u}_{ij}^\gamma} \right] \end{aligned}$$

A.2 Computation of dissipative terms

Once established $d\tilde{\mathbf{x}}$ by the ansatz in Eq. (10), the rest of the viscous dynamics can be straightforwardly computed using the fluctuation-dissipation theorem Eq. (9) and substituting the components of the friction matrix \mathbf{M} and $\nabla \cdot \mathbf{M}$:

$$\begin{aligned} \begin{bmatrix} d\mathbf{r}_i \\ d\mathbf{v}_i \\ d\tilde{S}_i \end{bmatrix}_{\text{irr}} &= \sum_{j \in \mathcal{N}_i} \frac{d\tilde{\mathbf{x}} d\tilde{\mathbf{x}}^T}{2k_B} \begin{bmatrix} \mathbf{0} \\ \mathbf{0} \\ 1 \end{bmatrix} + k_B \sum_{j \in \mathcal{N}_i} \frac{\partial}{\partial \mathbf{x}_j} \cdot \frac{d\tilde{\mathbf{x}} d\tilde{\mathbf{x}}^T}{2k_B} + d\tilde{\mathbf{x}}_i \\ &= \frac{1}{2k_B} \sum_{j \in \mathcal{N}_i} \begin{bmatrix} \mathbf{0} & \mathbf{0} & \mathbf{0} \\ \mathbf{0} & d\tilde{\mathbf{v}}_i d\tilde{\mathbf{v}}_j^T & d\tilde{\mathbf{v}}_i d\tilde{S}_j \\ \mathbf{0} & d\tilde{S}_i d\tilde{\mathbf{v}}_j^T & d\tilde{S}_i d\tilde{S}_j \end{bmatrix} \begin{bmatrix} \mathbf{0} \\ \mathbf{0} \\ 1 \end{bmatrix} + \frac{1}{2} \sum_{j \in \mathcal{N}_i} \frac{\partial}{\partial \mathbf{x}_j} \cdot \begin{bmatrix} \mathbf{0} & \mathbf{0} & \mathbf{0} \\ \mathbf{0} & d\tilde{\mathbf{v}}_i d\tilde{\mathbf{v}}_j^T & d\tilde{\mathbf{v}}_i d\tilde{S}_j \\ \mathbf{0} & d\tilde{S}_i d\tilde{\mathbf{v}}_j^T & d\tilde{S}_i d\tilde{S}_j \end{bmatrix} + d\tilde{\mathbf{x}}_i \\ &= \frac{1}{2k_B} \sum_{j \in \mathcal{N}_i} \begin{bmatrix} \mathbf{0} \\ d\tilde{\mathbf{v}}_i d\tilde{S}_j \\ d\tilde{S}_i d\tilde{S}_j \end{bmatrix} + \frac{1}{2} \sum_{j \in \mathcal{N}_i} \begin{bmatrix} \mathbf{0} \\ \frac{\partial}{\partial \mathbf{v}_j} \cdot d\tilde{\mathbf{v}}_i d\tilde{\mathbf{v}}_j^T + \frac{\partial}{\partial S_j} \cdot d\tilde{\mathbf{v}}_i d\tilde{S}_j \\ \frac{\partial}{\partial \mathbf{v}_j} \cdot d\tilde{S}_i d\tilde{\mathbf{v}}_j^T + \frac{\partial}{\partial S_j} \cdot d\tilde{S}_i d\tilde{S}_j \end{bmatrix} + \begin{bmatrix} \mathbf{0} \\ d\tilde{\mathbf{v}}_i \\ d\tilde{S}_i \end{bmatrix}. \end{aligned}$$

By operating each term, we obtain the following expressions for the irreversible part of the dynamics:

$$\begin{aligned} d\mathbf{v}_i|_{\text{irr}} &= \frac{1}{2k_B} \sum_{j \in \mathcal{N}_i} d\tilde{\mathbf{v}}_i d\tilde{S}_j + \frac{1}{2} \sum_{j \in \mathcal{N}_i} \left(\frac{\partial}{\partial \mathbf{v}_j} \cdot d\tilde{\mathbf{v}}_i d\tilde{\mathbf{v}}_j^T + \frac{\partial}{\partial S_j} \cdot d\tilde{\mathbf{v}}_i d\tilde{S}_j \right) + d\tilde{\mathbf{v}}_i, \\ d\tilde{S}_i|_{\text{irr}} &= \frac{1}{2k_B} \sum_{j \in \mathcal{N}_i} d\tilde{S}_i d\tilde{S}_j + \frac{1}{2} \sum_{j \in \mathcal{N}_i} \left(\frac{\partial}{\partial \mathbf{v}_j} \cdot d\tilde{S}_i d\tilde{\mathbf{v}}_j^T + \frac{\partial}{\partial S_j} \cdot d\tilde{S}_i d\tilde{S}_j \right) + d\tilde{S}_i. \end{aligned}$$

In this section we focus in the derivation of each term. First, we need to establish some important identities.

Lemma A.1. *Given $d\mathbf{W}_{ii'}$ and $d\mathbf{W}_{jj'}$ two matrix-valued Wiener processes with the properties stated in Eq. (11), the following identities hold:*

1. $\text{tr}(d\mathbf{W}_{ii'}) \text{tr}(d\mathbf{W}_{jj'}) = D(\delta_{ij}\delta_{i'j'} + \delta_{i'j}\delta_{ij'}) dt.$
2. $\text{tr}(d\mathbf{W}_{ii'}) d\bar{\mathbf{W}}_{jj'} = 0.$
3. $d\bar{\mathbf{W}}_{ii'}^{\alpha\alpha'} d\bar{\mathbf{W}}_{jj'}^{\beta\beta'} = (\delta_{ij}\delta_{i'j'} + \delta_{i'j}\delta_{ij'}) \left[\frac{1}{2}(\delta^{\alpha\beta}\delta^{\alpha'\beta'} + \delta^{\alpha'\beta}\delta^{\alpha\beta'}) - \frac{1}{D}\delta^{\alpha\alpha'}\delta^{\beta\beta'} \right] dt.$
4. $\left[A_{ii'} d\bar{\mathbf{W}}_{ii'}^{\alpha\alpha'} + B_{ii'} \frac{\delta^{\alpha\alpha'}}{D} \text{tr}(d\mathbf{W}_{ii'}) \right] \left[A_{jj'} d\bar{\mathbf{W}}_{jj'}^{\beta\beta'} + B_{jj'} \frac{\delta^{\beta\beta'}}{D} \text{tr}(d\mathbf{W}_{jj'}) \right]$
 $= (\delta_{ij}\delta_{i'j'} + \delta_{i'j}\delta_{ij'}) \left[\frac{1}{2} A_{ii'} A_{jj'} (\delta^{\alpha\beta}\delta^{\alpha'\beta'} + \delta^{\alpha'\beta}\delta^{\alpha\beta'}) + (B_{ii'} B_{jj'} - A_{ii'} A_{jj'}) \frac{1}{D} \delta^{\alpha\alpha'} \delta^{\beta\beta'} \right] dt.$

Proof. First, it is important to remember some of the properties of Kronecker delta operations, which are intimately related to the properties of identity matrices:

- Symmetric property: $\delta^{\alpha\beta} = \delta^{\beta\alpha}$
- Summation property: $\sum_{\sigma} \delta^{\alpha\sigma} \delta^{\sigma\beta} = \delta^{\alpha\beta}$
- Cumulative summation: $\sum_{\alpha,\beta} \delta^{\alpha\beta} = D$ where D is the dimension of the problem.
- Conmutativity: $\delta^{\alpha\alpha'} \delta^{\beta\beta'} = \delta^{\beta\beta'} \delta^{\alpha\alpha'}$

By recalling the definition of $d\overline{\mathbf{W}}_{ij}$ in Eq. (12) and the correlation rules of the Wiener processes defined in Eq. (11), the proofs are completed with straightforward algebraic manipulations:

$$\begin{aligned}
 \text{tr}(d\mathbf{W}_{ii'}) \text{tr}(d\mathbf{W}_{jj'}) &= \sum_{\alpha} d\mathbf{W}_{ii'}^{\alpha\alpha} \sum_{\beta} d\mathbf{W}_{jj'}^{\beta\beta} = \sum_{\alpha,\beta} d\mathbf{W}_{ii'}^{\alpha\alpha} d\mathbf{W}_{jj'}^{\beta\beta} \\
 &= \sum_{\alpha,\beta} (\delta_{ij} \delta_{i'j'} + \delta_{i'j} \delta_{ij'}) \delta^{\alpha\beta} \delta^{\alpha\beta} dt \\
 &= (\delta_{ij} \delta_{i'j'} + \delta_{i'j} \delta_{ij'}) \sum_{\alpha,\beta} \delta^{\alpha\beta} dt \\
 &= D(\delta_{ij} \delta_{i'j'} + \delta_{i'j} \delta_{ij'}) dt.
 \end{aligned}$$

$$\begin{aligned}
 \text{tr}(d\mathbf{W}_{ii'}) d\overline{\mathbf{W}}_{jj'} &= \text{tr}(d\mathbf{W}_{ii'}) \left[\frac{1}{2} (d\mathbf{W}_{jj'}^{\alpha\beta} + d\mathbf{W}_{jj'}^{\beta\alpha}) - \frac{\delta^{\alpha\beta}}{D} \text{tr}(d\mathbf{W}_{jj'}) \right] \\
 &= \text{tr}(d\mathbf{W}_{ii'}) \frac{1}{2} (d\mathbf{W}_{jj'}^{\alpha\beta} + d\mathbf{W}_{jj'}^{\beta\alpha}) - \frac{\delta^{\alpha\beta}}{D} \text{tr}(d\mathbf{W}_{ii'}) \text{tr}(d\mathbf{W}_{jj'}) \\
 &= \sum_{\sigma} \left[d\mathbf{W}_{ii'}^{\sigma\sigma} \frac{1}{2} (d\mathbf{W}_{jj'}^{\alpha\beta} + d\mathbf{W}_{jj'}^{\beta\alpha}) \right] - \frac{\delta^{\alpha\beta}}{D} \text{tr}(d\mathbf{W}_{ii'}) \text{tr}(d\mathbf{W}_{jj'}) \\
 &\stackrel{(1)}{=} \frac{1}{2} \sum_{\sigma} \left[d\mathbf{W}_{ii'}^{\sigma\sigma} d\mathbf{W}_{jj'}^{\alpha\beta} + d\mathbf{W}_{ii'}^{\sigma\sigma} d\mathbf{W}_{jj'}^{\beta\alpha} \right] - \frac{\delta^{\alpha\beta}}{D} D(\delta_{ij} \delta_{i'j'} + \delta_{i'j} \delta_{ij'}) dt \\
 &= \frac{1}{2} \sum_{\sigma} \left[(\delta_{ij} \delta_{i'j'} + \delta_{i'j} \delta_{ij'}) (\delta^{\sigma\alpha} \delta^{\sigma\beta} + \delta^{\sigma\beta} \delta^{\sigma\alpha}) \right] dt - \delta^{\alpha\beta} (\delta_{ij} \delta_{i'j'} + \delta_{i'j} \delta_{ij'}) dt \\
 &= (\delta_{ij} \delta_{i'j'} + \delta_{i'j} \delta_{ij'}) \left[\frac{1}{2} \sum_{\sigma} 2\delta^{\sigma\alpha} \delta^{\sigma\beta} - \delta^{\alpha\beta} \right] dt \\
 &= (\delta_{ij} \delta_{i'j'} + \delta_{i'j} \delta_{ij'}) (\delta^{\alpha\beta} - \delta^{\alpha\beta}) dt = 0.
 \end{aligned}$$

$$\begin{aligned}
 d\overline{\mathbf{W}}_{ii'}^{\alpha\alpha'} d\overline{\mathbf{W}}_{jj'}^{\beta\beta'} &= \left[\frac{1}{2} (d\mathbf{W}_{ii'}^{\alpha\alpha'} + d\mathbf{W}_{ii'}^{\alpha'\alpha}) - \frac{\delta^{\alpha\alpha'}}{D} \text{tr}(d\mathbf{W}_{ii'}) \right] d\overline{\mathbf{W}}_{jj'}^{\beta\beta'} \\
 &\stackrel{(2)}{=} \frac{1}{2} (d\mathbf{W}_{ii'}^{\alpha\alpha'} + d\mathbf{W}_{ii'}^{\alpha'\alpha}) \left[\frac{1}{2} (d\mathbf{W}_{jj'}^{\beta\beta'} + d\mathbf{W}_{jj'}^{\beta'\beta}) - \frac{\delta^{\beta\beta'}}{D} \text{tr}(d\mathbf{W}_{jj'}) \right] \\
 &= \frac{1}{4} (d\mathbf{W}_{ii'}^{\alpha\alpha'} d\mathbf{W}_{jj'}^{\beta\beta'} + d\mathbf{W}_{ii'}^{\alpha\alpha'} d\mathbf{W}_{jj'}^{\beta'\beta} + d\mathbf{W}_{ii'}^{\alpha'\alpha} d\mathbf{W}_{jj'}^{\beta\beta'} + d\mathbf{W}_{ii'}^{\alpha'\alpha} d\mathbf{W}_{jj'}^{\beta'\beta}) \\
 &\quad - \frac{\delta^{\beta\beta'}}{2D} (d\mathbf{W}_{ii'}^{\alpha\alpha'} + d\mathbf{W}_{ii'}^{\alpha'\alpha}) \text{tr}(d\mathbf{W}_{jj'}) \\
 &\stackrel{(1)}{=} (\delta_{ij} \delta_{i'j'} + \delta_{i'j} \delta_{ij'}) \left[\frac{1}{4} (\delta^{\alpha\beta} \delta^{\alpha'\beta'} + \delta^{\alpha\beta'} \delta^{\alpha'\beta} + \delta^{\alpha'\beta} \delta^{\alpha\beta'} + \delta^{\alpha'\beta'} \delta^{\alpha\beta}) \right] dt \\
 &\quad - \frac{\delta^{\beta\beta'}}{2D} \sum_{\sigma} (d\mathbf{W}_{ii'}^{\alpha\alpha'} d\mathbf{W}_{jj'}^{\sigma\sigma} + d\mathbf{W}_{ii'}^{\alpha'\alpha} d\mathbf{W}_{jj'}^{\sigma\sigma}) \\
 &= (\delta_{ij} \delta_{i'j'} + \delta_{i'j} \delta_{ij'}) \left[\frac{1}{4} (2\delta^{\alpha\beta} \delta^{\alpha'\beta'} + 2\delta^{\alpha'\beta} \delta^{\alpha\beta'}) - \frac{\delta^{\beta\beta'}}{2D} \sum_{\sigma} (\delta^{\alpha\sigma} \delta^{\alpha'\sigma} + \delta^{\alpha'\sigma} \delta^{\alpha\sigma}) \right] dt \\
 &= (\delta_{ij} \delta_{i'j'} + \delta_{i'j} \delta_{ij'}) \left[\frac{1}{2} (\delta^{\alpha\beta} \delta^{\alpha'\beta'} + \delta^{\alpha'\beta} \delta^{\alpha\beta'}) - \frac{\delta^{\beta\beta'}}{2D} \sum_{\sigma} 2\delta^{\alpha\sigma} \delta^{\alpha'\sigma} \right] dt
 \end{aligned}$$

$$= (\delta_{ij}\delta_{i'j'} + \delta_{i'j}\delta_{ij'}) \left[\frac{1}{2}(\delta^{\alpha\beta}\delta^{\alpha'\beta'} + \delta^{\alpha'\beta}\delta^{\alpha\beta'}) - \frac{1}{D}\delta^{\alpha\alpha'}\delta^{\beta\beta'} \right] dt.$$

$$\begin{aligned} & \left[A_{ii'}d\overline{\mathbf{W}}_{ii'}^{\alpha\alpha'} + B_{ii'}\frac{\delta^{\alpha\alpha'}}{D}\text{tr}(d\mathbf{W}_{ii'}) \right] \left[A_{jj'}d\overline{\mathbf{W}}_{jj'}^{\beta\beta'} + B_{jj'}\frac{\delta^{\beta\beta'}}{D}\text{tr}(d\mathbf{W}_{jj'}) \right] \\ &= A_{ii'}A_{jj'}d\overline{\mathbf{W}}_{ii'}^{\alpha\alpha'}d\overline{\mathbf{W}}_{jj'}^{\beta\beta'} + A_{ii'}B_{jj'}\frac{\delta^{\beta\beta'}}{D}d\overline{\mathbf{W}}_{ii'}^{\alpha\alpha'}\text{tr}(d\mathbf{W}_{jj'}) \\ & \quad + B_{ii'}A_{jj'}\frac{\delta^{\alpha\alpha'}}{D}\text{tr}(d\mathbf{W}_{ii'})d\overline{\mathbf{W}}_{jj'}^{\beta\beta'} + B_{ii'}B_{jj'}\frac{\delta^{\alpha\alpha'}\delta^{\beta\beta'}}{D^2}\text{tr}(d\mathbf{W}_{ii'})\text{tr}(d\mathbf{W}_{jj'}) \\ & \stackrel{(2)}{=} A_{ii'}A_{jj'}d\overline{\mathbf{W}}_{ii'}^{\alpha\alpha'}d\overline{\mathbf{W}}_{jj'}^{\beta\beta'} + B_{ii'}B_{jj'}\frac{\delta^{\alpha\alpha'}\delta^{\beta\beta'}}{D^2}\text{tr}(d\mathbf{W}_{ii'})\text{tr}(d\mathbf{W}_{jj'}) \\ & \stackrel{(1,3)}{=} (\delta_{ij}\delta_{i'j'} + \delta_{i'j}\delta_{ij'}) \left[\frac{A_{ii'}A_{jj'}}{2}(\delta^{\alpha\beta}\delta^{\alpha'\beta'} + \delta^{\alpha'\beta}\delta^{\alpha\beta'}) - \frac{A_{ii'}A_{jj'}}{D}\delta^{\alpha\alpha'}\delta^{\beta\beta'} + \frac{B_{ii'}B_{jj'}}{D^2}\delta^{\alpha\alpha'}\delta^{\beta\beta'} D \right] dt \\ &= (\delta_{ij}\delta_{i'j'} + \delta_{i'j}\delta_{ij'}) \left[\frac{A_{ii'}A_{jj'}}{2}(\delta^{\alpha\beta}\delta^{\alpha'\beta'} + \delta^{\alpha'\beta}\delta^{\alpha\beta'}) + \frac{B_{ii'}B_{jj'} - A_{ii'}A_{jj'}}{D}\delta^{\alpha\alpha'}\delta^{\beta\beta'} \right] dt. \end{aligned}$$

□

Now we can compute the M matrix by blocks using the fluctuation-dissipation theorem in Eq. (9),

$$\mathbf{M}_{ij}dt = \frac{d\tilde{\mathbf{x}}_i d\tilde{\mathbf{x}}_j^T}{2k_B} = \frac{1}{2k_B} \begin{bmatrix} \mathbf{0} & \mathbf{0} & \mathbf{0} \\ \mathbf{0} & d\tilde{\mathbf{v}}_i d\tilde{\mathbf{v}}_j^T & d\tilde{\mathbf{v}}_i d\tilde{S}_j \\ \mathbf{0} & d\tilde{S}_i d\tilde{\mathbf{v}}_j^T & d\tilde{S}_i d\tilde{S}_j \end{bmatrix}.$$

Note that the complete M matrix is symmetric, but the individual blocks M_{ij} are not. We first need to apply the ansatz of $d\tilde{\mathbf{x}}$ in Eq. (10). For convenience, we will compute the individual components of the vectorial quantities, such as \mathbf{v}^α or \mathbf{e}^α , by using the Einstein summation convention (only for the greek superscripts). We will need the following summation rules for the Kronecker deltas:

- Index contraction: $\delta^{\alpha\beta}\mathbf{v}^\alpha = \sum_\alpha \delta^{\alpha\beta}\mathbf{v}^\alpha = \mathbf{v}^\beta$
- Dot product: $\mathbf{v}^\alpha \delta^{\alpha\beta} \mathbf{e}^\beta = \sum_{\alpha,\beta} \mathbf{v}^\alpha \delta^{\alpha\beta} \mathbf{e}^\beta = \sum_\alpha \mathbf{v}^\alpha \mathbf{e}^\alpha = \mathbf{v} \cdot \mathbf{e}$

We will also need to apply the symmetry of the coefficients $A_{ij} = A_{ji}$, $B_{ij} = B_{ji}$ and $C_{ij} = C_{ji}$, the skew-symmetry of $\mathbf{e}_{ij} = -\mathbf{e}_{ji}$ and the unitary modulus of $\mathbf{e}_{ij} \cdot \mathbf{e}_{ij} = 1$. Now, we can compute the individual components by using Lemma A.1. First, we will contract the Greek superscripts and then the Roman subscripts.

$$\begin{aligned} m^2 \frac{d\tilde{\mathbf{v}}_i^\alpha d\tilde{\mathbf{v}}_j^\beta}{2k_B} &= \sum_{i',j'} \left[A_{ii'}d\overline{\mathbf{W}}_{ii'}^{\alpha\alpha'} + B_{ii'}\frac{\delta^{\alpha\alpha'}}{D}\text{tr}(d\mathbf{W}_{ii'}) \right] \mathbf{e}_{ii'}^{\alpha'} \left[A_{jj'}d\overline{\mathbf{W}}_{jj'}^{\beta\beta'} + B_{jj'}\frac{\delta^{\beta\beta'}}{D}\text{tr}(d\mathbf{W}_{jj'}) \right] \mathbf{e}_{jj'}^{\beta'} \\ &= \sum_{i',j'} (\delta_{ij}\delta_{i'j'} + \delta_{i'j}\delta_{ij'}) \left[\frac{A_{ii'}A_{jj'}}{2}(\delta^{\alpha\beta}\delta^{\alpha'\beta'} + \delta^{\alpha'\beta}\delta^{\alpha\beta'}) + \frac{B_{ii'}B_{jj'} - A_{ii'}A_{jj'}}{D}\delta^{\alpha\alpha'}\delta^{\beta\beta'} \right] \mathbf{e}_{ii'}^{\alpha'} \mathbf{e}_{jj'}^{\beta'} dt \\ &= \sum_{i',j'} (\delta_{ij}\delta_{i'j'} + \delta_{i'j}\delta_{ij'}) \left[\frac{A_{ii'}A_{jj'}}{2}(\delta^{\alpha\beta} \mathbf{e}_{ii'} \cdot \mathbf{e}_{jj'} + \mathbf{e}_{ii'}^\beta \mathbf{e}_{jj'}^\alpha) + \frac{B_{ii'}B_{jj'} - A_{ii'}A_{jj'}}{D} \mathbf{e}_{ii'}^\alpha \mathbf{e}_{jj'}^\beta \right] dt \\ &= \delta_{ij} \sum_{k \in \mathcal{N}_i} \left[\frac{A_{ik}A_{jk}}{2}(\delta^{\alpha\beta} \mathbf{e}_{ik} \cdot \mathbf{e}_{jk} + \mathbf{e}_{ik}^\beta \mathbf{e}_{jk}^\alpha) + \frac{B_{ik}B_{jk} - A_{ik}A_{jk}}{D} \mathbf{e}_{ik}^\alpha \mathbf{e}_{jk}^\beta \right] dt \\ & \quad + \left[\frac{A_{ij}A_{ji}}{2}(\delta^{\alpha\beta} \mathbf{e}_{ij} \cdot \mathbf{e}_{ji} + \mathbf{e}_{ij}^\beta \mathbf{e}_{ji}^\alpha) + \frac{B_{ij}B_{ji} - A_{ij}A_{ji}}{D} \mathbf{e}_{ij}^\alpha \mathbf{e}_{ji}^\beta \right] dt \\ &= \delta_{ij} \sum_{k \in \mathcal{N}_i} \left[\frac{A_{ik}^2}{2}(\delta^{\alpha\beta} + \mathbf{e}_{ik}^\alpha \mathbf{e}_{ik}^\beta) + \frac{B_{ik}^2 - A_{ik}^2}{D} \mathbf{e}_{ik}^\alpha \mathbf{e}_{ik}^\beta \right] dt - \left[\frac{A_{ij}^2}{2}(\delta^{\alpha\beta} + \mathbf{e}_{ij}^\alpha \mathbf{e}_{ij}^\beta) + \frac{B_{ij}^2 - A_{ij}^2}{D} \mathbf{e}_{ij}^\alpha \mathbf{e}_{ij}^\beta \right] dt. \end{aligned}$$

We can use very similar proofs for the remaining terms. Remember that the Wiener processes dV_{ij} are independent of $d\mathbf{W}_{ij}$ by Eq. (11), so the C_{ij} terms only appear in the entropic term of the matrix. Also, we will need to use the skew-symmetry of $\mathbf{v}_{ij} = -\mathbf{v}_{ji}$.

$$\begin{aligned}
 mT_j \frac{d\tilde{\mathbf{v}}_i^\alpha d\tilde{S}_j}{2k_B} &= \sum_{i',j'} \left[A_{ii'} d\overline{\mathbf{W}}_{ii'}^{\alpha\alpha'} + B_{ii'} \frac{\delta^{\alpha\alpha'}}{D} \text{tr}(d\mathbf{W}_{ii'}) \right] \mathbf{e}_{ii'}^\alpha \left(-\frac{1}{2} \left[A_{jj'} d\overline{\mathbf{W}}_{jj'}^{\beta\beta'} + B_{jj'} \frac{\delta^{\beta\beta'}}{D} \text{tr}(d\mathbf{W}_{jj'}) \right] \mathbf{e}_{jj'}^\beta \mathbf{v}_{jj'}^\beta \right. \\
 &\quad \left. + C_{jj'} dV_{jj'} \right) \\
 &= -\sum_{i',j'} (\delta_{ij} \delta_{i'j'} + \delta_{i'j} \delta_{ij'}) \left[\frac{A_{ii'} A_{jj'}}{2} (\delta^{\alpha\beta} \delta^{\alpha'\beta'} + \delta^{\alpha'\beta} \delta^{\alpha\beta'}) + \frac{B_{ii'} B_{jj'} - A_{ii'} A_{jj'}}{D} \delta^{\alpha\alpha'} \delta^{\beta\beta'} \right] \mathbf{e}_{ii'}^\alpha \mathbf{e}_{jj'}^\beta \frac{\mathbf{v}_{jj'}^\beta}{2} dt \\
 &= -\sum_{i',j'} (\delta_{ij} \delta_{i'j'} + \delta_{i'j} \delta_{ij'}) \left[\frac{A_{ii'} A_{jj'}}{2} \left(\frac{\mathbf{v}_{jj'}^\alpha}{2} \mathbf{e}_{ii'} \cdot \mathbf{e}_{jj'} + \mathbf{e}_{ii'} \cdot \frac{\mathbf{v}_{jj'}^\alpha}{2} \mathbf{e}_{jj'} \right) + \frac{B_{ii'} B_{jj'} - A_{ii'} A_{jj'}}{D} \mathbf{e}_{ii'}^\alpha \mathbf{e}_{jj'} \cdot \frac{\mathbf{v}_{jj'}}{2} \right] dt \\
 &= -\delta_{ij} \sum_{k \in \mathcal{N}_i} \left[\frac{A_{ik} A_{jk}}{2} \left(\frac{\mathbf{v}_{jk}^\alpha}{2} \mathbf{e}_{ik} \cdot \mathbf{e}_{jk} + \mathbf{e}_{ik} \cdot \frac{\mathbf{v}_{jk}^\alpha}{2} \mathbf{e}_{jk} \right) + \frac{B_{ik} B_{jk} - A_{ik} A_{jk}}{D} \mathbf{e}_{ik}^\alpha \mathbf{e}_{jk} \cdot \frac{\mathbf{v}_{jk}}{2} \right] dt \\
 &\quad - \left[\frac{A_{ij} A_{ji}}{2} \left(\frac{\mathbf{v}_{ji}^\alpha}{2} \mathbf{e}_{ij} \cdot \mathbf{e}_{ji} + \mathbf{e}_{ij} \cdot \frac{\mathbf{v}_{ji}^\alpha}{2} \mathbf{e}_{ji} \right) + \frac{B_{ij} B_{ji} - A_{ij} A_{ji}}{D} \mathbf{e}_{ij}^\alpha \mathbf{e}_{ji} \cdot \frac{\mathbf{v}_{ji}}{2} \right] dt \\
 &= -\delta_{ij} \sum_{k \in \mathcal{N}_i} \left[\frac{A_{ik}^2}{2} \left(\frac{\mathbf{v}_{ik}^\alpha}{2} + \mathbf{e}_{ik} \cdot \frac{\mathbf{v}_{ik}^\alpha}{2} \mathbf{e}_{ik} \right) + \frac{B_{ik}^2 - A_{ik}^2}{D} \mathbf{e}_{ik}^\alpha \mathbf{e}_{ik} \cdot \frac{\mathbf{v}_{ik}}{2} \right] dt \\
 &\quad - \left[\frac{A_{ij}^2}{2} \left(\frac{\mathbf{v}_{ij}^\alpha}{2} + \mathbf{e}_{ij} \cdot \frac{\mathbf{v}_{ij}^\alpha}{2} \mathbf{e}_{ij} \right) + \frac{B_{ij}^2 - A_{ij}^2}{D} \mathbf{e}_{ij}^\alpha \mathbf{e}_{ij} \cdot \frac{\mathbf{v}_{ij}}{2} \right] dt.
 \end{aligned}$$

$$\begin{aligned}
 mT_i \frac{d\tilde{S}_i d\tilde{\mathbf{v}}_j^\alpha}{2k_B} &= \sum_{i',j'} \left(-\frac{1}{2} \left[A_{ii'} d\overline{\mathbf{W}}_{ii'}^{\beta\beta'} + B_{ii'} \frac{\delta^{\beta\beta'}}{D} \text{tr}(d\mathbf{W}_{ii'}) \right] \mathbf{e}_{ii'}^\beta \mathbf{v}_{ii'}^\beta + C_{ii'} dV_{ii'} \right) \left[A_{jj'} d\overline{\mathbf{W}}_{jj'}^{\alpha\alpha'} + B_{jj'} \frac{\delta^{\alpha\alpha'}}{D} \text{tr}(d\mathbf{W}_{jj'}) \right] \mathbf{e}_{jj'}^\alpha \\
 &= -\sum_{i',j'} (\delta_{ij} \delta_{i'j'} + \delta_{ij'} \delta_{i'j}) \left[\frac{A_{ii'} A_{jj'}}{2} (\delta^{\alpha\beta} \delta^{\alpha'\beta'} + \delta^{\alpha'\beta} \delta^{\alpha\beta'}) + \frac{B_{ii'} B_{jj'} - A_{ii'} A_{jj'}}{D} \delta^{\alpha\alpha'} \delta^{\beta\beta'} \right] \mathbf{e}_{ii'}^\beta \frac{\mathbf{v}_{ii'}^\beta}{2} \mathbf{e}_{jj'}^\alpha dt \\
 &= -\sum_{i',j'} (\delta_{ij} \delta_{i'j'} + \delta_{ij'} \delta_{i'j}) \left[\frac{A_{ii'} A_{jj'}}{2} \left(\frac{\mathbf{v}_{ii'}^\alpha}{2} \mathbf{e}_{ii'} \cdot \mathbf{e}_{jj'} + \mathbf{e}_{ii'} \cdot \frac{\mathbf{v}_{ii'}^\alpha}{2} \mathbf{e}_{jj'} \right) + \frac{B_{ii'} B_{jj'} - A_{ii'} A_{jj'}}{D} \mathbf{e}_{jj'}^\alpha \mathbf{e}_{ii'} \cdot \frac{\mathbf{v}_{ii'}}{2} \right] dt \\
 &= -\delta_{ij} \sum_{k \in \mathcal{N}_i} \left[\frac{A_{ik} A_{jk}}{2} \left(\frac{\mathbf{v}_{jk}^\alpha}{2} \mathbf{e}_{ik} \cdot \mathbf{e}_{jk} + \mathbf{e}_{jk} \cdot \frac{\mathbf{v}_{jk}^\alpha}{2} \mathbf{e}_{ik} \right) + \frac{B_{ik} B_{jk} - A_{ik} A_{jk}}{D} \mathbf{e}_{jk}^\alpha \mathbf{e}_{ik} \cdot \frac{\mathbf{v}_{ik}}{2} \right] dt \\
 &\quad - \left[\frac{A_{ij} A_{ji}}{2} \left(\frac{\mathbf{v}_{ij}^\alpha}{2} \mathbf{e}_{ij} \cdot \mathbf{e}_{ji} + \mathbf{e}_{ji} \cdot \frac{\mathbf{v}_{ij}^\alpha}{2} \mathbf{e}_{ij} \right) + \frac{B_{ij} B_{ji} - A_{ij} A_{ji}}{D} \mathbf{e}_{ji}^\alpha \mathbf{e}_{ij} \cdot \frac{\mathbf{v}_{ij}}{2} \right] dt \\
 &= -\delta_{ij} \sum_{k \in \mathcal{N}_i} \left[\frac{A_{ik}^2}{2} \left(\frac{\mathbf{v}_{ik}^\alpha}{2} + \mathbf{e}_{ik} \cdot \frac{\mathbf{v}_{ik}^\alpha}{2} \mathbf{e}_{ik} \right) + \frac{B_{ik}^2 - A_{ik}^2}{D} \mathbf{e}_{ik}^\alpha \mathbf{e}_{ik} \cdot \frac{\mathbf{v}_{ik}}{2} \right] dt \\
 &\quad + \left[\frac{A_{ij}^2}{2} \left(\frac{\mathbf{v}_{ij}^\alpha}{2} + \mathbf{e}_{ij} \cdot \frac{\mathbf{v}_{ij}^\alpha}{2} \mathbf{e}_{ij} \right) + \frac{B_{ij}^2 - A_{ij}^2}{D} \mathbf{e}_{ij}^\alpha \mathbf{e}_{ij} \cdot \frac{\mathbf{v}_{ij}}{2} \right] dt.
 \end{aligned}$$

$$\begin{aligned}
 T_i T_j \frac{d\tilde{S}_i d\tilde{S}_j}{2k_B} &= \sum_{i',j'} \left(-\frac{1}{2} \left[A_{ii'} d\overline{\mathbf{W}}_{ii'}^{\alpha\alpha'} + B_{ii'} \frac{\delta^{\alpha\alpha'}}{D} \text{tr}(d\mathbf{W}_{ii'}) \right] \mathbf{e}_{ii'}^\alpha \mathbf{v}_{ii'}^\alpha + C_{ii'} dV_{ii'} \right) \left(-\frac{1}{2} \left[A_{jj'} d\overline{\mathbf{W}}_{jj'}^{\beta\beta'} \right. \right. \\
 &\quad \left. \left. + B_{jj'} \frac{\delta^{\beta\beta'}}{D} \text{tr}(d\mathbf{W}_{jj'}) \right] \mathbf{e}_{jj'}^\beta \mathbf{v}_{jj'}^\beta + C_{jj'} dV_{jj'} \right) \\
 &= \sum_{i,j'} (\delta_{ij} \delta_{i'j'} + \delta_{ij'} \delta_{i'j}) \left[\frac{A_{ii'} A_{jj'}}{2} (\delta^{\alpha\beta} \delta^{\alpha'\beta'} + \delta^{\alpha'\beta} \delta^{\alpha\beta'}) + \frac{B_{ii'} B_{jj'} - A_{ii'} A_{jj'}}{D} \delta^{\alpha\alpha'} \delta^{\beta\beta'} \right] \mathbf{e}_{ii'}^\alpha \frac{\mathbf{v}_{ii'}^\alpha}{2} \mathbf{e}_{jj'}^\beta \frac{\mathbf{v}_{jj'}^\beta}{2} dt \\
 &\quad + \sum_{i',j'} (\delta_{ij} \delta_{i'j'} - \delta_{ij'} \delta_{i'j}) C_{ii'} C_{jj'} dt
 \end{aligned}$$

$$\begin{aligned}
 &= \sum_{i,j'} (\delta_{ij} \delta_{i'j'} + \delta_{ij'} \delta_{i'j}) \left(\frac{A_{ii'} A_{jj'}}{2} \left[\left(\frac{\mathbf{v}_{ii'}}{2} \cdot \frac{\mathbf{v}_{jj'}}{2} \right) \mathbf{e}_{ii'} \cdot \mathbf{e}_{jj'} + \left(\mathbf{e}_{ii'} \cdot \frac{\mathbf{v}_{jj'}}{2} \right) \left(\mathbf{e}_{jj'} \cdot \frac{\mathbf{v}_{ii'}}{2} \right) \right] \right. \\
 &\quad \left. + \frac{B_{ii'} B_{jj'} - A_{ii'} A_{jj'}}{D} \left(\mathbf{e}_{ii'} \cdot \frac{\mathbf{v}_{ii'}}{2} \right) \left(\mathbf{e}_{jj'} \cdot \frac{\mathbf{v}_{jj'}}{2} \right) \right) dt + \sum_{i',j'} (\delta_{ij} \delta_{i'j'} - \delta_{ij'} \delta_{i'j}) C_{ii'} C_{jj'} dt \\
 &= \delta_{ij} \sum_{k \in \mathcal{N}_i} \left(\frac{A_{ik} A_{jk}}{2} \left[\left(\frac{\mathbf{v}_{ik}}{2} \cdot \frac{\mathbf{v}_{jk}}{2} \right) \mathbf{e}_{ik} \cdot \mathbf{e}_{jk} + \left(\mathbf{e}_{ik} \cdot \frac{\mathbf{v}_{jk}}{2} \right) \left(\mathbf{e}_{jk} \cdot \frac{\mathbf{v}_{ik}}{2} \right) \right] \right. \\
 &\quad \left. + \frac{B_{ik} B_{jk} - A_{ik} A_{jk}}{D} \left(\mathbf{e}_{ik} \cdot \frac{\mathbf{v}_{ik}}{2} \right) \left(\mathbf{e}_{jk} \cdot \frac{\mathbf{v}_{jk}}{2} \right) \right) dt \\
 &\quad + \frac{A_{ij} A_{ji}}{2} \left[\left(\frac{\mathbf{v}_{ij}}{2} \cdot \frac{\mathbf{v}_{ji}}{2} \right) \mathbf{e}_{ij} \cdot \mathbf{e}_{ji} + \left(\mathbf{e}_{ij} \cdot \frac{\mathbf{v}_{ji}}{2} \right) \left(\mathbf{e}_{ji} \cdot \frac{\mathbf{v}_{ij}}{2} \right) \right] + \frac{B_{ij} B_{ji} - A_{ij} A_{ji}}{D} \left(\mathbf{e}_{ij} \cdot \frac{\mathbf{v}_{ij}}{2} \right) \left(\mathbf{e}_{ji} \cdot \frac{\mathbf{v}_{ji}}{2} \right) dt \\
 &\quad + \delta_{ij} \sum_{k \in \mathcal{N}_i} C_{ik} C_{jk} dt - C_{ij} C_{ji} dt \\
 &= \delta_{ij} \sum_{k \in \mathcal{N}_i} \left(\frac{A_{ik}^2}{2} \left[\left(\frac{\mathbf{v}_{ik}}{2} \right)^2 + \left(\mathbf{e}_{ik} \cdot \frac{\mathbf{v}_{ik}}{2} \right)^2 \right] + \frac{B_{ik}^2 - A_{ik}^2}{D} \left(\mathbf{e}_{ik} \cdot \frac{\mathbf{v}_{ik}}{2} \right)^2 + C_{ik}^2 \right) dt \\
 &\quad + \left(\frac{A_{ij}^2}{2} \left[\left(\frac{\mathbf{v}_{ij}}{2} \right)^2 + \left(\mathbf{e}_{ij} \cdot \frac{\mathbf{v}_{ij}}{2} \right)^2 \right] + \frac{B_{ij}^2 - A_{ij}^2}{D} \left(\mathbf{e}_{ij} \cdot \frac{\mathbf{v}_{ij}}{2} \right)^2 - C_{ij}^2 \right) dt.
 \end{aligned}$$

First, lets compute the M contributions to the dynamics:

$$\begin{aligned}
 m \sum_{j \in \mathcal{N}_i} \frac{d\tilde{\mathbf{v}}_i d\tilde{\mathbf{S}}_j}{2k_B} &= - \sum_{j \in \mathcal{N}_i} \frac{1}{T_j} \delta_{ij} \sum_{k \in \mathcal{N}_i} \left[\frac{A_{ik}^2}{2} \left(\frac{\mathbf{v}_{ik}}{2} + \mathbf{e}_{ik} \cdot \frac{\mathbf{v}_{ik}}{2} \mathbf{e}_{ik} \right) + \frac{B_{ik}^2 - A_{ik}^2}{D} \mathbf{e}_{ik} \mathbf{e}_{ik} \cdot \frac{\mathbf{v}_{ik}}{2} \right] dt \\
 &\quad - \sum_{j \in \mathcal{N}_i} \frac{1}{T_j} \left[\frac{A_{ij}^2}{2} \left(\frac{\mathbf{v}_{ij}}{2} + \mathbf{e}_{ij} \cdot \frac{\mathbf{v}_{ij}}{2} \mathbf{e}_{ij} \right) + \frac{B_{ij}^2 - A_{ij}^2}{D} \mathbf{e}_{ij} \mathbf{e}_{ij} \cdot \frac{\mathbf{v}_{ij}}{2} \right] dt \\
 &= - \frac{1}{2T_i} \sum_{j \in \mathcal{N}_i} \left[\frac{A_{ij}^2}{2} (\mathbf{v}_{ij} + \mathbf{e}_{ij} \cdot \mathbf{v}_{ij} \mathbf{e}_{ij}) + \frac{B_{ij}^2 - A_{ij}^2}{D} \mathbf{e}_{ij} \mathbf{e}_{ij} \cdot \mathbf{v}_{ij} \right] dt \\
 &\quad - \frac{1}{2} \sum_{j \in \mathcal{N}_i} \frac{1}{T_j} \left[\frac{A_{ij}^2}{2} (\mathbf{v}_{ij} + \mathbf{e}_{ij} \cdot \mathbf{v}_{ij} \mathbf{e}_{ij}) + \frac{B_{ij}^2 - A_{ij}^2}{D} \mathbf{e}_{ij} \mathbf{e}_{ij} \cdot \mathbf{v}_{ij} \right] dt \\
 &= - \frac{1}{2} \sum_{j \in \mathcal{N}_i} \left(\frac{1}{T_i} + \frac{1}{T_j} \right) \left[\frac{A_{ij}^2}{2} (\mathbf{v}_{ij} + \mathbf{e}_{ij} \cdot \mathbf{v}_{ij} \mathbf{e}_{ij}) + \frac{B_{ij}^2 - A_{ij}^2}{D} \mathbf{e}_{ij} \mathbf{e}_{ij} \cdot \mathbf{v}_{ij} \right] dt \\
 &= - \frac{1}{2} \sum_{j \in \mathcal{N}_i} \left(\frac{1}{T_i} + \frac{1}{T_j} \right) \left[\frac{A_{ij}^2}{2} \mathbf{v}_{ij} + \left(\frac{A_{ij}^2}{2} + \frac{B_{ij}^2 - A_{ij}^2}{D} \right) \mathbf{e}_{ij} \cdot \mathbf{v}_{ij} \mathbf{e}_{ij} \right] dt.
 \end{aligned}$$

$$\begin{aligned}
 T_i \sum_{j \in \mathcal{N}_i} \frac{d\tilde{\mathbf{S}}_i d\tilde{\mathbf{S}}_j}{2k_B} &= \sum_{j \in \mathcal{N}_i} \frac{1}{T_j} \delta_{ij} \sum_{k \in \mathcal{N}_i} \left(\frac{A_{ik}^2}{2} \left[\left(\frac{\mathbf{v}_{ik}}{2} \right)^2 + \left(\mathbf{e}_{ik} \cdot \frac{\mathbf{v}_{ik}}{2} \right)^2 \right] + \frac{B_{ik}^2 - A_{ik}^2}{D} \left(\mathbf{e}_{ik} \cdot \frac{\mathbf{v}_{ik}}{2} \right)^2 + C_{ik}^2 \right) dt \\
 &\quad + \sum_{j \in \mathcal{N}_i} \frac{1}{T_j} \left(\frac{A_{ij}^2}{2} \left[\left(\frac{\mathbf{v}_{ij}}{2} \right)^2 + \left(\mathbf{e}_{ij} \cdot \frac{\mathbf{v}_{ij}}{2} \right)^2 \right] + \frac{B_{ij}^2 - A_{ij}^2}{D} \left(\mathbf{e}_{ij} \cdot \frac{\mathbf{v}_{ij}}{2} \right)^2 - C_{ij}^2 \right) dt \\
 &= \frac{1}{T_i} \sum_{j \in \mathcal{N}_i} \left(\frac{A_{ij}^2}{2} \left[\left(\frac{\mathbf{v}_{ij}}{2} \right)^2 + \left(\mathbf{e}_{ij} \cdot \frac{\mathbf{v}_{ij}}{2} \right)^2 \right] + \frac{B_{ij}^2 - A_{ij}^2}{D} \left(\mathbf{e}_{ij} \cdot \frac{\mathbf{v}_{ij}}{2} \right)^2 + C_{ij}^2 \right) dt \\
 &\quad + \sum_{j \in \mathcal{N}_i} \frac{1}{T_j} \left(\frac{A_{ij}^2}{2} \left[\left(\frac{\mathbf{v}_{ij}}{2} \right)^2 + \left(\mathbf{e}_{ij} \cdot \frac{\mathbf{v}_{ij}}{2} \right)^2 \right] + \frac{B_{ij}^2 - A_{ij}^2}{D} \left(\mathbf{e}_{ij} \cdot \frac{\mathbf{v}_{ij}}{2} \right)^2 - C_{ij}^2 \right) dt \\
 &= \frac{1}{4} \sum_{j \in \mathcal{N}_i} \left(\frac{1}{T_i} + \frac{1}{T_j} \right) \left(\frac{A_{ij}^2}{2} [\mathbf{v}_{ij}^2 + (\mathbf{v}_{ij} \cdot \mathbf{e}_{ij})^2] + \frac{B_{ij}^2 - A_{ij}^2}{D} (\mathbf{v}_{ij} \cdot \mathbf{e}_{ij})^2 \right) dt + \sum_{j \in \mathcal{N}_i} \left(\frac{1}{T_i} - \frac{1}{T_j} \right) C_{ij}^2 dt
 \end{aligned}$$

$$= \frac{1}{4} \sum_{j \in \mathcal{N}_i} \left(\frac{1}{T_i} + \frac{1}{T_j} \right) \left[\frac{A_{ij}^2}{2} \mathbf{v}_{ij}^2 + \left(\frac{A_{ij}^2}{2} + \frac{B_{ij}^2 - A_{ij}^2}{D} \right) (\mathbf{v}_{ij} \cdot \mathbf{e}_{ij})^2 \right] dt + \sum_{j \in \mathcal{N}_i} \left(\frac{1}{T_i} - \frac{1}{T_j} \right) C_{ij}^2 dt.$$

Last, we derive the divergence terms $\nabla \cdot \mathbf{M}$. Note that we need to define the heat capacity at constant volume C_i as the following expression:

$$\frac{\partial T_i}{\partial S_i} = \frac{T_i}{C_i}.$$

We also need to establish the following divergence identities

$$\begin{aligned} \frac{\partial}{\partial \mathbf{v}_i} \cdot \mathbf{v}_{ij} &= \frac{\partial}{\partial \mathbf{v}_i} \cdot (\mathbf{v}_i - \mathbf{v}_j) = \frac{\partial}{\partial \mathbf{v}_i} \cdot \mathbf{v}_i = D, \\ \frac{\partial}{\partial \mathbf{v}_j} \cdot \mathbf{v}_{ij} &= \frac{\partial}{\partial \mathbf{v}_j} \cdot (\mathbf{v}_i - \mathbf{v}_j) = -\frac{\partial}{\partial \mathbf{v}_j} \cdot \mathbf{v}_j = -D, \\ \frac{\partial}{\partial \mathbf{v}_j} \cdot (\mathbf{e}_{ij} \cdot \mathbf{v}_{ij} \mathbf{e}_{ij}) &= \frac{\partial}{\partial \mathbf{v}_j^\beta} e_{ij}^\alpha v_{ij}^\alpha e_{ij}^\beta = -\frac{\partial}{\partial \mathbf{v}_j^\beta} e_{ij}^\alpha v_{ji}^\alpha e_{ij}^\beta = -\mathbf{e}_{ij}^\beta e_{ij}^\beta = -1, \end{aligned}$$

and usual derivatives

$$\frac{\partial}{\partial S_i} \left(\frac{1}{T_i} \right) = -\frac{1}{T_i C_i}, \quad \frac{\partial}{\partial S_i} \left(\frac{1}{T_i^2} \right) = -\frac{2}{T_i^2 C_i}, \quad \frac{\partial A_{ij}}{\partial S_i} = \frac{\partial A_{ij}}{\partial T_i} \frac{\partial T_i}{\partial S_i} = \frac{\partial A_{ij}}{\partial T_i} \frac{T_i}{C_i}.$$

Now we can compute the remaining terms:

$$\begin{aligned} m^2 \sum_{j \in \mathcal{N}_i} \frac{\partial}{\partial \mathbf{v}_j} \cdot \frac{d\tilde{\mathbf{v}}_i d\tilde{\mathbf{v}}_j^T}{2k_B} &= \sum_{j \in \mathcal{N}_i} \frac{\partial}{\partial \mathbf{v}_j} \cdot \delta_{ij} \sum_{k \in \mathcal{N}_i} \left[\frac{A_{ik}^2}{2} (\mathbf{I} + \mathbf{e}_{ik} \mathbf{e}_{ik}^T) + \frac{B_{ik}^2 - A_{ik}^2}{D} \mathbf{e}_{ik} \mathbf{e}_{ik}^T \right] dt \\ &\quad - \sum_{j \in \mathcal{N}_i} \frac{\partial}{\partial \mathbf{v}_j} \cdot \left[\frac{A_{ij}^2}{2} (\mathbf{I} + \mathbf{e}_{ij} \mathbf{e}_{ij}^T) + \frac{B_{ij}^2 - A_{ij}^2}{D} \mathbf{e}_{ij} \mathbf{e}_{ij}^T \right] dt = \mathbf{0}. \end{aligned}$$

$$\begin{aligned} m \sum_{j \in \mathcal{N}_i} \frac{\partial}{\partial S_j} \cdot \frac{d\tilde{\mathbf{v}}_i d\tilde{S}_j}{2k_B} &= - \sum_{j \in \mathcal{N}_i} \frac{\partial}{\partial S_j} \cdot \frac{1}{T_j} \delta_{ij} \sum_{k \in \mathcal{N}_i} \left[\frac{A_{ik}^2}{2} \left(\frac{\mathbf{v}_{ik}}{2} + \mathbf{e}_{ik} \cdot \frac{\mathbf{v}_{ik}}{2} \mathbf{e}_{ik} \right) + \frac{B_{ik}^2 - A_{ik}^2}{D} \mathbf{e}_{ik} \mathbf{e}_{ik} \cdot \frac{\mathbf{v}_{ik}}{2} \right] dt \\ &\quad - \sum_{j \in \mathcal{N}_i} \frac{\partial}{\partial S_j} \cdot \frac{1}{T_j} \left[\frac{A_{ij}^2}{2} \left(\frac{\mathbf{v}_{ij}}{2} + \mathbf{e}_{ij} \cdot \frac{\mathbf{v}_{ij}}{2} \mathbf{e}_{ij} \right) + \frac{B_{ij}^2 - A_{ij}^2}{D} \mathbf{e}_{ij} \mathbf{e}_{ij} \cdot \frac{\mathbf{v}_{ij}}{2} \right] dt \\ &= -\frac{1}{2} \frac{\partial}{\partial S_i} \cdot \frac{1}{T_i} \sum_{j \in \mathcal{N}_i} \left[\frac{A_{ij}^2}{2} (\mathbf{v}_{ij} + \mathbf{e}_{ij} \cdot \mathbf{v}_{ij} \mathbf{e}_{ij}) + \frac{B_{ij}^2 - A_{ij}^2}{D} \mathbf{e}_{ij} \mathbf{e}_{ij} \cdot \mathbf{v}_{ij} \right] dt \\ &\quad - \frac{1}{2} \sum_{j \in \mathcal{N}_i} \frac{\partial}{\partial S_j} \cdot \frac{1}{T_j} \left[\frac{A_{ij}^2}{2} (\mathbf{v}_{ij} + \mathbf{e}_{ij} \cdot \mathbf{v}_{ij} \mathbf{e}_{ij}) + \frac{B_{ij}^2 - A_{ij}^2}{D} \mathbf{e}_{ij} \mathbf{e}_{ij} \cdot \mathbf{v}_{ij} \right] dt \\ &= \frac{1}{2} \sum_{j \in \mathcal{N}_i} \left(\frac{1}{T_i C_i} + \frac{1}{T_j C_j} \right) \left[\frac{A_{ij}^2}{2} \mathbf{v}_{ij} + \left(\frac{A_{ij}^2}{2} + \frac{B_{ij}^2 - A_{ij}^2}{D} \right) \mathbf{e}_{ij} \cdot \mathbf{v}_{ij} \mathbf{e}_{ij} \right] dt \\ &\quad - \frac{1}{2} \sum_{j \in \mathcal{N}_i} \frac{1}{T_i} \left[A_{ij} \frac{\partial A_{ij}}{\partial S_i} \mathbf{v}_{ij} + \left(A_{ij} \frac{\partial A_{ij}}{\partial S_i} + \frac{2}{D} B_{ij} \frac{\partial B_{ij}}{\partial S_i} - \frac{2}{D} A_{ij} \frac{\partial A_{ij}}{\partial S_i} \right) \mathbf{e}_{ij} \cdot \mathbf{v}_{ij} \mathbf{e}_{ij} \right] dt \\ &\quad - \frac{1}{2} \sum_{j \in \mathcal{N}_i} \frac{1}{T_j} \left[A_{ij} \frac{\partial A_{ij}}{\partial S_j} \mathbf{v}_{ij} + \left(A_{ij} \frac{\partial A_{ij}}{\partial S_j} + \frac{2}{D} B_{ij} \frac{\partial B_{ij}}{\partial S_j} - \frac{2}{D} A_{ij} \frac{\partial A_{ij}}{\partial S_j} \right) \mathbf{e}_{ij} \cdot \mathbf{v}_{ij} \mathbf{e}_{ij} \right] dt \\ &= \frac{1}{2} \sum_{j \in \mathcal{N}_i} \left(\frac{1}{T_i C_i} + \frac{1}{T_j C_j} \right) \left[\frac{A_{ij}^2}{2} \mathbf{v}_{ij} + \left(\frac{A_{ij}^2}{2} + \frac{B_{ij}^2 - A_{ij}^2}{D} \right) \mathbf{e}_{ij} \cdot \mathbf{v}_{ij} \mathbf{e}_{ij} \right] dt \\ &\quad - \frac{1}{2} \sum_{j \in \mathcal{N}_i} \frac{1}{C_i} \left[A_{ij} \frac{\partial A_{ij}}{\partial T_i} \mathbf{v}_{ij} + \left(A_{ij} \frac{\partial A_{ij}}{\partial T_i} + \frac{2}{D} B_{ij} \frac{\partial B_{ij}}{\partial T_i} - \frac{2}{D} A_{ij} \frac{\partial A_{ij}}{\partial T_i} \right) \mathbf{e}_{ij} \cdot \mathbf{v}_{ij} \mathbf{e}_{ij} \right] dt \end{aligned}$$

$$-\frac{1}{2} \sum_{j \in \mathcal{N}_i} \frac{1}{C_j} \left[A_{ij} \frac{\partial A_{ij}}{\partial T_j} \mathbf{v}_{ij} + \left(A_{ij} \frac{\partial A_{ij}}{\partial T_j} + \frac{2}{D} B_{ij} \frac{\partial B_{ij}}{\partial T_j} - \frac{2}{D} A_{ij} \frac{\partial A_{ij}}{\partial T_j} \right) \mathbf{e}_{ij} \cdot \mathbf{v}_{ij} \mathbf{e}_{ij} \right] dt$$

$$\begin{aligned} T_i \sum_{j \in \mathcal{N}_i} \frac{\partial}{\partial \mathbf{v}_j} \cdot \frac{d\tilde{S}_i d\tilde{\mathbf{v}}_j^T}{2k_B} &= - \sum_{j \in \mathcal{N}_i} \frac{\partial}{\partial \mathbf{v}_j} \cdot \frac{1}{m} \delta_{ij} \sum_{k \in \mathcal{N}_i} \left[\frac{A_{ik}^2}{2} \left(\frac{\mathbf{v}_{ik}}{2} + \mathbf{e}_{ik} \cdot \frac{\mathbf{v}_{ik}}{2} \mathbf{e}_{ik} \right) + \frac{B_{ik}^2 - A_{ik}^2}{D} \mathbf{e}_{ik} \mathbf{e}_{ik} \cdot \frac{\mathbf{v}_{ik}}{2} \right] dt \\ &+ \sum_{j \in \mathcal{N}_i} \frac{\partial}{\partial \mathbf{v}_j} \cdot \frac{1}{m} \left[\frac{A_{ij}^2}{2} \left(\frac{\mathbf{v}_{ij}}{2} + \mathbf{e}_{ij} \cdot \frac{\mathbf{v}_{ij}}{2} \mathbf{e}_{ij} \right) + \frac{B_{ij}^2 - A_{ij}^2}{D} \mathbf{e}_{ij} \mathbf{e}_{ij} \cdot \frac{\mathbf{v}_{ij}}{2} \right] dt \\ &= -\frac{1}{2m} \frac{\partial}{\partial \mathbf{v}_i} \cdot \sum_{j \in \mathcal{N}_i} \left[\frac{A_{ij}^2}{2} (\mathbf{v}_{ij} + \mathbf{e}_{ij} \cdot \mathbf{v}_{ij} \mathbf{e}_{ij}) + \frac{B_{ij}^2 - A_{ij}^2}{D} \mathbf{e}_{ij} \mathbf{e}_{ij} \cdot \mathbf{v}_{ij} \right] dt \\ &+ \frac{1}{2m} \sum_{j \in \mathcal{N}_i} \frac{\partial}{\partial \mathbf{v}_j} \cdot \left[\frac{A_{ij}^2}{2} (\mathbf{v}_{ij} + \mathbf{e}_{ij} \cdot \mathbf{v}_{ij} \mathbf{e}_{ij}) + \frac{B_{ij}^2 - A_{ij}^2}{D} \mathbf{e}_{ij} \mathbf{e}_{ij} \cdot \mathbf{v}_{ij} \right] dt \\ &= -\frac{1}{m} \sum_{j \in \mathcal{N}_i} \left[(D+1) \frac{A_{ij}^2}{2} + \frac{B_{ij}^2 - A_{ij}^2}{D} \right] dt. \end{aligned}$$

$$\begin{aligned} \sum_{j \in \mathcal{N}_i} \frac{\partial}{\partial S_j} \cdot \frac{d\tilde{S}_i d\tilde{S}_j}{2k_B} &= \sum_{j \in \mathcal{N}_i} \frac{\partial}{\partial S_j} \cdot \frac{1}{T_i T_j} \delta_{ij} \sum_{k \in \mathcal{N}_i} \left(\frac{A_{ik}^2}{2} \left[\left(\frac{\mathbf{v}_{ik}}{2} \right)^2 + \left(\mathbf{e}_{ik} \cdot \frac{\mathbf{v}_{ik}}{2} \right)^2 \right] + \frac{B_{ik}^2 - A_{ik}^2}{D} \left(\mathbf{e}_{ik} \cdot \frac{\mathbf{v}_{ik}}{2} \right)^2 + C_{ik}^2 \right) dt \\ &+ \sum_{j \in \mathcal{N}_i} \frac{\partial}{\partial S_j} \cdot \frac{1}{T_i T_j} \left(\frac{A_{ij}^2}{2} \left[\left(\frac{\mathbf{v}_{ij}}{2} \right)^2 + \left(\mathbf{e}_{ij} \cdot \frac{\mathbf{v}_{ij}}{2} \right)^2 \right] + \frac{B_{ij}^2 - A_{ij}^2}{D} \left(\mathbf{e}_{ij} \cdot \frac{\mathbf{v}_{ij}}{2} \right)^2 - C_{ij}^2 \right) dt \\ &= \frac{\partial}{\partial S_i} \cdot \frac{1}{T_i^2} \sum_{j \in \mathcal{N}_i} \left(\frac{A_{ij}^2}{2} \left[\left(\frac{\mathbf{v}_{ij}}{2} \right)^2 + \left(\mathbf{e}_{ij} \cdot \frac{\mathbf{v}_{ij}}{2} \right)^2 \right] + \frac{B_{ij}^2 - A_{ij}^2}{D} \left(\mathbf{e}_{ij} \cdot \frac{\mathbf{v}_{ij}}{2} \right)^2 + C_{ij}^2 \right) dt \\ &+ \sum_{j \in \mathcal{N}_i} \frac{\partial}{\partial S_j} \cdot \frac{1}{T_i T_j} \left(\frac{A_{ij}^2}{2} \left[\left(\frac{\mathbf{v}_{ij}}{2} \right)^2 + \left(\mathbf{e}_{ij} \cdot \frac{\mathbf{v}_{ij}}{2} \right)^2 \right] + \frac{B_{ij}^2 - A_{ij}^2}{D} \left(\mathbf{e}_{ij} \cdot \frac{\mathbf{v}_{ij}}{2} \right)^2 - C_{ij}^2 \right) dt \\ &= -\frac{1}{4T_i} \sum_{j \in \mathcal{N}_i} \left(\frac{2}{T_i C_i} + \frac{1}{T_j C_j} \right) \left[\frac{A_{ij}^2}{2} \mathbf{v}_{ij}^2 + \left(\frac{A_{ij}^2}{2} + \frac{B_{ij}^2 - A_{ij}^2}{D} \right) (\mathbf{v}_{ij} \cdot \mathbf{e}_{ij})^2 \right] dt \\ &- \frac{1}{T_i} \sum_{j \in \mathcal{N}_i} \left(\frac{2}{T_i C_i} - \frac{1}{T_j C_j} \right) C_{ij}^2 dt \\ &+ \frac{1}{4T_i} \sum_{j \in \mathcal{N}_i} \frac{1}{T_i} \left[A_{ij} \frac{\partial A_{ij}}{\partial S_i} \mathbf{v}_{ij}^2 + \left(A_{ij} \frac{\partial A_{ij}}{\partial S_i} + \frac{2}{D} B_{ij} \frac{\partial B_{ij}}{\partial S_i} - \frac{2}{D} A_{ij} \frac{\partial A_{ij}}{\partial S_i} \right) (\mathbf{v}_{ij} \cdot \mathbf{e}_{ij})^2 \right] dt \\ &+ \frac{1}{4T_i} \sum_{j \in \mathcal{N}_i} \frac{1}{T_j} \left[A_{ij} \frac{\partial A_{ij}}{\partial S_j} \mathbf{v}_{ij}^2 + \left(A_{ij} \frac{\partial A_{ij}}{\partial S_j} + \frac{2}{D} B_{ij} \frac{\partial B_{ij}}{\partial S_j} - \frac{2}{D} A_{ij} \frac{\partial A_{ij}}{\partial S_j} \right) (\mathbf{v}_{ij} \cdot \mathbf{e}_{ij})^2 \right] dt \\ &+ \frac{1}{T_i} \sum_{j \in \mathcal{N}_i} \left(\frac{1}{T_i} 2C_{ij} \frac{\partial C_{ij}}{\partial S_i} - \frac{1}{T_j} 2C_{ij} \frac{\partial C_{ij}}{\partial S_j} \right) dt \\ &= -\frac{1}{4T_i} \sum_{j \in \mathcal{N}_i} \left(\frac{2}{T_i C_i} + \frac{1}{T_j C_j} \right) \left[\frac{A_{ij}^2}{2} \mathbf{v}_{ij}^2 + \left(\frac{A_{ij}^2}{2} + \frac{B_{ij}^2 - A_{ij}^2}{D} \right) (\mathbf{v}_{ij} \cdot \mathbf{e}_{ij})^2 \right] dt \\ &- \frac{1}{T_i} \sum_{j \in \mathcal{N}_i} \left(\frac{2}{T_i C_i} - \frac{1}{T_j C_j} \right) C_{ij}^2 dt \\ &+ \frac{1}{4T_i} \sum_{j \in \mathcal{N}_i} \frac{1}{C_i} \left[A_{ij} \frac{\partial A_{ij}}{\partial T_i} \mathbf{v}_{ij}^2 + \left(A_{ij} \frac{\partial A_{ij}}{\partial T_i} + \frac{2}{D} B_{ij} \frac{\partial B_{ij}}{\partial T_i} - \frac{2}{D} A_{ij} \frac{\partial A_{ij}}{\partial T_i} \right) (\mathbf{v}_{ij} \cdot \mathbf{e}_{ij})^2 \right] dt \\ &+ \frac{1}{4T_i} \sum_{j \in \mathcal{N}_i} \frac{1}{C_j} \left[A_{ij} \frac{\partial A_{ij}}{\partial T_j} \mathbf{v}_{ij}^2 + \left(A_{ij} \frac{\partial A_{ij}}{\partial T_j} + \frac{2}{D} B_{ij} \frac{\partial B_{ij}}{\partial T_j} - \frac{2}{D} A_{ij} \frac{\partial A_{ij}}{\partial T_j} \right) (\mathbf{v}_{ij} \cdot \mathbf{e}_{ij})^2 \right] dt \end{aligned}$$

$$+ \frac{2}{T_i} \sum_{j \in \mathcal{N}_i} \left(\frac{1}{C_i} C_{ij} \frac{\partial C_{ij}}{\partial T_i} - \frac{1}{C_j} C_{ij} \frac{\partial C_{ij}}{\partial T_j} \right) dt.$$

A.3 Complete equations

With the parameterization specified we finally can summarize the dynamic equations of the method.

$$\begin{aligned} d\mathbf{r}_i &= \mathbf{v}_i dt, \\ m d\mathbf{v}_i &= \sum_{j \in \mathcal{N}_i} \left[\frac{P_j}{d_j^2} \frac{\partial W_{ji}}{\partial \mathbf{r}_{ji}} - \frac{P_i}{d_i^2} \frac{\partial W_{ij}}{\partial \mathbf{r}_{ij}} \right] dt + \sum_j \left[\tau_j \frac{\partial \bar{W}_{ji}}{\partial \mathbf{u}_{ji}} - \tau_i \frac{\partial \bar{W}_{ij}}{\partial \mathbf{u}_{ij}} \right] \\ &\quad - \frac{1}{2} \sum_{j \in \mathcal{N}_i} \left(\frac{1}{T_i} + \frac{1}{T_j} \right) \left[\frac{A_{ij}^2}{2} \mathbf{v}_{ij} + \left(\frac{A_{ij}^2}{2} + \frac{B_{ij}^2 - A_{ij}^2}{D} \right) \mathbf{e}_{ij} \cdot \mathbf{v}_{ij} \mathbf{e}_{ij} \right] dt \\ &\quad + \frac{k_B}{2} \sum_{j \in \mathcal{N}_i} \left(\frac{1}{T_i C_i} + \frac{1}{T_j C_j} \right) \left[\frac{A_{ij}^2}{2} \mathbf{v}_{ij} + \left(\frac{A_{ij}^2}{2} + \frac{B_{ij}^2 - A_{ij}^2}{D} \right) \mathbf{e}_{ij} \cdot \mathbf{v}_{ij} \mathbf{e}_{ij} \right] dt \\ &\quad - \frac{k_B}{2} \sum_{j \in \mathcal{N}_i} \frac{1}{C_i} \left[A_{ij} \frac{\partial A_{ij}}{\partial T_i} \mathbf{v}_{ij} + \left(A_{ij} \frac{\partial A_{ij}}{\partial T_i} + \frac{2}{D} B_{ij} \frac{\partial B_{ij}}{\partial T_i} - \frac{2}{D} A_{ij} \frac{\partial A_{ij}}{\partial T_i} \right) \mathbf{e}_{ij} \cdot \mathbf{v}_{ij} \mathbf{e}_{ij} \right] dt \\ &\quad - \frac{k_B}{2} \sum_{j \in \mathcal{N}_i} \frac{1}{C_j} \left[A_{ij} \frac{\partial A_{ij}}{\partial T_j} \mathbf{v}_{ij} + \left(A_{ij} \frac{\partial A_{ij}}{\partial T_j} + \frac{2}{D} B_{ij} \frac{\partial B_{ij}}{\partial T_j} - \frac{2}{D} A_{ij} \frac{\partial A_{ij}}{\partial T_j} \right) \mathbf{e}_{ij} \cdot \mathbf{v}_{ij} \mathbf{e}_{ij} \right] dt \\ &\quad + \sqrt{2k_B} \sum_{j \in \mathcal{N}_i} \left[A_{ij} d\bar{W}_{ij} + B_{ij} \frac{1}{D} \text{tr}(d\mathbf{W}_{ij}) \right] \mathbf{e}_{ij}, \\ T_i dS_i &= \frac{1}{4} \sum_{j \in \mathcal{N}_i} \left(\frac{1}{T_i} + \frac{1}{T_j} \right) \left[\frac{A_{ij}^2}{2} \mathbf{v}_{ij}^2 + \left(\frac{A_{ij}^2}{2} + \frac{B_{ij}^2 - A_{ij}^2}{D} \right) (\mathbf{v}_{ij} \cdot \mathbf{e}_{ij})^2 \right] dt + \sum_{j \in \mathcal{N}_i} \left(\frac{1}{T_i} - \frac{1}{T_j} \right) C_{ij}^2 dt \\ &\quad - \frac{k_B}{m} \sum_{j \in \mathcal{N}_i} \left[(D+1) \frac{A_{ij}^2}{2} + \frac{B_{ij}^2 - A_{ij}^2}{D} \right] dt \\ &\quad - \frac{k_B}{4} \sum_{j \in \mathcal{N}_i} \left(\frac{2}{T_i C_i} + \frac{1}{T_j C_j} \right) \left[\frac{A_{ij}^2}{2} \mathbf{v}_{ij}^2 + \left(\frac{A_{ij}^2}{2} + \frac{B_{ij}^2 - A_{ij}^2}{D} \right) (\mathbf{v}_{ij} \cdot \mathbf{e}_{ij})^2 \right] dt - k_B \sum_{j \in \mathcal{N}_i} \left(\frac{2}{T_i C_i} - \frac{1}{T_j C_j} \right) C_{ij}^2 dt \\ &\quad + \frac{k_B}{4} \sum_{j \in \mathcal{N}_i} \frac{1}{C_i} \left[A_{ij} \frac{\partial A_{ij}}{\partial T_i} \mathbf{v}_{ij}^2 + \left(A_{ij} \frac{\partial A_{ij}}{\partial T_i} + \frac{2}{D} B_{ij} \frac{\partial B_{ij}}{\partial T_i} - \frac{2}{D} A_{ij} \frac{\partial A_{ij}}{\partial T_i} \right) (\mathbf{v}_{ij} \cdot \mathbf{e}_{ij})^2 \right] dt \\ &\quad + \frac{k_B}{4} \sum_{j \in \mathcal{N}_i} \frac{1}{C_j} \left[A_{ij} \frac{\partial A_{ij}}{\partial T_j} \mathbf{v}_{ij}^2 + \left(A_{ij} \frac{\partial A_{ij}}{\partial T_j} + \frac{2}{D} B_{ij} \frac{\partial B_{ij}}{\partial T_j} - \frac{2}{D} A_{ij} \frac{\partial A_{ij}}{\partial T_j} \right) (\mathbf{v}_{ij} \cdot \mathbf{e}_{ij})^2 \right] dt \\ &\quad + 2k_B \sum_{j \in \mathcal{N}_i} \left(\frac{1}{C_i} C_{ij} \frac{\partial C_{ij}}{\partial T_i} - \frac{1}{C_j} C_{ij} \frac{\partial C_{ij}}{\partial T_j} \right) dt \\ &\quad - \frac{\sqrt{2k_B}}{2} \sum_{j \in \mathcal{N}_i} \left[A_{ij} d\bar{W}_{ij} + B_{ij} \frac{1}{D} \text{tr}(d\mathbf{W}_{ij}) \right] : \mathbf{e}_{ij} \mathbf{v}_{ij} + \sqrt{2k_B} \sum_{j \in \mathcal{N}_i} C_{ij} dV_{ij}. \end{aligned}$$

In the next section we prove that the proposed methodology fulfills the required thermodynamics and conservation laws.

B Conservation laws

Proposition B.1. *The metriplectic equation in Eq. (4) satisfies momentum conservation $d\mathbf{P} = \mathbf{0}$.*

Proof. This is a direct consequence of the skew-symmetry of the particle pair forces over index swapping. The total deterministic momentum over all particles is $\mathbf{P} = \sum_i m \mathbf{v}_i$. By using Itô's lemma, we have that:

$$d\mathbf{P} = \frac{\partial \mathbf{P}}{\partial \mathbf{x}} \cdot d\mathbf{x} + \frac{1}{2} \frac{\partial^2 \mathbf{P}}{\partial \mathbf{x}^2} : d\tilde{\mathbf{x}} d\tilde{\mathbf{x}}^T,$$

which is equivalent, by using the fluctuation dissipation theorem, to

$$d\mathbf{P} = \frac{\partial \mathbf{P}}{\partial \mathbf{x}} \cdot d\mathbf{x} + k_B \frac{\partial^2 \mathbf{P}}{\partial \mathbf{x}^2} : \mathbf{M} = \frac{\partial \mathbf{P}}{\partial \mathbf{x}} \cdot \left[\left(\mathbf{L} \frac{\partial E}{\partial \mathbf{x}} + \mathbf{M} \frac{\partial S}{\partial \mathbf{x}} + k_B \frac{\partial}{\partial \mathbf{x}} \cdot \mathbf{M} \right) dt + d\tilde{\mathbf{x}} \right] + k_B \frac{\partial^2 \mathbf{P}}{\partial \mathbf{x}^2} : \mathbf{M}.$$

We now show each summand is zero. The first term, by expanding the gradient of the internal energy from Eq. (13):

$$\frac{\partial \mathbf{P}}{\partial \mathbf{x}} \cdot \mathbf{L} \frac{\partial E}{\partial \mathbf{x}} = \sum_i [0, m\mathbf{1}, 0] \frac{1}{m} \begin{bmatrix} m\mathbf{v}_i \\ -\frac{\partial U}{\partial \mathbf{r}_i} \\ 0 \end{bmatrix} = \sum_i -\frac{\partial U}{\partial \mathbf{r}_i} = \sum_i \sum_{j \in \mathcal{N}_i} \left[\frac{P_j}{d_j^2} \frac{\partial W_{ji}}{\partial \mathbf{r}_{ji}} - \frac{P_i}{d_i^2} \frac{\partial W_{ij}}{\partial \mathbf{r}_{ij}} + \boldsymbol{\tau}_j : \frac{\partial \bar{\mathbf{W}}_{ji}}{\partial \mathbf{u}_{ji}} - \boldsymbol{\tau}_i : \frac{\partial \bar{\mathbf{W}}_{ij}}{\partial \mathbf{u}_{ij}} \right].$$

As the particle interactions are defined within a fixed neighbourhood \mathcal{N}_i for each particle, we can split the set of interactions in three subsets: $\{(i, j)\} = \{(i', j')\} \cup \{(j', i')\} \cup \{(i', i')\}$. This means that every particle interaction (i', j') has a mirror interaction with swapped indices (j', i') for $i' \neq j'$, as well as self interactions of a particle with itself (i', i') when $i' = j'$. The position vectors are $\mathbf{r}_{i'j'} = -\mathbf{r}_{j'i'}$ and $\mathbf{r}_{i'i'} = \mathbf{0}$ respectively. By applying the index swapping to the derivative and the condition of a spherical symmetric kernel $\nabla W(\mathbf{0}) = \mathbf{0}$, we get the following split sum:

$$\begin{aligned} \frac{\partial \mathbf{P}}{\partial \mathbf{x}} \cdot \mathbf{L} \frac{\partial E}{\partial \mathbf{x}} &= \sum_{i', j'} \left[\frac{P_{j'}}{d_{j'}^2} \frac{\partial W_{j'i'}}{\partial \mathbf{r}_{j'i'}} - \frac{P_{i'}}{d_{i'}^2} \frac{\partial W_{i'j'}}{\partial \mathbf{r}_{i'j'}} \right] + \sum_{j', i'} \left[\frac{P_{i'}}{d_{i'}^2} \frac{\partial W_{i'j'}}{\partial \mathbf{r}_{i'j'}} - \frac{P_{j'}}{d_{j'}^2} \frac{\partial W_{j'i'}}{\partial \mathbf{r}_{j'i'}} \right] + \sum_{i', i'} 2 \frac{P_{i'}}{d_{i'}^2} \frac{\partial W_{i'i'}}{\partial \mathbf{r}_{i'i'}} \\ &+ \sum_{i', j'} \left[\boldsymbol{\tau}_{j'} : \frac{\partial \bar{\mathbf{W}}_{j'i'}}{\partial \mathbf{u}_{j'i'}} - \boldsymbol{\tau}_{i'} : \frac{\partial \bar{\mathbf{W}}_{i'j'}}{\partial \mathbf{u}_{i'j'}} \right] + \sum_{j', i'} \left[\boldsymbol{\tau}_{i'} : \frac{\partial \bar{\mathbf{W}}_{i'j'}}{\partial \mathbf{u}_{i'j'}} - \boldsymbol{\tau}_{j'} : \frac{\partial \bar{\mathbf{W}}_{j'i'}}{\partial \mathbf{u}_{j'i'}} \right] + \mathbf{0} = \mathbf{0}. \end{aligned}$$

We can gather the divergence and second order term into a single divergence term

$$\frac{\partial \mathbf{P}}{\partial \mathbf{x}} \cdot k_B \frac{\partial}{\partial \mathbf{x}} \cdot \mathbf{M} + k_B \frac{\partial^2 \mathbf{P}}{\partial \mathbf{x}^2} : \mathbf{M} = k_B \frac{\partial}{\partial \mathbf{x}} \cdot \left(\mathbf{M} \frac{\partial \mathbf{P}}{\partial \mathbf{x}} \right) = \mathbf{0}.$$

By decomposing \mathbf{M} on its dyadic $d\mathbf{x}d\mathbf{x}^T = 2k_B \mathbf{M} dt$ we get that the sufficient condition is that $\frac{\partial \mathbf{P}}{\partial \mathbf{x}} \cdot d\tilde{\mathbf{x}} = \mathbf{0}$. By expanding and using the noise ansatz,

$$\frac{\partial \mathbf{P}}{\partial \mathbf{x}} \cdot d\tilde{\mathbf{x}} = \sum_i [0, m\mathbf{1}, 0] \begin{bmatrix} \mathbf{0} \\ d\tilde{\mathbf{v}}_i \\ d\tilde{S}_i \end{bmatrix} = \sum_i m d\tilde{\mathbf{v}}_i = \sum_i \sqrt{2k_B} \sum_{j \in \mathcal{N}_i} \left[A_{ij} d\bar{\mathbf{W}}_{ij} + B_{ij} \frac{1}{D} \text{tr}(d\mathbf{W}_{ij}) \right] \mathbf{e}_{ij}.$$

We obtain the desired cancellation by a similar reasoning as before: pairwise interactions cancel out due to the symmetries of A_{ij} , B_{ij} and $d\mathbf{W}_{ij}$ and skew-symmetry of the interdistance unit vectors $\mathbf{e}_{ij} = -\mathbf{e}_{ji}$ and $\mathbf{e}_{ii} = \mathbf{0}$. Thus, the fluctuating velocities do not contribute to the total momentum.

$$\begin{aligned} \frac{\partial \mathbf{P}}{\partial \mathbf{x}} \cdot d\tilde{\mathbf{x}} &= \sqrt{2k_B} \sum_{i', j'} \left[A_{i'j'} d\bar{\mathbf{W}}_{i'j'} + B_{i'j'} \frac{1}{D} \text{tr}(d\mathbf{W}_{i'j'}) \right] \mathbf{e}_{i'j'} + \sqrt{2k_B} \sum_{j', i'} \left[A_{j'i'} d\bar{\mathbf{W}}_{j'i'} + B_{j'i'} \frac{1}{D} \text{tr}(d\mathbf{W}_{j'i'}) \right] \mathbf{e}_{j'i'} \\ &+ \sqrt{2k_B} \sum_{i', i'} \left[A_{i'i'} d\bar{\mathbf{W}}_{i'i'} + B_{i'i'} \frac{1}{D} \text{tr}(d\mathbf{W}_{i'i'}) \right] \mathbf{e}_{i'i'} \\ &= \sqrt{2k_B} \sum_{i', j'} \left[A_{i'j'} d\bar{\mathbf{W}}_{i'j'} + B_{i'j'} \frac{1}{D} \text{tr}(d\mathbf{W}_{i'j'}) \right] \mathbf{e}_{i'j'} - \sqrt{2k_B} \sum_{i', j'} \left[A_{i'j'} d\bar{\mathbf{W}}_{i'j'} + B_{i'j'} \frac{1}{D} \text{tr}(d\mathbf{W}_{i'j'}) \right] \mathbf{e}_{i'j'} = \mathbf{0}. \end{aligned}$$

The second and fourth terms are $\mathbf{M} \frac{\partial \mathbf{P}}{\partial \mathbf{x}}$ and $\frac{\partial \mathbf{P}}{\partial \mathbf{x}} \cdot d\tilde{\mathbf{x}}$ respectively, already proven to be zero. □

Proposition B.2. Eq. (4) satisfies energy conservation $dE = 0$ if $\mathbf{M} \nabla E = \mathbf{0}$ and $d\tilde{\mathbf{x}} \cdot \nabla E = 0$.

Proof. By Itô's lemma, we have that

$$dE = \frac{\partial E}{\partial \mathbf{x}} \cdot d\mathbf{x} + \frac{1}{2} \frac{\partial^2 E}{\partial \mathbf{x}^2} : d\tilde{\mathbf{x}}d\tilde{\mathbf{x}}^T,$$

which is equivalent, by using the fluctuation dissipation theorem, to

$$dE = \frac{\partial E}{\partial \mathbf{x}} \cdot d\mathbf{x} + k_B \frac{\partial^2 E}{\partial \mathbf{x}^2} : \mathbf{M} = \frac{\partial E}{\partial \mathbf{x}} \cdot \left[\left(\mathbf{L} \frac{\partial E}{\partial \mathbf{x}} + \mathbf{M} \frac{\partial S}{\partial \mathbf{x}} + k_B \frac{\partial}{\partial \mathbf{x}} \cdot \mathbf{M} \right) dt + d\tilde{\mathbf{x}} \right] + k_B \frac{\partial^2 E}{\partial \mathbf{x}^2} : \mathbf{M}.$$

We now show each summand is zero.

Due to the skew-symmetry of \mathbf{L} we have that the first summand is

$$\frac{\partial E}{\partial \mathbf{x}} \cdot \mathbf{L} \frac{\partial E}{\partial \mathbf{x}} = 0.$$

For the second, following the symmetric positive semi-definiteness and degeneracy condition for \mathbf{M}

$$\frac{\partial E}{\partial \mathbf{x}} \cdot \mathbf{M} \frac{\partial S}{\partial \mathbf{x}} = \frac{\partial S}{\partial \mathbf{x}} \cdot \mathbf{M} \frac{\partial E}{\partial \mathbf{x}} = 0.$$

We can gather the divergence and second order term into a single divergence which can be cancelled via the degeneracy condition

$$\frac{\partial E}{\partial \mathbf{x}} \cdot k_B \frac{\partial}{\partial \mathbf{x}} \cdot \mathbf{M} + k_B \frac{\partial^2 E}{\partial \mathbf{x}^2} : \mathbf{M} = k_B \frac{\partial}{\partial \mathbf{x}} \cdot \left(\mathbf{M} \frac{\partial E}{\partial \mathbf{x}} \right) = 0.$$

The final stochastic differential term is zero by assumption:

$$\frac{\partial E}{\partial \mathbf{x}} \cdot d\tilde{\mathbf{x}} = d\tilde{\mathbf{x}} \cdot \frac{\partial E}{\partial \mathbf{x}} = 0.$$

□

Proposition B.3. *The metriplectic equation in Eq. (4) satisfies the degeneracy conditions $\mathbf{L}\nabla S = \mathbf{M}\nabla E = \mathbf{0}$ and $d\tilde{\mathbf{x}} \cdot \nabla E = 0$, thus it satisfies energy conservation.*

Proof. The first degeneracy condition is satisfied trivially by the definition of the entropy as a state variable and the zero block structure of the Poisson matrix,

$$\mathbf{L} \frac{\partial S}{\partial \mathbf{x}} = \sum_{j \in \mathcal{N}_i} \frac{1}{m} \begin{bmatrix} \mathbf{0} & -\mathbf{I}\delta_{ij} & \mathbf{0} \\ \mathbf{I}\delta_{ij} & \mathbf{0} & \mathbf{0} \\ \mathbf{0} & \mathbf{0} & \mathbf{0} \end{bmatrix} \begin{bmatrix} \mathbf{0} \\ \mathbf{0} \\ 1 \end{bmatrix} = \mathbf{0}.$$

For the second degeneracy, we need to use the factorization of the friction matrix into the dyadic of the noise differentials $d\mathbf{x}d\mathbf{x}^T = 2k_B \mathbf{M} dt$ in the following way,

$$d\tilde{\mathbf{x}}d\tilde{\mathbf{x}}^T \frac{\partial E}{\partial \mathbf{x}} = 2k_B \mathbf{M} dt \frac{\partial E}{\partial \mathbf{x}}.$$

Now we can prove that the left term is equal to zero, which also holds for the right term. Considering that $2k_B dt \neq 0$, it implies that the second degeneracy is zero. By applying the definition of ∇E and expanding the relative velocity $\mathbf{v}_{ij} = \mathbf{v}_i - \mathbf{v}_j$ we get

$$\begin{aligned} d\tilde{\mathbf{x}} \cdot \frac{\partial E}{\partial \mathbf{x}} &= \sum_i \left[\mathbf{0}, d\tilde{\mathbf{v}}_i, d\tilde{S}_i \right] \begin{bmatrix} -\frac{\partial U}{\partial \mathbf{r}_i} \\ m\mathbf{v}_i \\ T_i \end{bmatrix} = \sum_i (m\mathbf{v}_i \cdot d\tilde{\mathbf{v}}_i + T_i d\tilde{S}_i) = \sum_i \mathbf{v}_i \cdot \sqrt{2k_B} \sum_{j \in \mathcal{N}_i} [A_{ij} d\bar{\mathbf{W}}_{ij} + B_{ij} \frac{1}{D} \text{tr}(d\mathbf{W}_{ij})] \mathbf{e}_{ij} \\ &+ \sum_i -\frac{\sqrt{2k_B}}{2} \sum_{j \in \mathcal{N}_i} \left[A_{ij} d\bar{\mathbf{W}}_{ij} + B_{ij} \frac{1}{D} \text{tr}(d\mathbf{W}_{ij}) \right] : \mathbf{e}_{ij} \mathbf{v}_{ij} + \sum_i \sqrt{2k_B} \sum_{j \in \mathcal{N}_i} C_{ij} dV_{ij} \\ &= \sqrt{2k_B} \sum_{i,j} \left[A_{ij} d\bar{\mathbf{W}}_{ij} + B_{ij} \frac{1}{D} \text{tr}(d\mathbf{W}_{ij}) \right] \mathbf{e}_{ij} \cdot \mathbf{v}_i - \frac{\sqrt{2k_B}}{2} \sum_{i,j} \left[A_{ij} d\bar{\mathbf{W}}_{ij} + B_{ij} \frac{1}{D} \text{tr}(d\mathbf{W}_{ij}) \right] \mathbf{e}_{ij} \cdot \mathbf{v}_i \\ &+ \frac{\sqrt{2k_B}}{2} \sum_{i,j} \left[A_{ij} d\bar{\mathbf{W}}_{ij} + B_{ij} \frac{1}{D} \text{tr}(d\mathbf{W}_{ij}) \right] \mathbf{e}_{ij} \cdot \mathbf{v}_j \\ &= \sqrt{2k_B} \sum_{i,j} \left[A_{ij} d\bar{\mathbf{W}}_{ij} + B_{ij} \frac{1}{D} \text{tr}(d\mathbf{W}_{ij}) \right] \mathbf{e}_{ij} \cdot \mathbf{v}_i - \sqrt{2k_B} \sum_{i,j} \left[A_{ij} d\bar{\mathbf{W}}_{ij} + B_{ij} \frac{1}{D} \text{tr}(d\mathbf{W}_{ij}) \right] \mathbf{e}_{ij} \cdot \mathbf{v}_i = 0. \end{aligned}$$

We have used the same index swapping cancellations between pairwise particles as in Proposition B.1. The independent term vanishes due to the skew-symmetry of dV_{ij} and symmetry of C_{ij} , which makes a cancellation for each pair of particles. Similarly, we have performed an index swap by exploiting the symmetries of A_{ij} , B_{ij} , C_{ij} and $d\mathbf{W}_{ij}$.

□

Proposition B.4. *The degeneracies $\mathbf{M}\nabla E = \mathbf{0}$ and $d\tilde{\mathbf{x}} \cdot \nabla E = 0$ are satisfied if $Q_{ji} = C_{ijk} \frac{\partial E}{\partial \mathbf{x}_k}$ where C_{ijk} is a 3-tensor with the following skew-symmetry $C_{ijk} = -C_{ikj}$.*

Proof. The noise vector is described by $d\tilde{\mathbf{x}} = \mathbf{Q}d\mathbf{W}$ where $d\mathbf{W}$ denotes a vector of independent and identically distributed (IID) increments of a Wiener process. From the degeneracy $d\tilde{\mathbf{x}} \cdot \nabla E = d\mathbf{W}^T \mathbf{Q}^T \nabla E = \mathbf{0}$ we obtain the constraint that $\mathbf{Q}^T \nabla E = \mathbf{0}$ implies $d\tilde{\mathbf{x}} \cdot \nabla E = 0$ for any sample $d\mathbf{W}$. The other degeneracy condition follows immediately $\mathbf{M} \nabla E = \mathbf{Q} \mathbf{Q}^T \nabla E = \mathbf{0}$.

Now we proof the condition $\mathbf{Q}^T \nabla E = \mathbf{0}$. By using the 3-tensor skew-symmetric parametrization we get:

$$Q_{ji} \frac{\partial E}{\partial x_j} = C_{ijk} \frac{\partial E}{\partial x_k} \frac{\partial E}{\partial x_j} = C_{ikj} \frac{\partial E}{\partial x_j} \frac{\partial E}{\partial x_k} = -C_{ijk} \frac{\partial E}{\partial x_k} \frac{\partial E}{\partial x_j} = -Q_{ji} \frac{\partial E}{\partial x_j}.$$

By rearranging the first and last terms of the equality, we have

$$Q_{ji} \frac{\partial E}{\partial x_j} + Q_{ji} \frac{\partial E}{\partial x_j} = 2Q_{ji} \frac{\partial E}{\partial x_j} = 0 \rightarrow Q_{ji} \frac{\partial E}{\partial x_j} = 0.$$

□

Remark. The proposed parametrization can be constructed in several ways, designing specific parameters θ in increasing level of complexity and respecting the required skew-symmetry:

- Nodal parameters + edge skew-symmetry: $C_{ijk} = \theta_i(\theta'_{jk} - \theta'_{kj})$.
- Edge parameters + edge skew-symmetry: $C_{ijk} = \theta_{ij}(\theta'_{jk} - \theta'_{kj})$.
- General tensor skew-symmetry: $C_{ijk} = \theta_{ijk} - \theta_{ikj}$.

Remark. This parametrization can also be extended in case there are more than one entropic variables: S_1, \dots, S_N by using a higher rank tensor with similar symmetries $C_{ijk_1 \dots k_N} = -C_{ik_a k_1 \dots j \dots k_N}$ for all extra indices and defining $Q_{ji} = C_{ijk_1 \dots k_N} \frac{\partial E}{\partial x_{k_1}} \dots \frac{\partial E}{\partial x_{k_N}}$.

C Derivation of log-likelihood

Let $\mathcal{D} = \{(\mathbf{x}_{\text{rev}}^t, \mathbf{x}_{\text{rev}}^{t+1})\}_{t=0}^{N_{\text{train}}}$ be a dataset consisting of position-velocity pairs. To train the system, we construct a joint probability distribution $p(\mathbf{x}_{\text{rev}}^{t+1}, \mathbf{x}_{\text{irr}}^{t+1} | \mathbf{x}_{\text{rev}}^t, \mathbf{x}_{\text{irr}}^t)$ corresponding to a numerical integration of Eq. (4) and train the architectures with maximum likelihood. Recall that for a general drift-diffusion SDE

$$d\mathbf{x} = f(\mathbf{x}, t)dt + g(\mathbf{x}, t)d\mathbf{W},$$

application of the Euler-Maruyama integrator provides a Gaussian increment

$$\mathbf{x}^{t+1} | \mathbf{x}^t \sim \mathcal{N}(\boldsymbol{\mu}^{t+1} = \mathbf{x}^t + f(\mathbf{x}^t, t)\Delta t, \boldsymbol{\Sigma}^{t+1} = g(\mathbf{x}^t, t)^2 \Delta t). \quad (14)$$

Under a Markovian assumption, we can thus define a joint distribution for the complete time series and derive the negative log-likelihood.

$$\text{NLL}(x^1, \dots, x^T) = - \sum_{t=1}^T \log p(x^t | x^{t-1}).$$

To obtain robust long-term rollouts, we specialize this candidate log-likelihood function to Eq. (4) and modify the transition probabilities slightly to develop a semi-implicit Euler scheme. We denote all trainable parameters via

$$\Theta = \{\theta_V, \theta_U, \theta_A, \theta_B, \theta_C, \theta_S, k_B, m\}$$

and define the maximum log-likelihood objective

$$\Theta^* = \arg \min_{\Theta} \text{NLL}(x^1, \dots, x^T).$$

To modify Eq. (14), we identify a transition probability $p(x^t | x^{t-1})$ consistent with the update rule.

$$\begin{aligned} \mathbf{v}^{t+1} &= \mathbf{v}^t + \frac{d\mathbf{v}^t}{dt} \Delta t + \Delta \tilde{\mathbf{v}}^t, \\ \mathbf{r}^{t+1} &= \mathbf{r}^t + \mathbf{v}^{t+1} \Delta t, \\ S^{t+1} &= S^t + \frac{dS^t}{dt} \Delta t + \Delta \tilde{S}^t. \end{aligned}$$

For small Δt , this is provided by the multivariate normal distribution $\mathbf{x}^{t+1}|\mathbf{x}^t \sim N(\boldsymbol{\mu}^{t+1}, \boldsymbol{\Sigma}^{t+1})$ with mean and covariance

$$\boldsymbol{\mu}^{t+1} = \begin{bmatrix} \mathbf{r}^t + \mathbf{v}^t \Delta t + \frac{d\mathbf{v}^t}{dt} \Delta t^2 \\ \mathbf{v}^t + \frac{d\mathbf{v}^t}{dt} \Delta t \\ S^t + \frac{dS^t}{dt} \Delta t \end{bmatrix}, \quad \boldsymbol{\Sigma}^{t+1} = \begin{bmatrix} \Delta \tilde{\mathbf{v}} \Delta \tilde{\mathbf{v}}^T \Delta t^2 & \Delta \tilde{\mathbf{v}} \Delta \tilde{\mathbf{v}}^T \Delta t & \Delta \tilde{\mathbf{v}} \Delta \tilde{S} \Delta t \\ \Delta \tilde{\mathbf{v}} \Delta \tilde{\mathbf{v}}^T \Delta t & \Delta \tilde{\mathbf{v}} \Delta \tilde{\mathbf{v}}^T & \Delta \tilde{\mathbf{v}} \Delta \tilde{S} \\ \Delta \tilde{S} \Delta \tilde{\mathbf{v}}^T \Delta t & \Delta \tilde{S} \Delta \tilde{\mathbf{v}}^T & \Delta \tilde{S} \Delta \tilde{S} \end{bmatrix}.$$

Now we can define the loss function to be the standard negative log-likelihood of the observations as

$$\mathcal{L} = \sum_{t=0}^{N_{\text{train}}} \left[\frac{1}{2} \ln |\boldsymbol{\Sigma}^{t+1}| + \frac{1}{2} (\mathbf{x}^{t+1} - \boldsymbol{\mu}^{t+1})^T (\boldsymbol{\Sigma}^{t+1})^{-1} (\mathbf{x}^{t+1} - \boldsymbol{\mu}^{t+1}) \right].$$

There are two problems with this approach. First, the computation of $\boldsymbol{\Sigma}$ involves the explicit construction of the global M matrix which has a space complexity scaling of $O(N^2)$, so it is very expensive in terms of memory usage and computation time for the determinant and inverse operations. We can overcome this problem by using only the marginal covariances $\boldsymbol{\Sigma}_{ii}$ of each particle, which scales linearly with the number of particles $O(N)$. Second, the covariance matrix $\boldsymbol{\Sigma}$ is singular because the position has a deterministic relationship with the velocity up to a linear scaling of Δt . We overcome this by also marginalizing over the dependent position variable, which solves the rank deficiency.

Now we can split the problem as a particle-wise problem with the following statistical properties:

$$\boldsymbol{\mu}_i^{t+1} = \begin{bmatrix} \mathbf{v}_i^t + \frac{d\mathbf{v}_i^t}{dt} \Delta t \\ S_i^t + \frac{dS_i^t}{dt} \Delta t \end{bmatrix}, \quad \boldsymbol{\Sigma}_{ii}^{t+1} = \begin{bmatrix} \Delta \tilde{\mathbf{v}}_i \Delta \tilde{\mathbf{v}}_i^T & \Delta \tilde{\mathbf{v}}_i \Delta \tilde{S}_i \\ \Delta \tilde{S}_i \Delta \tilde{\mathbf{v}}_i^T & \Delta \tilde{S}_i \Delta \tilde{S}_i \end{bmatrix}.$$

Thus the final loss function is defined as

$$\mathcal{L} = \frac{1}{N_{\text{train}}} \sum_{t=0}^{N_{\text{train}}} \frac{1}{N} \sum_{i=0}^N \left[\frac{1}{2} \ln |\boldsymbol{\Sigma}_{ii}^{t+1}| + \frac{1}{2} (\mathbf{x}_i^{t+1} - \boldsymbol{\mu}_i^{t+1})^T (\boldsymbol{\Sigma}_{ii}^{t+1})^{-1} (\mathbf{x}_i^{t+1} - \boldsymbol{\mu}_i^{t+1}) \right].$$

C.1 Computation of marginal covariances

For the marginal covariances, we need to get the $i = j$ components of the complete covariance matrix M , whose components were already computed in the previous section. By the following properties $\delta_{ii} = 1$, $\mathbf{e}_{ii} = \mathbf{v}_{ii} = 0$ and the fact the the summation over $j \in \mathcal{N}_i$ only contains nodes different than i , we obtain the following contributions:

$$\begin{aligned} m^2 \frac{d\tilde{\mathbf{v}}_i d\tilde{\mathbf{v}}_i^T}{2k_B} &= \delta_{ii} \sum_{k \in \mathcal{N}_i} \left[\frac{A_{ik}^2}{2} (\mathbf{I} + \mathbf{e}_{ik} \mathbf{e}_{ik}^T) + \frac{B_{ik}^2 - A_{ik}^2}{D} \mathbf{e}_{ik} \mathbf{e}_{ik}^T \right] dt - \left[\frac{A_{ii}^2}{2} (\mathbf{I} + \mathbf{e}_{ii} \mathbf{e}_{ii}^T) + \frac{B_{ii}^2 - A_{ii}^2}{D} \mathbf{e}_{ii} \mathbf{e}_{ii}^T \right] dt \\ &= \sum_{j \in \mathcal{N}_i} \left[\frac{A_{ij}^2}{2} \mathbf{I} + \left(\frac{A_{ij}^2}{2} + \frac{B_{ij}^2 - A_{ij}^2}{D} \right) \mathbf{e}_{ij} \mathbf{e}_{ij}^T \right] dt. \end{aligned}$$

$$\begin{aligned} mT_i \frac{d\tilde{\mathbf{v}}_i d\tilde{S}_i}{2k_B} &= -\delta_{ii} \sum_{k \in \mathcal{N}_i} \left[\frac{A_{ik}^2}{2} \left(\frac{\mathbf{v}_{ik}}{2} + \mathbf{e}_{ik} \cdot \frac{\mathbf{v}_{ik}}{2} \mathbf{e}_{ik} \right) + \frac{B_{ik}^2 - A_{ik}^2}{D} \mathbf{e}_{ik} \mathbf{e}_{ik} \cdot \frac{\mathbf{v}_{ik}}{2} \right] dt \\ &\quad - \left[\frac{A_{ii}^2}{2} \left(\frac{\mathbf{v}_{ii}}{2} + \mathbf{e}_{ii} \cdot \frac{\mathbf{v}_{ii}}{2} \mathbf{e}_{ii} \right) + \frac{B_{ii}^2 - A_{ii}^2}{D} \mathbf{e}_{ii} \mathbf{e}_{ii} \cdot \frac{\mathbf{v}_{ii}}{2} \right] dt \\ &= -\frac{1}{2} \sum_{j \in \mathcal{N}_i} \left[\frac{A_{ij}^2}{2} \mathbf{v}_{ij} + \left(\frac{A_{ij}^2}{2} + \frac{B_{ij}^2 - A_{ij}^2}{D} \right) \mathbf{e}_{ij} \cdot \mathbf{v}_{ij} \mathbf{e}_{ij} \right] dt. \end{aligned}$$

$$\begin{aligned} mT_i \frac{d\tilde{S}_i d\tilde{\mathbf{v}}_i^T}{2k_B} &= -\delta_{ii} \sum_{k \in \mathcal{N}_i} \left[\frac{A_{ik}^2}{2} \left(\frac{\mathbf{v}_{ik}^T}{2} + \mathbf{e}_{ik} \cdot \frac{\mathbf{v}_{ik}}{2} \mathbf{e}_{ik}^T \right) + \frac{B_{ik}^2 - A_{ik}^2}{D} \mathbf{e}_{ik}^T \mathbf{e}_{ik} \cdot \frac{\mathbf{v}_{ik}}{2} \right] dt \\ &\quad + \left[\frac{A_{ii}^2}{2} \left(\frac{\mathbf{v}_{ii}^T}{2} + \mathbf{e}_{ii} \cdot \frac{\mathbf{v}_{ii}}{2} \mathbf{e}_{ii}^T \right) + \frac{B_{ii}^2 - A_{ii}^2}{D} \mathbf{e}_{ii}^T \mathbf{e}_{ii} \cdot \frac{\mathbf{v}_{ii}}{2} \right] dt \end{aligned}$$

$$= -\frac{1}{2} \sum_{j \in \mathcal{N}_i} \left[\frac{A_{ij}^2}{2} \mathbf{v}_{ij}^T + \left(\frac{A_{ij}^2}{2} + \frac{B_{ij}^2 - A_{ij}^2}{D} \right) \mathbf{e}_{ij} \cdot \mathbf{v}_{ij} \mathbf{e}_{ij}^T \right] dt.$$

$$\begin{aligned} T_i^2 \frac{d\tilde{S}_i d\tilde{S}_i}{2k_B} &= \delta_{ii} \sum_{k \in \mathcal{N}_i} \left(\frac{A_{ik}^2}{2} \left[\left(\frac{\mathbf{v}_{ik}}{2} \right)^2 + \left(\mathbf{e}_{ik} \cdot \frac{\mathbf{v}_{ik}}{2} \right)^2 \right] + \frac{B_{ik}^2 - A_{ik}^2}{D} \left(\mathbf{e}_{ik} \cdot \frac{\mathbf{v}_{ik}}{2} \right)^2 + C_{ik}^2 \right) dt \\ &+ \left(\frac{A_{ii}^2}{2} \left[\left(\frac{\mathbf{v}_{ii}}{2} \right)^2 + \left(\mathbf{e}_{ii} \cdot \frac{\mathbf{v}_{ii}}{2} \right)^2 \right] + \frac{B_{ii}^2 - A_{ii}^2}{D} \left(\mathbf{e}_{ii} \cdot \frac{\mathbf{v}_{ii}}{2} \right)^2 - C_{ii}^2 \right) dt \\ &= \sum_{j \in \mathcal{N}_i} \left(\frac{A_{ij}^2}{2} \left[\left(\frac{\mathbf{v}_{ij}}{2} \right)^2 + \left(\mathbf{e}_{ij} \cdot \frac{\mathbf{v}_{ij}}{2} \right)^2 \right] + \frac{B_{ij}^2 - A_{ij}^2}{D} \left(\mathbf{e}_{ij} \cdot \frac{\mathbf{v}_{ij}}{2} \right)^2 + C_{ij}^2 \right) dt \\ &= \frac{1}{4} \sum_{j \in \mathcal{N}_i} \left[\frac{A_{ij}^2}{2} \mathbf{v}_{ij}^2 + \left(\frac{A_{ij}^2}{2} + \frac{B_{ij}^2 - A_{ij}^2}{D} \right) \left(\mathbf{e}_{ij} \cdot \mathbf{v}_{ij} \right)^2 \right] dt + \sum_{j \in \mathcal{N}_i} C_{ij}^2 dt. \end{aligned}$$

Note that the resulting marginal covariance matrices are symmetric, as expected. Furthermore, as the complete covariance matrix \mathbf{M} is positive semidefinite by construction, all its leading minors are also positive semidefinite matrices. Thus, all the marginal covariance matrices are valid.

D Constrained monotonic neural networks

The purpose of Constrained Monotonic Neural Networks [121] is to construct a universal approximator with a precondition of (partial) monotonicity and/or convexity of a multivariate, multidimensional function. The basic building block is a monotone constrained fully connected layer:

$$\mathbf{h} = \rho^s(|\mathbf{W}^T|_{\mathbf{t}} \mathbf{x} + \mathbf{b})$$

where $\mathbf{x} \in \mathbb{R}^n$ is the input vector, $\mathbf{h} \in \mathbb{R}^m$ is the output vector, $\mathbf{W} \in \mathbb{R}^{n \times m}$ and $\mathbf{b} \in \mathbb{R}^m$ are the weights and biases, ρ^s is the combined activation function, and \mathbf{t} is the monotonicity indicator vector. This is a usual MLP architecture whose weights and activation functions are specifically chosen to ensure monotonicity and convexity of the output results.

In particular, we need to model the internal energy $U_i = U(S_i, \mathcal{V}_i)$ scalar function which is increasing in entropy S_i and decreasing in volume \mathcal{V}_i , both scalar quantities. Thus, the monotonicity indicator vector is $\mathbf{t} = [1, -1]$ and the weight matrix is modified by the operation $|\mathbf{W}^T|_{\mathbf{t}}$ which assigns the following sign change:

$$w'_{ji} = \begin{cases} |w_{ji}| & \text{if } t_i = 1 \\ -|w_{ji}| & \text{if } t_i = -1 \\ w_{ji} & \text{otherwise} \end{cases}.$$

For the subsequent hidden layers, monotonic dense units with the indicator vector \mathbf{t} always being set to 1 are used in order to preserve monotonicity. Last, we enforce convexity with respect to both inputs by using a convex activation function ρ^s . In our experiments, we have used a softmax activation. It is noteworthy that even with the imposed constraints on weights and activation functions, the network retains its universal approximation property. The complete proof is provided in [121].

E Training and testing algorithms

Algorithm 1 Training algorithm for the proposed method.

Input: State variables: $(\mathbf{r}^t, \mathbf{v}^t)$
for each particle i **do**
 Compute neighbour particles $j \in \mathcal{N}_i$
 Estimate entropy S_i :
 $S_i = \text{NN}(\mathbf{r}_{ij}, \mathbf{v}_{ij})$
 Compute particle volume \mathcal{V}_i and traceless strain tensor $\bar{\boldsymbol{\varepsilon}}_i$:
 $d_i = \text{NN}(\mathbf{r}_{ij})$
 $\bar{\boldsymbol{\varepsilon}}_i = \text{NN}(\mathbf{r}_{ij}, \mathbf{r}_{ij}^0)$
 Compute internal energy U_i :
 $U_i = \text{NN}(S_i, \mathcal{V}_i, \bar{\boldsymbol{\varepsilon}}_i)$
 $P_i = -\frac{\partial U_i}{\partial \mathcal{V}_i}, T_i = \frac{\partial U_i}{\partial S_i}, \boldsymbol{\tau}_i = \frac{\partial U_i}{\partial \bar{\boldsymbol{\varepsilon}}_i}$
 Compute prediction statistics:
 $A_{ij}, B_{ij}, C_{ij} = \text{NN}(\mathbf{r}_{ij}, T_i, T_j)$
 Compute Σ_{ii}^{t+1} and $\boldsymbol{\mu}_i^{t+1}$
end for
 Compute negative log-likelihood loss \mathcal{L}

Algorithm 2 Testing algorithm for the proposed method.

Input: Initial conditions: $(\mathbf{r}^0, \mathbf{v}^0)$
 Estimate initial entropy $S^0 = \text{NN}(\mathbf{r}_{ij}^0, \mathbf{v}_{ij}^0)$
for each snapshot t **do**
 for each particle i **do**
 Compute neighbour particles $j \in \mathcal{N}_i$
 Compute particle volume \mathcal{V}_i and traceless strain tensor $\bar{\boldsymbol{\varepsilon}}_i$:
 $d_i = \text{NN}(\mathbf{r}_{ij})$
 $\bar{\boldsymbol{\varepsilon}}_i = \text{NN}(\mathbf{r}_{ij}, \mathbf{r}_{ij}^0)$
 Compute internal energy U_i :
 $U_i = \text{NN}(S_i, \mathcal{V}_i, \bar{\boldsymbol{\varepsilon}}_i)$
 $P_i = -\frac{\partial U_i}{\partial \mathcal{V}_i}, T_i = \frac{\partial U_i}{\partial S_i}, \boldsymbol{\tau}_i = \frac{\partial U_i}{\partial \bar{\boldsymbol{\varepsilon}}_i}$
 Compute stochastic increments $d\tilde{\mathbf{x}}_i$:
 $A_{ij}, B_{ij}, C_{ij} = \text{NN}(\mathbf{r}_{ij}, T_i, T_j)$
 Random numbers $d\mathbf{W}_{ij}$ and dV_{ij}
 Compute $d\tilde{\mathbf{x}}_i = (\mathbf{0}, d\tilde{\mathbf{v}}_i, d\tilde{S}_i)$
 end for
 Solve dynamics \mathbf{x}^{t+1} via GENERIC
 Update state vector: $\mathbf{x}^t \leftarrow \mathbf{x}^{t+1}$
end for

F Alternative architectures

F.1 GNS

Graph Network-based Simulator (GNS) [107] is a deep learning architecture specifically designed for capturing the dynamical behaviour of complex fluids. For GNS, we use the original deterministic acceleration prediction based on positions and velocities. We use the following encoder-processor-decoder message-passing structure:

- Encoder: Following the original paper, the nodal features are chosen to be the velocities of the particles \mathbf{v}_i , and the edge features the relative positions \mathbf{r}_{ij} and distances $|\mathbf{r}_{ij}|$. Those are encoded in node \mathbf{z}_i and edge \mathbf{z}_{ij} latent vectors by using two networks:

$$\mathbf{z}_{ij} = \text{MLP}_e \left(\frac{\mathbf{r}_{ij}}{h}, \frac{|\mathbf{r}_{ij}|}{h} \right), \quad \mathbf{z}_i = \text{MLP}_v(\mathbf{v}_i).$$

- Processor: The latent nodes and edges are then processed with a message passing layer with mean aggregation function. This scheme is repeated M times with residual connections in order for the information to transverse the complete graph.

$$\mathbf{z}_{ij}^{l+1} = \mathbf{z}_{ij}^l + \text{MLP}_m^l(\mathbf{z}_i^l, \mathbf{z}_j^l, \mathbf{z}_{ij}^l), \quad \mathbf{z}_i^{l+1} = \mathbf{z}_i^l + \text{MLP}_v^l\left(\mathbf{z}_i^l, \frac{1}{|\mathcal{N}_i|} \sum_{j \in \mathcal{N}_i} \mathbf{z}_{ij}^{l+1}\right).$$

- Decoder: The decoder extracts the dynamic information from the latent nodes as an acceleration prediction:

$$\mathbf{a}_i = \text{MLP}_d(\mathbf{z}_i^M) dt.$$

The dynamic equations are then the following:

$$\begin{aligned} d\mathbf{r}_i &= \mathbf{v}_i dt \\ d\mathbf{v}_i &= \text{GNS}(\mathbf{r}_i, \mathbf{v}_i) dt = \mathbf{a}_i dt \end{aligned}$$

F.2 GNS-SDE

The original GNS paper does not account for stochastic effects. We have adapted the methodology to account for stochastic effects in a second architecture which we refer to as GNS-SDE [108]. The idea is to have two independent GNS which account for the drift and diffusion terms of a generic stochastic differential equation as follows:

$$\begin{aligned} d\mathbf{r}_i &= \mathbf{v}_i dt, \\ d\mathbf{v}_i &= \text{GNS}_{\text{drift}}(\mathbf{r}_i, \mathbf{v}_i) dt + \text{GNS}_{\text{diff}}(\mathbf{r}_i, \mathbf{v}_i) d\mathbf{w} \end{aligned}$$

where $\text{GNS}_{\text{drift}}(\mathbf{x})$ and $\text{GNS}_{\text{diff}}(\mathbf{x})$ are the drift and diffusion coefficients respectively and $d\mathbf{w}$ is a Wiener process with zero mean and unit variance.

F.3 DPD

As a traditional coarse-graining baseline, we use the standard Dissipative Particle Dynamics (DPD) force decomposition in conservative, dissipative and random forces between particles as:

$$\begin{aligned} d\mathbf{r}_i &= \mathbf{v}_i dt, \\ m d\mathbf{v}_i &= \sum_{j \in \mathcal{N}_i} (\mathbf{F}_{ij}^C dt + \mathbf{F}_{ij}^D dt + \mathbf{F}_{ij}^R d\mathbf{w}) \end{aligned}$$

where each force is computed using:

$$\begin{aligned} \mathbf{F}_{ij}^C &= \alpha w^C(|\mathbf{r}_{ij}|) \mathbf{e}_{ij}, \\ \mathbf{F}_{ij}^D &= -\gamma w^D(|\mathbf{r}_{ij}|) (\mathbf{e}_{ij} \cdot \mathbf{v}_{ij}) \mathbf{e}_{ij}, \\ \mathbf{F}_{ij}^R &= \sigma w^R(|\mathbf{r}_{ij}|) \mathbf{e}_{ij}. \end{aligned}$$

The conservative and random pairwise weight function is chosen to be the usual linear function of the normalized distance

$$w^C(|\mathbf{r}_{ij}|) = w^R(|\mathbf{r}_{ij}|) = 1 - \frac{|\mathbf{r}_{ij}|}{h}.$$

The dissipative forces are fully determined by the fluctuation-dissipation theorem:

$$\begin{aligned} \sigma^2 &= 2\gamma k_B T, \\ w^D(|\mathbf{r}_{ij}|) &= w^R(|\mathbf{r}_{ij}|)^2. \end{aligned}$$

To sum up, this model has 4 trainable parameters: the force amplitudes α and σ , the particle mass m and the thermal energy $k_B T$.

G Hyperparameters

G.1 Datasets

The datasets were generated using the following hyperparameters:

- Number of CG particles (N): Discretization of the domain in coarse-grained particles.
- Length of the domain (L): Length of the cubic box in 2D and 3D. For molecular dynamics examples, the periodic boundary conditions are applied.
- Cutoff radius (h): The radius which determines the neighbourhood from which the interactions are active, following the minimum image convention for periodic boundary conditions.
- Time step (Δt): Time step of the coarse-grained learnt simulation. In molecular dynamics examples, several orders of magnitude bigger than the original time scale. In solid mechanics example, it is determined by the CFL condition and the measured data availability.

Table 1: Dataset hyperparameters.

	N	L	h	Δt
IDEAL GAS	500	1.00 (3D periodic)	0.20	5.0e-4
STAR POLYMER 11	1000	30.18 (3D periodic)	4.75	2.5e-2
STAR POLYMER 51	2000	63.41 (3D periodic)	7.61	4.0e-2
VISCOELASTIC	900	2 (2D)	0.13	1.0e-2
COLLOIDS	1135	2 (2D)	0.11	5.0e-4

G.1.1 IDEAL GAS

The first example is the simulation of $N = 500$ coarse-grained particles in a 3D periodic box of length $L = 1$. The fluid has a shear and bulk viscosity of $\eta = \zeta = 0.1$ and thermal conductivity of $\kappa = 0.1$. The equation of state is assumed to be an monoatomic ideal gas,

$$U(S, \mathcal{V}) = \frac{3h_p^2 N_p^2}{4\pi m} \left(\frac{N_p}{\mathcal{V}} \right)^{\frac{2}{3}} \exp\left(\frac{2S}{3k_B N_p} - \frac{5}{3} \right),$$

where h_p is the Planck constant and N_p the number of particles per fluid particle. We select units in which $N_p h_p = 1$, $N_p k_B = 10$ and $m = 1$. The dataset was generated directly in the coarse-grained domain using the methodology described in [30].

G.1.2 STAR POLYMER 11 and STAR POLYMER 51

The second example is a polymer melt in a 3D periodic box. Each polymer is composed of a core atom and 10 arms bonded by a FENE potential, whereas the interaction between polymers is modelled by a Lennard-Jones potential. Two different internal configurations are considered: 1 and 5 beads per arm, which results in less and higher coarse-graining levels. The fully resolved datasets are generated using LAMMPS [106] and then coarse-grained by computing the center of mass position and velocity of each polymer.

G.1.3 VISCOELASTIC

The 2D solid square domain of length $L = 2$ with a imposed shear displacement of $\Delta L_x = 1$ in the X axis. The material is chosen to be a Mooney-Rivlin model with density $\rho = 1000$ and parameters $C_{10} = 1.5 \cdot 10^6$, $C_{01} = 5 \cdot 10^5$ and $D_1 = 10^{-7}$. A time-dependant viscoelastic behaviour was included as a two-term Prony series with shear relaxation modulus ratio and relaxation time of $G_1 = 0.5$, $\tau_1 = 0.2$ and $G_2 = 0.49$, $\tau_2 = 0.3$ respectively. The system is discretized in $N = 900$ coarse graining particles. The reference solution was computed using the finite element solver Abaqus.

G.1.4 COLLOIDS

The last example is a real measured dataset of a jammed 2D monolayer of repulsive microspheres under cyclic shear forcing. The system consists of sulfate latex particles adsorbed at a water-decane interface, forming a soft jammed material due to electrostatic dipole-dipole repulsion. The material is sheared using an interfacial stress rheometer (ISR), where a magnetized needle applies oscillatory shear stress within a confined channel [111, 32]. High-resolution optical microscopy is used to capture

the positions of each particle, processed with a computer vision particle tracking algorithm, and the velocities are obtained with finite differences. The system is discretized in $N = 1135$ coarse graining particles.

G.2 Training

The hyperparameters used to train the models are the following:

- Number of training snapshots (N_{train}): Time horizon considered for the training from the initial conditions. They are shuffled in 75% train and 25% validation split.
- Number of extrapolation snapshots (N_{extrap}): Sequential rollout of the model from the initial conditions. In molecular dynamics, the model is extrapolated to $N_{\text{extrap}} = 25N_{\text{train}}$ to reach the steady-state statistics.
- Learning rate (l_r): Initial learning rate for training.
- Number of epochs (N_{epoch}): Number of total training epochs.
- Number of hidden layers (N_h): Number of hidden layers of the MLPs. All the MLPs used are 2 hidden layers with SiLU activation functions [129].
- Number of parameters (N_{params}): Parameter count of the trained model..

Table 2: Training hyperparameters.

	N_{train}	N_{extrap}	l_r	N_{epoch}	N_h	N_{params}
IDEAL GAS	300	7.5e3	1.0e-2	5.0e3	50	16560
STAR POLYMER 11	400	1.0e4	1.0e-3	5.0e3	100	63110
STAR POLYMER 51	400	1.0e4	1.0e-3	1.0e4	50	16560
VISCOELASTIC	800	1000	1.0e-3	2.0e3	100	84517
COLLOIDS	2000	3500	1.0e-3	2.0e3	100	84517

H Additional figures

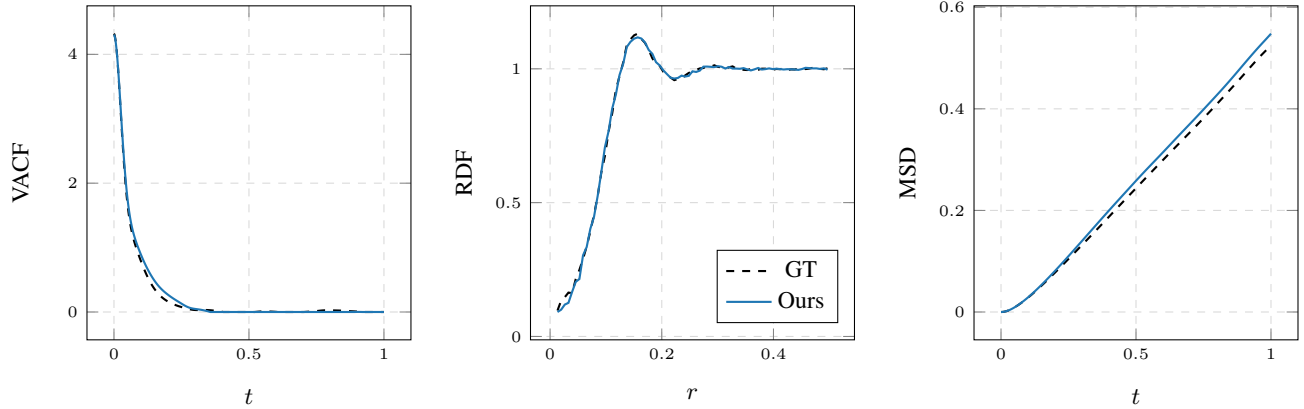


Figure 8: Correlation metrics for the TAYLOR-GREEN dataset trained with forcing conditions.

Table 3: L2 relative error (\downarrow) of correlation metrics for the IDEAL GAS interpolation and extrapolation experiments and STAR POLYMER examples.

		VACF	RDF	MSD
TAYLOR-GREEN	GNS	1.09e4	3.27e-1	2.24e4
	GNS-SDE	8.23e4	3.40e-1	1.70e5
	DPD	3.25e-1	4.41e-2	2.66e-1
	Ours	5.18e-2	9.82e-3	7.73e-2
SELF-DIFFUSION	GNS	1.02e4	3.15e-1	1.94e4
	GNS-SDE	6.46e4	3.27e-1	1.23e5
	DPD	4.52e-1	4.44e-2	4.65e-1
	Ours	4.19e-2	1.59e-2	4.54e-2
SHEAR FLOW	GNS	7.59e5	3.43e-1	3.45e-1
	GNS-SDE	1.47e5	2.94e-1	3.74e-1
	DPD	2.18e-1	3.68e-2	4.64e-2
	Ours	7.94e-2	1.12e-2	3.76e-2
STAR POLYMER 11	GNS	1.25e6	4.29e-1	2.09e6
	GNS-SDE	3.87e5	4.27e-1	6.45e5
	DPD	6.66e-1	2.26e-1	9.51e-1
	Ours	9.89e-2	1.99e-2	4.73e-2
STAR POLYMER 51	GNS	1.27e1	2.13e-1	2.12e1
	GNS-SDE	7.97e6	2.23e-1	1.61e7
	DPD	4.00e0	9.64e-2	7.63e0
	Ours	1.41e-1	5.28e-2	5.32e-2

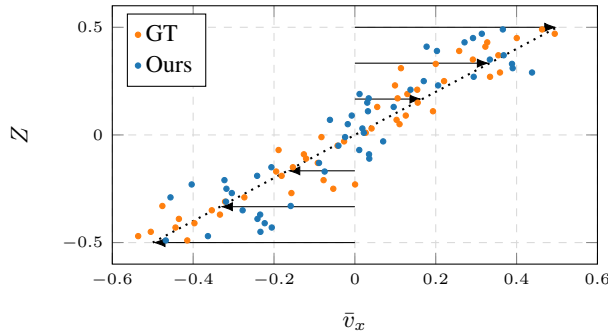


Figure 9: Velocity profile of the SHEAR FLOW test dataset averaged over the X axis. The forced boundary condition is represented as a dotted line.

 Table 4: Time performance (mean \pm std) in ms/step (\downarrow) for the evaluated methods and the fully resolved dynamics (full-order).

	IDEAL GAS	STAR POLYMER 11	STAR POLYMER 51
GNS	1.32 \pm 0.04	1.93 \pm 0.03	2.51 \pm 0.02
GNS-SDE	2.57 \pm 0.02	3.75 \pm 0.04	4.99 \pm 0.04
DPD	0.17 \pm 0.00	0.18 \pm 0.00	0.17 \pm 0.00
Ours	5.98 \pm 0.05	6.12 \pm 0.06	6.00 \pm 0.08
Full-order	-	21.87	74.40

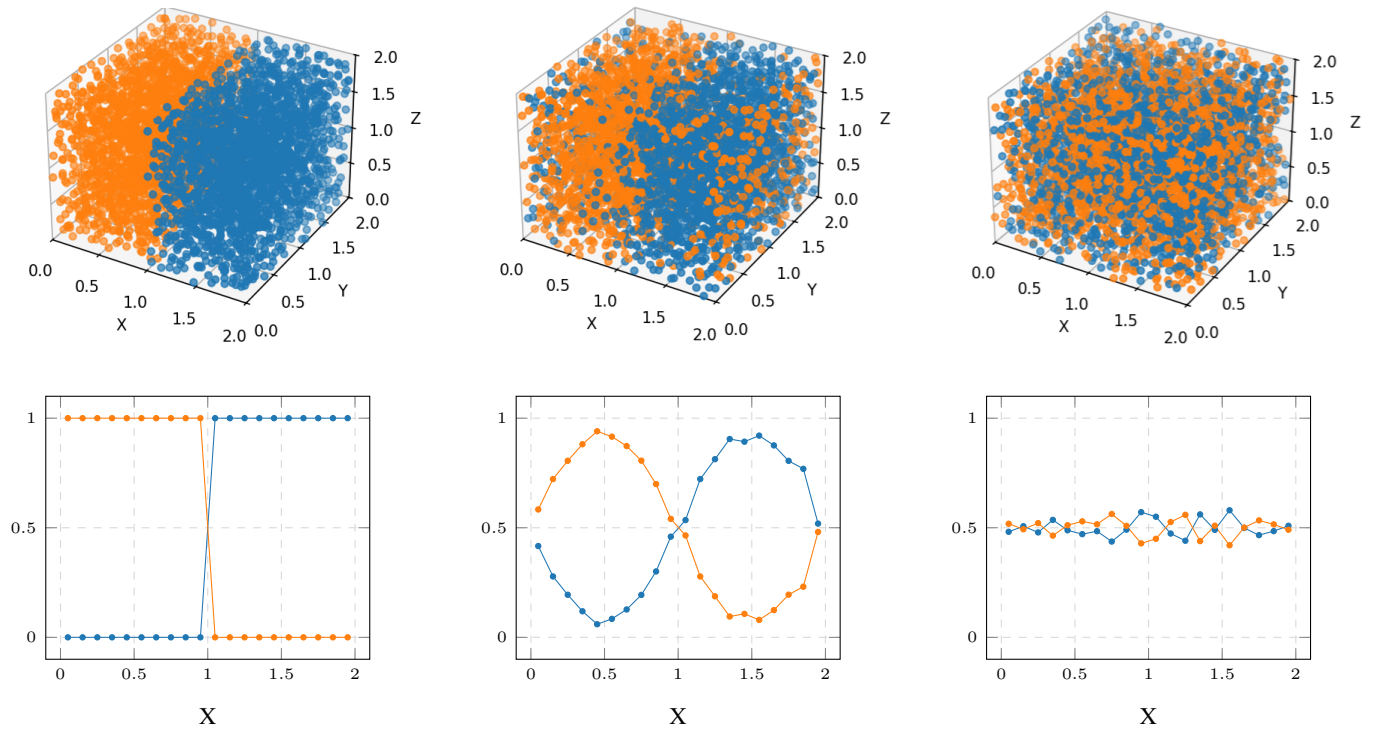


Figure 10: Visualization of the neural network inference simulation of the SELF DIFFUSION case with a bigger domain $L = 2$ at same density. The upper panels show several snapshots of the mixing of particles due to the thermal fluctuations. The lower panels represent the corresponding spatial concentration of red and blue particle profiles averaged over the X axis.

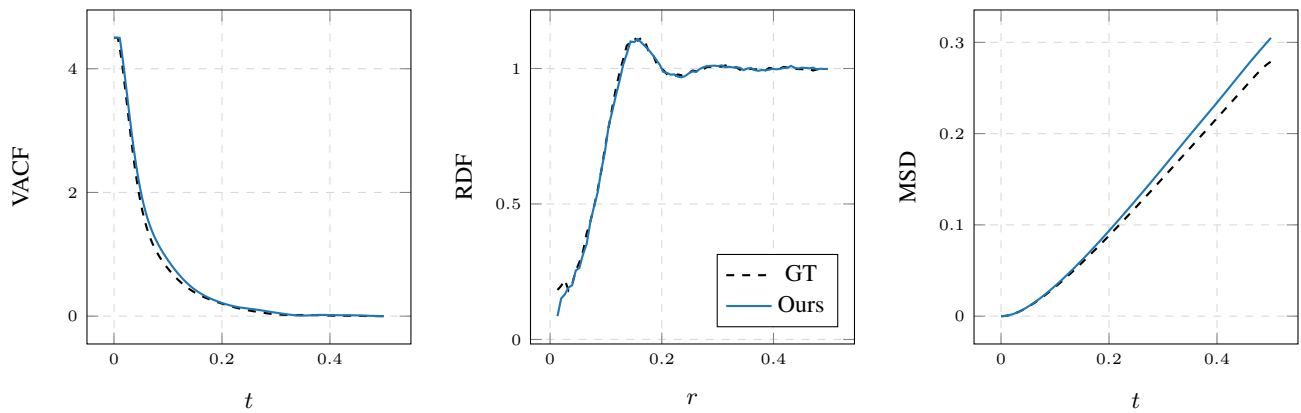


Figure 11: Correlation metrics for the TAYLOR-GREEN dataset trained with equilibrium conditions.

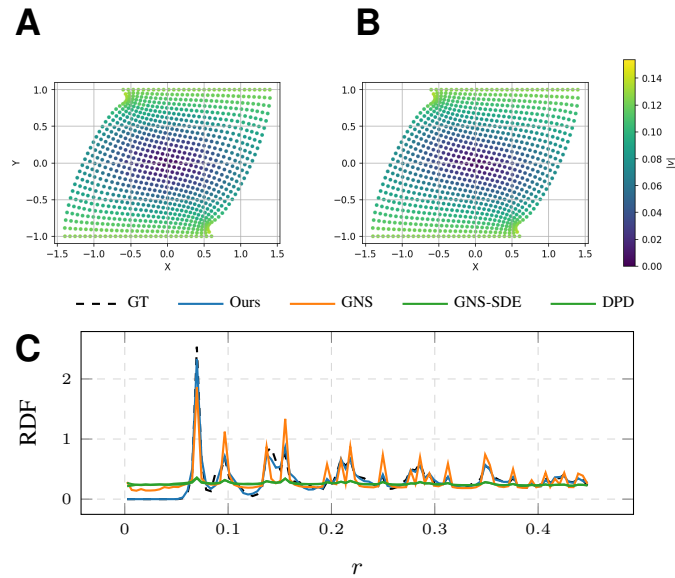


Figure 12: Results for the VISCOELASTIC dataset. Intermediate snapshot with color encoding velocity magnitude for (A) ground truth and (B) model prediction. (C) Radial Distribution Function, indicating the correct prediction of structural statistics.

Table 5: L2 relative error (\downarrow) of correlation metrics for the VISCOELASTIC and COLLOIDS examples.

		RDF
VISCOELASTIC	GNS	3.08e-1
	GNS-SDE	5.07e-1
	DPD	5.06e-1
	Ours no U^{dev}	1.84e-1
	Ours	9.17e-2
COLLOIDS	GNS	4.33e-1
	GNS-SDE	4.90e-1
	DPD	6.89e-1
	Ours no U^{dev}	4.49e-1
	Ours	9.22e-2

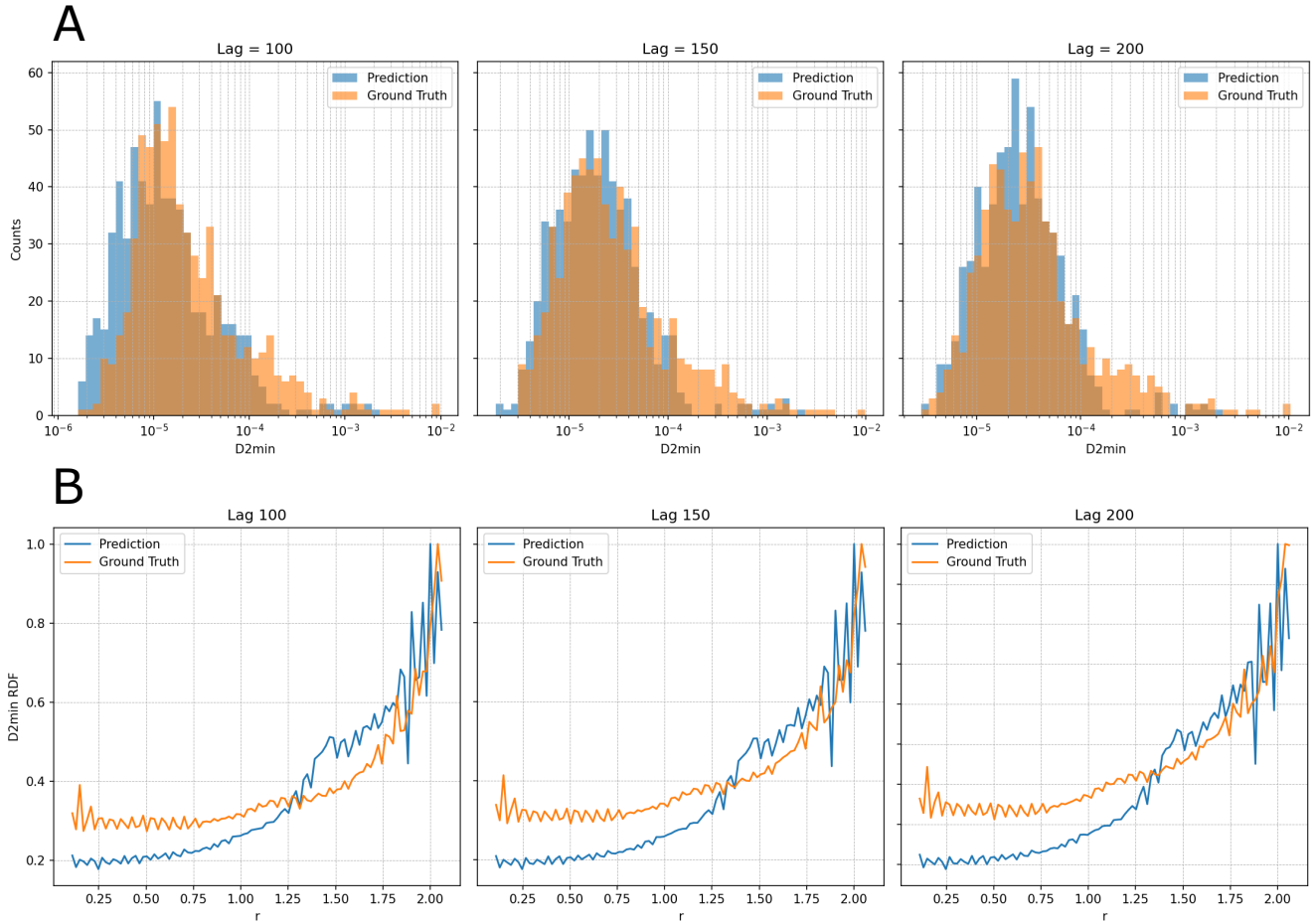


Figure 13: Dynamical properties for the COLLOIDS dataset with lag times 100, 150 and 200. (A) Histograms of non-affine displacements D_{\min}^2 for all the domain particles of the prediction and the reference solution. (B) Normalized radial distribution function of the local non-affine displacements.